THESIS

INVESTIGATION OF GOLD AS A MATERIAL FOR THERMAL RADIATION SHIELDING

Submitted by

Amit Harenkumar Munshi

Department of Mechanical Engineering

In partial fulfillment of the requirements

For the degree of Master of Science

Colorado State University

Fort Collins, Colorado

Spring 2013

Master's Committee:

Advisor: Walajabad Sampath

Allan Kirkpatrick
James Sites

ABSTRACT

INVESTIGATION OF GOLD AS A MATERIAL FOR THERMAL RADIATION SHIELDING

CdS/CdTe thin film solar cells technology is one of the fastest growing carbon neutral energy sources in the world today. In 2010, CdTe/CdS accounted for nearly 6% of all the solar cells installed worldwide. CdS/CdTe solar cells have achieved gigawatt-scale commercial production and has demonstrated the lowest reported manufacturing cost per watt.

Manufacturing of CdS/CdTe solar modules is carried out at temperature in the range of 620^{o}C under a vacuum of 40 millitorr using a Heated Pocket Deposition (HPD) system in the materials engineering laboratory. Since this system operates in vacuum, majority of the heat loss is due to thermal radiation. Heat losses due to conduction and convection are negligible. The concept here is to conserve the heat by reflecting the infrared radiation back into the deposition system thus increasing the thermal efficiency. Steel, aluminum, silver and gold are all possible solutions but gold exhibits properties that overcome the shortcomings of rest of the three elements.

A thin film of gold deposited uniformly on a surface of Pyrex or quartz can be used to reflect the infrared radiation efficiently. Calculations show, using two such consecutive shields can effectively reflect almost 97% of the incident radiation thus conserving substantial amount of energy in the entire production process.

What inhibits the use of gold film for this purpose is a phenomenon called thermal grooving or island formation. Thermal grooving occurs when the stress concentration at the grain boundaries causes grain separation. As the temperature is raised grains of gold are separated out forming isolated islands. This phenomenon is observed in thin gold films that are exposed to a temperature in excess of 350^{o}C for over 3 to 5 hours. In this study, these films are exposed to temperature upto 620^{o}C for cycles as long as 200 hours. It is obvious that this would render the gold film useless after one cycle. The goal of this research is to explore the solutions for elimination of the phenomenon of thermal grooving and thus

extract maximum life out of these thin gold films for conservation of heat. The advantage of using thin Gold film reflector was validated mathematically before any experiments were conducted.

After carefully exploring literature on past research and conducting experiments it was found that within the range of the films that were tested, a 2000 A^o film with a 150 A^o of Indium underlay showed the best performance after thermal annealing and testing.

ACKNOWLEDGEMENTS

I would like to take this opportunity to thank my advisor, Professor W.S. Sampath, for his guidance and patience. I would also like to thank my committee members, Professor James Sites and Professor Allan Kirkpatrick, for their time and commitment. I would like to thank the funding organization NSF I/UCRC (Industry & University Cooperative Research Program) for funding this study.

I highly appreciate the help of other members of the laboratory, especially Bhavin Patel and Brandon Kelly, whose advice and encouragement made my research possible. Also, Ritesh Banka who helped me write the program to calculate the temperatures at each radiation shield. I also like to show my appreciation for Russell Geisthardt and John Raguse of the CSU PV lab for testing the reflectance of the sample mirrors. Members of Colorado Nanofabrication Laboratory at University of Colorado, Boulder were instrumental in fabrication of Gold film samples, and I would like to thank them.

I thank Dr. Patrick McCurdy of the Central Instrumentation Facility for his instructions that allowed me to learn and use characterization equipment like Scanning Electron Microscope and Energy Dispersive X-ray Spectroscopy. Without the help and support of Jack Clark of Surface Analytics, LLC, I would have been unable to use Scanning White Light Interferometer which would have left this study incomplete.

Last but not the least; I am highly grateful to my friends and my entire family who inspired me throughout my academic career. My father Harenkumar Munshi and mother Bhargavi Munshi who was also my teacher at primary school supported me during my worst academic crisis that allowed me to emerge as a student I am today. I cannot thank my brother Jay Munshi and sister Jigna Jariwala enough for their support and encouragement throughout my life. Also, I show my gratitude to my grandparents Late Shri Prafulchandra Joshi and Late Smt. Jayvidya Joshi, whose blessings and confidence in my ability played a crucial role in carving my career and life.

DEDICATION

To the lotus feet of

My mother Bhargavi Munshi and my grandmother Late Mrs. Jayvidya Joshi

For their blessings and support through

Good and bad times.

TABLE OF CONTENTS

ABSTRACT ii

ACKNOWLEDGEMENTS iv

DEDICATION v

TABLE OF CONTENTS vi

LIST OF FIGURES ix

CHAPTER 1: INTRODUCTION 1

1.1 Global Energy Picture 1

1.2 CdS/CdTe Solar Cells 2

1.3 Manufacturing of CdS/CdTe Solar Cells 2

CHAPTER 2: ADVANCED THERMAL RADIATION SHIELD 7

2.1 Motivation 7

2.2 Basic Concept and Development 9

2.3 Advantages of Using Gold 10

2.4 Final Validation Prior to Experimentation 12

CHAPTER 3: PROBLEM STATEMENT AND EXPERIMENTAL APPROACH 17

3.1 Early Approach and First Test Plan 17

3.2 Experimental Setup 17

CHAPTER 4: MATERIAL ASPECT OF THE SHIELDS AND POTENTIAL SOLUTIONS 21

4.1 Overview of the Problem from Materials Perspective 21

4.2 Possible Solutions 23

4.3 Review of All Possible Solutions 24

4.3.1 Using thicker Gold Film 24

4.3.2 Using Silicon Oxide overlay 24

4.3.4 Doping with Tin (Tin underlay) 25

4.3.5 Doping with other metals 25

4.3.6 Doping with Chromium (Chromium underlay) 25
4.3.7 Doping with Indium (Indium underlay) 6
CHAPTER 5: ANALYTICAL TECHNIQUES FOR GOLD FILM CHARACTERIZATION 27
5.1 Overview 27
5.2 Scanning Electron Microscope Imaging 27
5.2.1 Principle and operation 27
5.3 Energy-Dispersion X-ray Spectroscopy 29
5.4 Scanning White Light Interferometer 31
5.5 UV-VIS-IR Spectrometer 33
CHAPTER 6: TEST AND ANALYSIS OF MIRROR SAMPLES FROM OPTICAL COMPONENT MANFACTURERES 34
6.1 Overview 34
6.2 Visual Inspection 34
6.3 Reflectivity Measurements using Spectrometer 36
6.4 Microscope Imaging and Evaluation 39
6.4.1 Microscope images of Edmund Optics samples 39
6.4.2Microscope images of Thor Laboratory samples 41
6.5 EDS Results for Samples After Test 43
6.6 SWLI Surface Roughness Measurement for Samples After Test 47
6.6.1SWLI roughness measurement for samples from Edmund Optics 47
6.6.2SWLI roughness measurement for samples from Thor Laboratory 48
6.7 Conclusion Derived from Analysis of First Phase of Experiments 51
CHAPTER 7: TEST AND ANALYSIS OF MIRRORS CUSTOM FABRICATED AT CNL 52
7.1 Overview 52
7.2 Colorado Nanofabrication Lab 52
7.3 Sample Specifications and Preparation 53

7.4 Visual Inspection of the Samples 54
7.5 Reflectivity Measurements using Spectrometer 56
7.6 Microscope Imaging and Evaluation 60
7.6.1 Microscope Images of Film with 50% Indium/800 A^o Gold 60
7.6.2 Microscope Images of Film with 6% Indium/1000 A^o Gold 62
7.6.3 Microscope Images of Film with 7.5% Indium/2000 A^o Gold 64
7.7 EDS Results for Samples Before and After Annealing 66
7.7.1 EDS scan of sample with 50% Indium under 800A^o of Gold 66
7.7.2 EDS scan of sample with 6% Indium under 1000A^o of Gold 70
7.7.3 EDS scan of sample with 7.5% Indium under 2000A^o of Gold 74
7.8 SWLI Surface Roughness Measurement for Samples Before and After Annealing 78
7.8.1 SWLI roughness measurement for samples with 50% Indium under 800 A^o Gold 78
7.8.2 SWLI roughness measurement for samples with 6% Indium under 1000 A^o Gold 80
7.8.3 SWLI roughness measurement for samples with 7.5% Indium under 2000 A^o Gold 82
CHAPTER 8: CONCLUSION AND FUTURE PROSPECT OF STUDY 85
8.1 Table of Observations 85
8.2 Conclusion 86
8.2 Scope of Future Study 86
REFERENCES 88
APPENDIX I 90

LIST OF FIGURES

Figure 1: Schematic Device Structure (Not to Scale) 2

Figure 2: Partial cross sectional view of thermal sublimation source 3

Figure 3: Flowchart of an exemplary process for manufacturing of CdTe/CdS photovoltaic module 5

Figure 4: (Left) Goldenrod Medium-Wave Infrared Lamps from Fannon Products
(Right) Heraeus Infrared Heaters Reflective tube 8

Figure 5: Principle heat losses from a vacuum flask 8

Figure 6: Schematic of the basic concept of Advanced Thermal Radiation Shield 10

Figure 7: Reflectivity of various materials. The x-axis on this graph is wavelength of electromagnetic radiation is nanometers and the y-axis shows the proportion of incident light that is reflected back. (Courtesy – HeraeusNoblelight) 12

Figure 8: A close approximation of an ideal black body 14

Figure 9: Conservation of heat using thin gold film on quartz/Pyrex substrate thermal radiation Shields 15

Figure 10: Schematic of Test Setup 18

Figure 11: High temperature tube furnace 19

Figure 12: High temperature tube furnace showing interiors 19

Figure 13: Typical programing and control unit with digital readout on a high temperature tube Furnace 20

Figure 14: Micrographs of gold film exposed to various temperatures and time. Magnification increases from bottom to top 22

Figure 15: Micrographs of gold film doped with Indium exposed to various temperatures and time. Magnification increases from bottom to top 26

Figure 16: Schematic cross-section of a Scanning Electron Microscope 28

Figure 17: (Left) species of characteristic radiation availed from the specimen surface (right) mechanism of back-scatter electron generation 28

Figure 18: Bohr's model and mechanism of release of radiation during EDS analysis 30

Figure 19: A typical EDS scan for an unknown sample containing Copper, Molybdenum, Oxygen and Potassium 31

Figure 20: Schematic layout of a typical Scanning White Light Interferometer 32

Figure 21: Standard laboratory setup of a Scanning White Light Interferometer 33

Figure 22: Mirror samples from Edmund Optics (left) after test (right) before test 35

Figure 23: Mirror samples from Thor Laboratories (left) before test (right) after test 36

Figure 24: Plot of percentage reflectivity v/s wavelength (nm) for Edmund Optics sample in Visible Spectrum before and after annealing 36

Figure 25: Plot of percentage reflectivity v/s wavelength (nm) for Edmund Optics sample in Infrared Spectrum before and after annealing 37

Figure 26: Plot of percentage reflectivity v/s wavelength (nm) for Thor Labs sample in Visible Spectrum before and after annealing 37

Figure 27: Plot of percentage reflectivity v/s wavelength (nm) for Thor Labs sample in Infrared Spectrum before and after annealing 38

Figure 28: Image of sample from Edmund Optics using a Scanning electron Microscope (Top left) at 10000x magnification (Top right) at 100000x magnification and (Bottom) at 220000x magnification before annealing 39

Figure 29: Image of sample from Edmund Optics using a Scanning electron Microscope (Top left) at 100x magnification (Top right) at 4500x magnification and (Bottom) at 10000x magnification after annealing 40

Figure 30: Image of sample from Thor Laboratory using a Scanning electron Microscope (Top left) at 33000x magnification (Top right) at 35000x magnification and (Bottom) at 80000x magnification before annealing 41

Figure 31: Image of sample from Edmund Optics using a Scanning electron Microscope (Top left) at 200x magnification (Top right) at 500x magnification and (Bottom) at 20000x magnification after annealing 42

Figure 32: EDS scan of a random region on the surface of annealed Edmund Optics mirror at 1500x magnification 43

Figure 33: EDS scan showing various phases in the region shown in figure 21. The phase 1 shows Gold dominant region, phase 2 shows Silicon Oxide region which is the substrate and phase 3 shows Chromium rich region 44

Figure 34: EDS scan of a random region on the surface of annealed Edmund Optics mirror at 1500x magnification……. 45

Figure 35: EDS scan showing various phases in the region shown in figure 23. The phase 1 shows Gold dominant region while phase 2 shows Silicon Oxide region which is the substrate and the overlay 46

Figure 36: SWLI scan of Edmund Optics mirror before annealing 47

Figure 37: SWLI scan of Edmund Optics mirror after annealing 48

Figure 38: SWLI scan of Thor Laboratory mirror before annealing..... 49

Figure 39: SWLI scan of Thor Laboratory mirror after annealing 50

Figure 40: SWLI scan of Thor Laboratory mirror after annealing 50

Figure 41: Schematic of Vacuum Thermal Evaporator at Colorado Nanofabrication Lab, CU Boulder 53

Figure 42: Samples prepared at CNL – (2) 6% In/1000A^{o} Au before annealing (1) 6% In/1000A^{o} Au after annealing (4) 50% In/800A^{o} Au before annealing (3) 50% In/800A^{o} Au after annealing (6) 7.5% In/2000A^{o} Au before annealing (5) 7.5% In/2000A^{o} Au after annealing 55

Figure 43: Schematic of Gold film with Indium underlay (7.5% Indium under 2000A^{o} of Gold) 55

Figure 44: Plot of percentage reflectivity v/s wavelength (nm) for 50% Indium under 800A^{o} Gold sample in Visible Spectrum before and after annealing 56

Figure 45: Plot of percentage reflectivity v/s wavelength (nm) for 50% Indium under 800A^{o} Gold sample in Infrared Spectrum before and after annealing..... 57

Figure 46: Plot of percentage reflectivity v/s wavelength (nm) for 6% Indium under 1000A^{o} Gold sample in Infrared Spectrum before and after annealing..... 57

Figure 47: Plot of percentage reflectivity v/s wavelength (nm) for 6% Indium under 1000A^{o} Gold sample in Infrared Spectrum before and after annealing..... 58

Figure 48: Plot of percentage reflectivity v/s wavelength (nm) for 7.5% Indium under 2000A^{o} Gold sample in Infrared Spectrum before and after annealing 58

Figure 49: Plot of percentage reflectivity v/s wavelength (nm) for 7.5% Indium under 2000A^{o} Gold sample in Infrared Spectrum before and after annealing 59

Figure 50: Image of the sample with 50% Indium under 800A^{o} Gold film before annealing 60

Figure 51: Image of the sample with 50% Indium under 800A^{o} Gold film after annealing 61

Figure 52: Image of the sample with 6% Indium under 1000A^{o} Gold film before annealing 62

Figure 53: Image of the sample with 6% Indium under 1000A^{o} Gold film after annealing 63

Figure 54: Image of the sample with 7.5% Indium under 2000A^{o} Gold film before annealing 64

Figure 55: Image of the sample with 7.5% Indium under 2000A^{o}Gold film after annealing 65

Figure 56: (Top) SEM image of region scanned (Bottom four) EDS material map of sample with 50% Indium under 800A^{o} of Gold before annealing (Acc. Voltage: 15.0 kV) 66

Figure 57: EDS scan of sample with 50% Indium under 800A^{o} of Gold before annealing (Acc. Voltage: 15.0 kV)…… 67

Figure 58: (Top) SEM image of region scanned (Bottom four) EDS material map of sample with 50% Indium under 800A^{o} of Gold after annealing (Acc. Voltage: 15.0 kV) 68

Figure 59: EDS scan of sample with 50% Indium under 800A^{o} of Gold after annealing (Acc. Voltage: 15.0 kV) 69

Figure 60: (Top) SEM image of region scanned (Bottom two) EDS material map of sample with 6% Indium under 1000A^{o} of Gold before annealing (Acc. Voltage: 15.0 kV) 70

Figure 61: EDS scan of sample with 6% Indium under 1000A^{o} of Gold before annealing (Acc. Voltage: 15.0 kV) 71

Figure 62: (Top) SEM image of region scanned (Bottom four) EDS material map of sample with 6% Indium under 1000A^{o} of Gold after annealing (Acc. Voltage: 15.0 kV) 72

Figure 63: EDS scan of sample with 6% Indium under 1000A^{o} of Gold before annealing (Acc. Voltage: 15.0 kV) 73

Figure 64: (Top) SEM image of region scanned (Bottom two) EDS material map of sample with 7.5% Indium under 2000A^{o} of Gold before annealing (Acc. Voltage: 15.0 kV) 74

Figure 65: EDS scan of sample with 7.5% Indium under 2000A^{o} of Gold before annealing (Acc. Voltage: 15.0 kV) 75

Figure 66: (Top) SEM image of region scanned (Bottom three) EDS material map of sample with 7.5% Indium under 2000A^{o} of Gold after annealing (Acc. Voltage: 15.0 kV) 76

Figure 67: EDS scan of sample with 7.5% Indium under 2000A^{o} of Gold after annealing (Acc. Voltage: 15.0 kV) 77

Figure 68: Image of SWLI roughness measurement for samples with 50% Indium under 800 A^{o} Gold before annealing 78

Figure 69: Image of SWLI roughness measurement for samples with 50% Indium under 800 A^{o} Gold after annealing 79

Figure 70: Image of SWLI roughness measurement for samples with 6% Indium under 1000 A^{o} Gold before annealing..... 80

Figure 71: Image of SWLI roughness measurement for samples with 6% Indium under 1000 A^{o} Gold after annealing..... 81

Figure 72: Image of SWLI roughness measurement for samples with 7.5% Indium under 2000 A^{o} Gold before annealing..... 82

Figure 73: Image of SWLI roughness measurement for samples with 7.5% Indium under 2000 A^{o} Gold after annealing..... 83

Figure 74: Indium Gold Phase Diagram 84

CHAPTER 1: INTRODUCTION

1.1 Global Energy Picture

Today, the vast majority of the world's energy needs are met through fossil fuels viz. coal, natural gas, and petroleum. 64% percent of grid electricity in the world is produced from these three fuels, with coal alone constituting 43%. As per forecast by Energy Information Administration (EIA) use of coal in developing countries will continue to increase at a rate of 2% per year [1]. The abundance and low cost of coal makes it an economically attractive option to meet the world's burgeoning energy demand. However, pollutants and greenhouse gases make the likely scenario of future electricity production through coal environmentally questionable. Again, coal is not a renewable energy source. As it begins to exhaust, even this would not remain an economically viable option.

Since coal is mainly carbon, it has the highest greenhouse gas emissions per unit energy of all the major energy sources [1]. The overwhelming scientific consensus is that CO_2 from burning fossil fuels is contributing to global warming. This is expected to cause an increase in global average temperature, changes in precipitation patterns, decreases in global snow and ice cover, increases in natural disasters, and rise in sea levels drowning coastal areas [2]. Additional concerns related to coal 2 are the other pollutants emitted by coal plants, the safety of coal mines (especially in developing countries), and the impacts of coal mining on the environment.

All these concerns put together, give rise to the need of an energy source that is eco-friendly, everlasting, abundant and safe. Hydro and wind energy are abundant and eco-friendly but their inconsistency and poor predictability do not allow them to be the primary source. Other sources like geothermal energy are still in the cradles and are expected to take decades before they can be used on a commercial scale. Bio-fuels, although theoretically are abundant, they are not eco-friendly and are surrounded by controversies regarding its production against necessity of edible agricultural products. All these together point to the potential of solar energy, photovoltaic in particular as a solution.

1.2CdS/CdTe Solar Cells

The CdS/CdTe solar cells are attractive for harness of solar energy mainly due to their low cost. It has the lowest reported manufacturing cost per watt. It accounts for the majority of the photovoltaic production in the U.S., and it is the leading thin-film technology worldwide [3]. As shown in figure below, CdS/CdTe solar cells typically are made of a glass substrate, a TCO (Transparent Conducting Oxide) layer, n-type CdS and p-type CdTe semiconductor layers, and a metallic back contact.

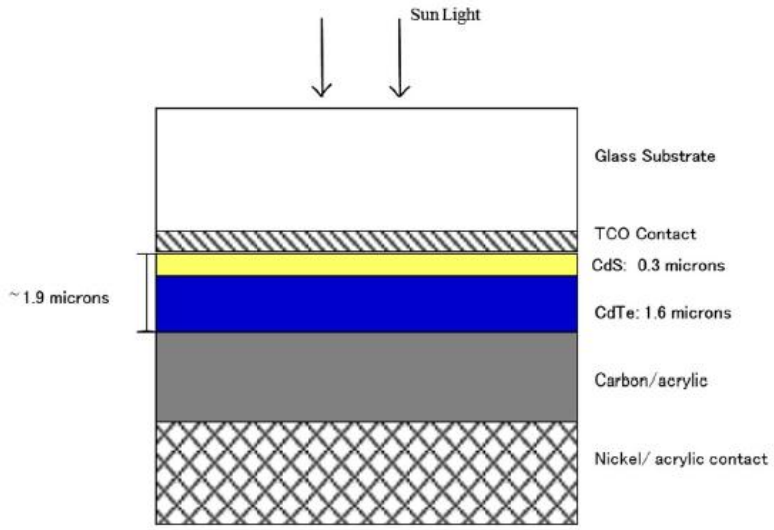

Figure 1: Schematic Device Structure (Not to Scale)

1.3 Manufacturing of CdS/CdTe Solar Cells

There are several steps involved in this process. The film sequence is such that the sun is positioned above the substrate and the light enters the module through the substrate glass that carries the transparent Conducting Oxide layer. Later CdS forms the n-type conductor film which is early transparent so as to allow the majority of the incoming light to the CdTe film underneath which acts as the p-type conductor film. The cheapest and the most commercially viable option for the substrate is float glass. The substrate temperature is kept between 400^{o}C and 620^{o}C at various stations. For the TCO layer a compromise has to be made between the maximum possible conduction and highest possible transmission of light. This layer must be so prepared that its transparency is maximum within the wavelength of light in which CdTe is most efficient and effective [4].

Most of the industrial methods for manufacturing CdTe/CdS solar panels involve thermal sublimation. An example of this is the Heated Pocket Deposition method. The apparatus for this method of manufacturing CdS/CdTe photovoltaic cells operates in a vacuum environment. The material thermally sublimes from a thermal sublimation source block and is deposited onto the substrate. The thermal sublimation source block is made such that it has a pocket where the lower surface holds an array of holes. These holes hold the deposition material. The graphite source is heated by radiation. Upon heating, the sublimation material sublimes from the surface of plug maintaining a constant surface area. This source block provides a spatially uniform thin film deposition rate across the lower surface of the substrate whose temperature is uniform[4].

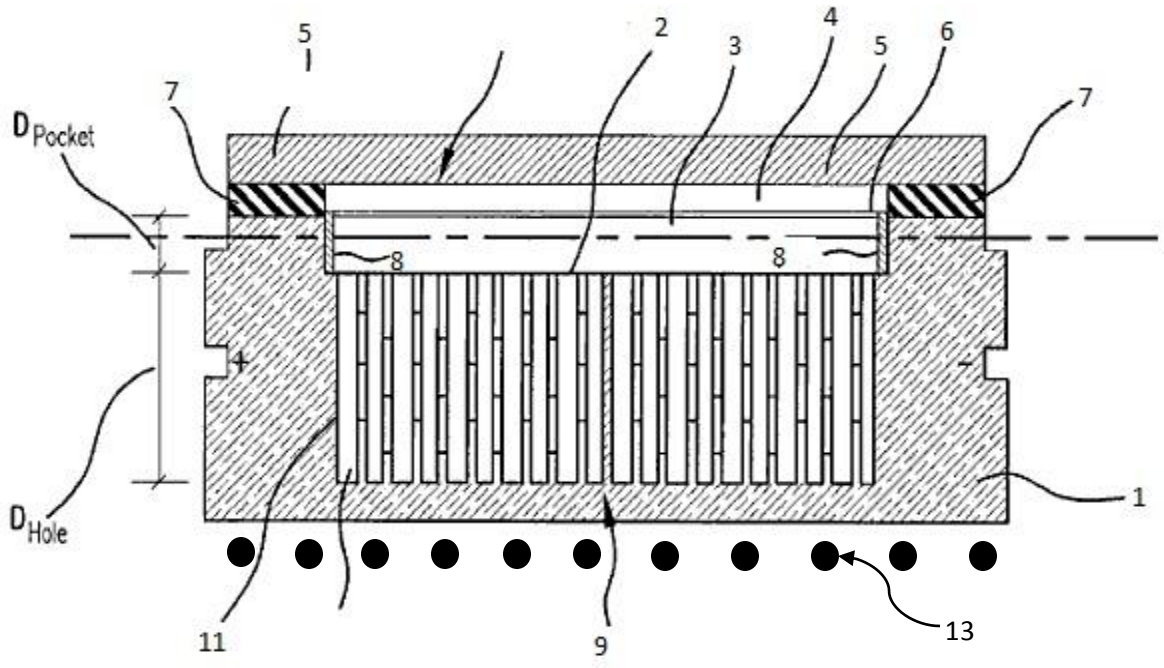

Figure 2: Partial cross sectional view of thermal sublimation source[4]

In the figure above:

1 Sublimation source block

2 Lower surface of pocket

3 Pocket

4 Separation distance

5 Substrate

6 Surface of substrate

7 Metal strip belts

8 Pocket walls

9 Array of holes

10 Hole (plug)

11 Inner surface of pocket

12 Lower surface of hole

13 Nichrome radiation heating coils

Process of manufacturing CdTe/CdS thin film photovoltaics involves several stages and various sub processes. Most of these processes are carried out under highly controlled atmosphere, environmental conditions, temperature and pressure. After acquiring the raw material for deposition the first in-house process is cleaning of the substrate and prepare for additional processing in vacuum. This includes ultrasonic cleaning of the substrate, rinsing with polar solvent including isopropyl alcohol, remove water from the surface of the substrate and drying in an environment similar to clear room. This substrate is soda lime glass with one side coated with TCO. The substrate is then transported into the vacuum chamber for processing through metal conveyer belts (as shown in figure above - 7) via an air-to-vacuum-to-air opening [4].

Within the vacuum environment, the substrate is heated to elevated temperature that is in the range of 500^{o}C to 560^{o}C. At this temperature CdS layer is deposited over the TCO layer and subsequently CdTe is deposited. After deposition of CdS and CdTe on the substrate, these layers are treated with $CdCl_2$ (Cadmium Chloride) to enhance the efficiency of the cell. During this treatment the temperature of the substrate is reduced and is maintained at a predetermined temperature between 300^{o}C and 500^{o}C. This process may be repeated several times within the vacuum chamber across various stations. Later the $CdCl_2$ is removed from the stake by annealing the layers between 400^{o}C and 450^{o}C. This completes the

$CdCl_2$ exposure process. Once this is done the substrate and film stack is cooled to a temperature between 20°C and 100°C to form an ohmic low-resistance contact on the surface of the CdTe layer [4].

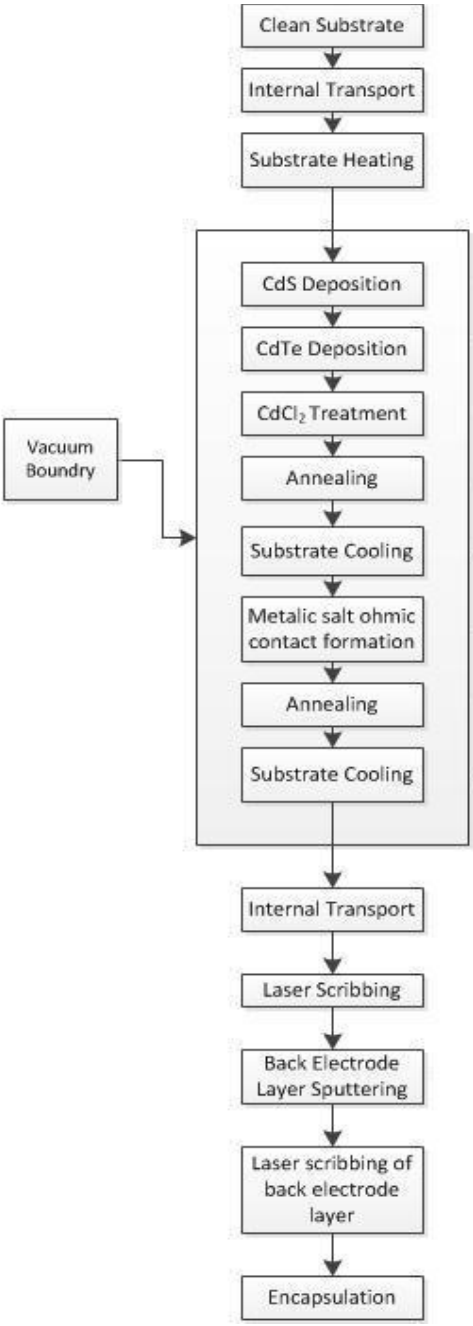

Figure 3: Flowchart of a process for manufacturing of CdTe/CdS photovoltaic module [4]

Many of the process steps involve radiation heating. At the end of these processes the module is cooled to a temperature between 25°C and 100°C in several steps and then the module is taken from the

vacuum chamber to the ambient atmosphere though another air-to-vacuum-to-air opening. As the next step, all the layers except the TCO layer are scribed in two steps using laser scribes. This operation may be performed outside the vacuum chamber. Later a conductive coating is applied onto the previously scribed carbon-containing coating to form a metallization layer. This coating may be Nickel (Ni), Molybdenum (Mo) or a combination of both with addition of other appropriate metals. Since the metallization takes place after scribing, the metal fills the space produced by the scribe. This produces an electrical connection between the back electrode of one cell and from electrode of another. In the next step is to form the third scribe through the layer of metallization. This process is applied to the metallization layer to complete an interconnection of individual photovoltaic module. This photovoltaic module is encapsulated in the next step to finish the process of manufacturing of the CdS/CdTe thin film solar module. These modules are now ready for installation [4].

CHAPTER 2: ADVANCED THERMAL RADIATION SHIELD

2.1 Motivation

The thermal sublimation source uses nichrome coils to heat the pocket for sublimation of CdTe and CdS on the substrate. These sublimation sources are made out of graphite and operate under a vacuum of about 40 millitorr. To maintain the desired temperature the source consumes over 10,000 KW of electricity for a vapor source for depositing on a 2' x 4' substrate (standard production size). The heat of sublimation for CdTe is given as 47.4 kcal/mol[5]. As per another source the heat of sublimation for CdTe is just under 58.3 kcal/mol[6]. One 2' x 4' module would contain 1.48 cc of CdTe. This is about 0.038 moles. The density is 6.2 g/cc., considering that each module takes 2 minutes for sublimation, there is a sublimation of 0.000317 moles/second. Based on these values and considering the heat of sublimation for CdTe has 47.4 kcal/mol, the actual required energy is only 63 watts [6]. This makes it clear that not even 0.01% of the heat input is actually being utilized for sublimation. A vast majority of the input energy is lost.

Since the source operates in a decent vacuum condition (typically, 40 millitorr), the heat lost due to conduction and convection is negligible. Under such condition the most prominent and active mode of heat loss is through radiation. If we can eliminate or substantially reduce this form of heat transfer we can reduce the consumption of energy to maintain the temperature of the system. Not only that, it would also improve the thermal uniformity of the system that will reduce the stress in the glass substrate caused due to temperature difference over the surface.

The initial concept of using thin film gold on quartz substrate was derived from similar use of Gold reflectors employed by companies like Fannon Products for their quartz infrared lamps. Another company Heraeus Noblelight also uses gold film reflectors for their infra-red heat lamps. These lamps are made for industrial heating and thin gold films on quartz substrate are used as reflectors to improve the effectiveness of these lamps and focus the heat as intended. This prompted this research to investigate the possibility and efficiency of such gold reflectors for thermal radiation shielding purpose.

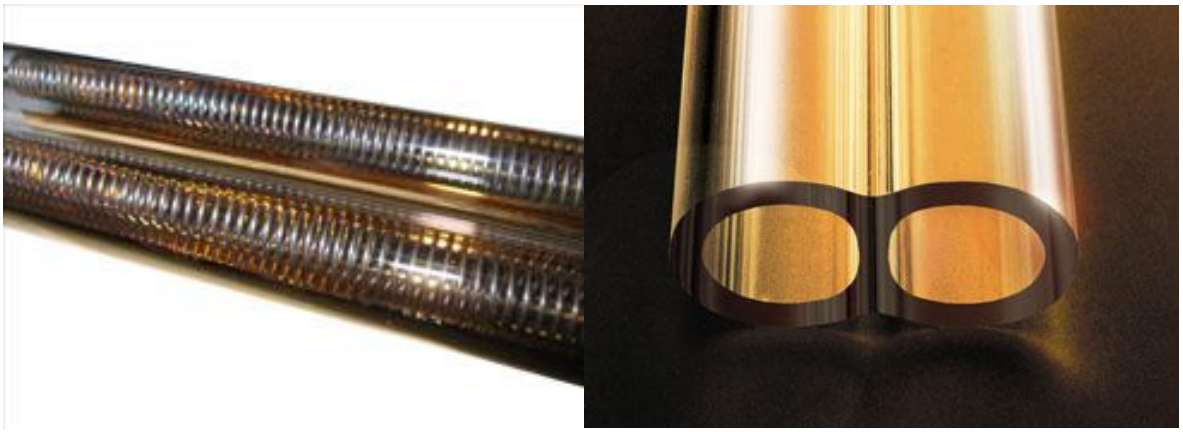

Figure 4:(Left) Goldenrod Medium-Wave Infrared Lamps from Fannon Products (Right) Heraeus Infrared Heaters Reflective tube

Further, it was necessary to utilize these shields in a form that would make these shields most effective. A conventional thermos flask design provided an example for this application. Since the entire process takes place in vacuum, a thermos flask design can be applied without the need of sophisticated pump setup to maintain vacuum between the two layers of the flask.

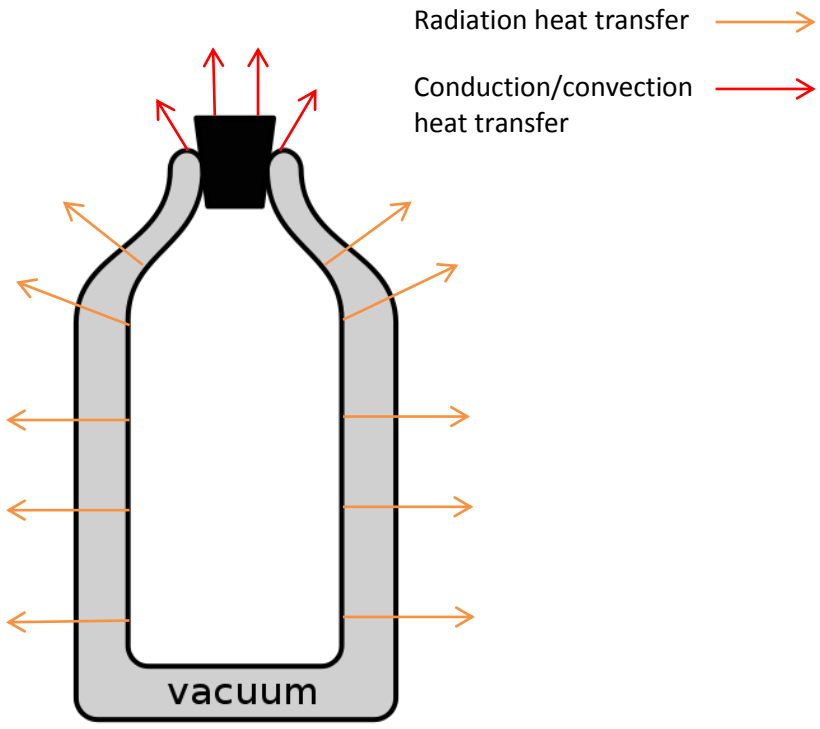

Figure 5: Principle heat losses from a vacuum flask

2.2 Basic Concept and Development

Based on the principles stated above and knowing the properties of metallic materials, investigation for appropriate design and optimum material was carried out. After initial literature search and applying some basic concepts of engineering the initial design for radiation shields was developed. Quartz was initially considered as an ideal substrate due to its near inert behavior at high temperatures and thin gold film as the reflective surface for its high reflectivity (nearly 97%) in the infra-red spectrum.

Later the need to reduce cost of these shields came into picture and so early investigation was performed using Pyrex glass. If the Pyrex glass failed, using of quartz instead would have been considered. However, using Pyrex would not only reduce cost but also availability of large transparent quartz sheets would be limited for the full scale industrial application.

Gold with quartz and later Pyrex was considered as an ideal combination due a couple of important reasons. First of all, quartz and gold are inert to each other. This means that even at elevated temperatures, there would be no reaction between them. It is important to have such a combination to ensure long and effective life of these shields. Also, other metallic substrates could not be used due to factors like heat transfer coefficient, tanning, oxidation, etc. having negative influence on the performance and life of the shields. Silicon based ceramic products like quartz, glass and Pyrex have great insulation properties and are also chemically as well as physically stable at very high temperatures which adds to the advantage.

Based on all the considerations and engineering principles a design that would supposedly be most effective was proposed. The efficiency and performance of these shields would be dependent of several other factors as we will see over the course of this text. Idea was to envelop the entire sublimation vapor source with two shields that have Pyrex as the substrate and coated with a fine thin film of gold that would act as the reflective surface. Pyrex would not only provide the base for gold deposition but has low thermal conductivity.

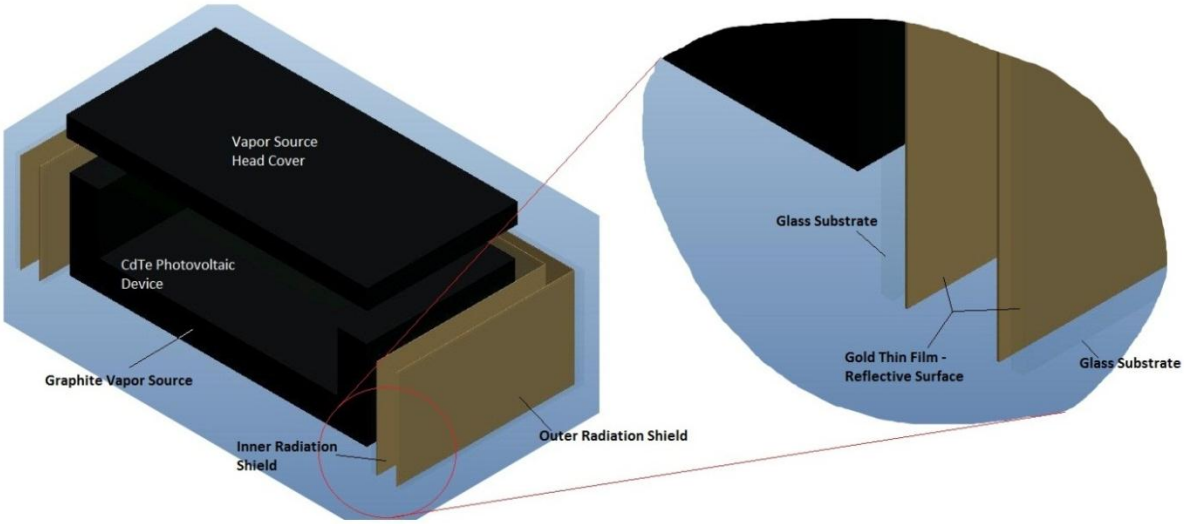

Figure 6: Schematic of the basic concept of Advanced Thermal Radiation Shield

The shields would be so arranged that the gold films would face each other similar to a conventional vacuum flask. The first shield will block a large amount of heat escaping the system and the second shield would further reduce the loss. The outside wall would, in this case, potentially be close to room temperature and most of the heat being list thought radiation would be conserved. Another idea was that if these shields were unable to perform as per expectation alone, adding one more layer of similar shields would provide ample shielding to conserve the energy. Moreover, if these shields had a long enough life, economically it would be a viable option. There were many other options and ideas that were discussed which will be explained in the next chapter along with their limitation proving this to be the best available option.

2.3 Advantages of Using Gold

The first question that would arise with use of gold would be regarding its cost. But the advantages of using gold for this kind of an application overshadow the cost factor to a large extent. Gold, although an expensive metal, has qualities and advantages that make it an important material not only for ornamental purpose but even industrial applications. However, a very small quantity of gold is needed to

create a thin film (less than 0.02 gm/m^2 sheet). High chemical stability, low vapor pressure and resistance to oxidation do not permit a huge loss of material over time. As a result, a film of gold can survive for long periods maintaining the properties that make it ideal for such applications.

Gold has several other advantages over other materials to be used as a reflector. It offers highest reflectivity in the infra-red spectrum of all materials. A thin film of gold on the back side of a quartz/glass forms an excellent industrial reflector. A precisely flat gold film will not only reflect majority of the infra-red radiation back but will also reduce scattering of radiation causing loss and heating of unwanted elements of the system. This not only increases the efficiency of system by conserving heat but also allows focusing of heat in the right direction of application. Gold has excellent malleability and ductility which allows it to be made into thin film or foils. This property is not too critical for application described here since the film is proposed to be deposited on the substrate using vacuum methods.

Taking a deeper look at the properties of gold from a quantative perspective creates greater interest in considering gold for such application. It has an emissivity (ε) of 0.02 to 0.03 depending on the luster of the polished surface, thickness of the film and the temperature at which the emissivity is measured. This means that out of all the incident radiation only 2% - 3% is absorbed by the material and the remaining is reflected back. The sublimation source that is being considered here operates close to a temperature of about 600^{o}C. At this temperature a film of gold that is 2 μm thick will have an emissivity of just under 0.03 (close to 0.028) [7]. This is close to ideal material for reflective application as compared to other materials like silver, steel, aluminum and platinum. For a film of platinum to act as efficiently as gold, its thickness would have to be over 4 times greater than the gold film giving similar performance [7]. The graph below shows a general comparison of a few materials that may be considered as good reflective materials. We can clearly see that in the infra-red region gold shows performance that is better than any other material.

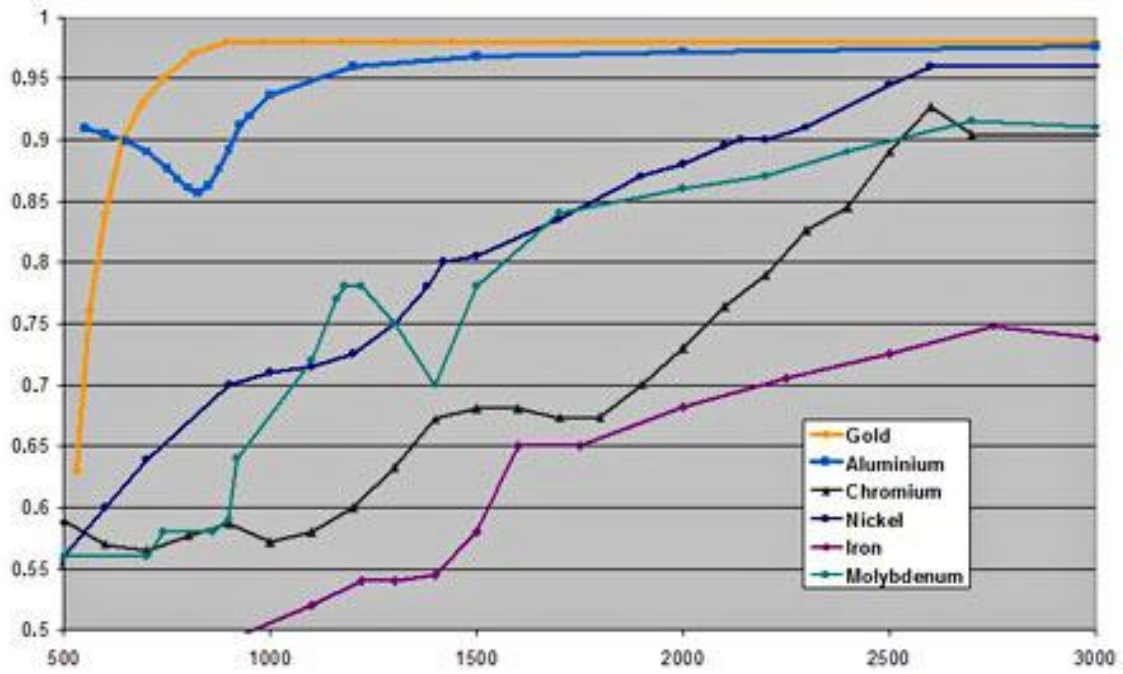

Figure 7: Reflectivity of various materials. The x-axis on this graph is wavelength of electromagnetic radiation is nanometers and the y-axis shows the proportion of incident light that is reflected back. (Courtesy – Heraeus Noblelight)[8]

This entire initial literature search provided enough evidence to consider gold as an excellent reflective material at high temperatures. It exhibited all the properties necessary for application as a reflector for infra-red radiation at high temperature. This included its chemical stability, high reflectivity, safe operation, ability to form uniform thin films, etc. There were no limitations that were evident at this stage that would act as a major road block in applying it for industrial application. Now it was necessary to validate the performance numerically and ensure that it was a good choice of material before getting into physical experimentation.

2.4 Final Validation Prior to Experimentation

Literature search clearly suggested that we were approaching the study on a correct path but it was necessary to validate the application mathematically. This was important to not only avoid expenditure over a wrong study but also for a systematic scientific approach. For this purpose, it is important to study and understand the concept of black body and black body radiation.

German physicist Gustav Robert Kirchhoff first gave the concept and coined the term *Blackbody Radiation* in the year 1860. A black body is an ideal physical body that would absorb all incident electromagnetic radiation irrespective of the frequency, angle of incidence or the wavelength. At thermal equilibrium such a body will emit electromagnetic radiation. This is called the black body radiation and according to Plank's Law it has a spectrum this is determined by only the temperature and the body's shape, composition or other physical factors have not effect. Such a body in thermal equilibrium is an ideal emitter. This means that it emits as much or more energy at all frequencies than any other body at the same temperature. It's another important property is that it is a diffuse emitter. This means that the energy emitted by such a body is radiated isotropically and is thus independent of direction [9]. According to Gustav Kirchhoff, 'the supposition that bodies can be imagined which, for infinitely small thicknesses, completely absorb all incident rays, and neither reflect nor transmit any shall be called bodies *perfectly black*, or, more briefly, *black bodies*.' Today an ideal black body is defined as the one that allows all incident radiation to pass into it and internally absorbs all of it with no energy getting transmitted through it and stands true for all wavelengths of electromagnetic radiation irrespective of the angle of incidence. Such a body is a perfect absorber of all incident radiation. In this modern definition, the term '*infinitely small thickness'* is dropped to expand the concept of an ideal black body [10].

A real material would emit energy at a fraction of the black body energy levels that is called emissivity. As per the definition of a black body, in thermal equilibrium a black body will have an emissivity of 1.0. That means 100% of the incident radiation will be absorbed and nothing be reflected back. Emissivity is usually denoted by the Greek alphabet ε. A body that has lower emissivity independent of frequency, wavelength and angle of incidence is called a gray body. An exact opposite of a black body is a white body and it is defined as the rough surface that reflects all incident radiation uniformly in all directions [9].

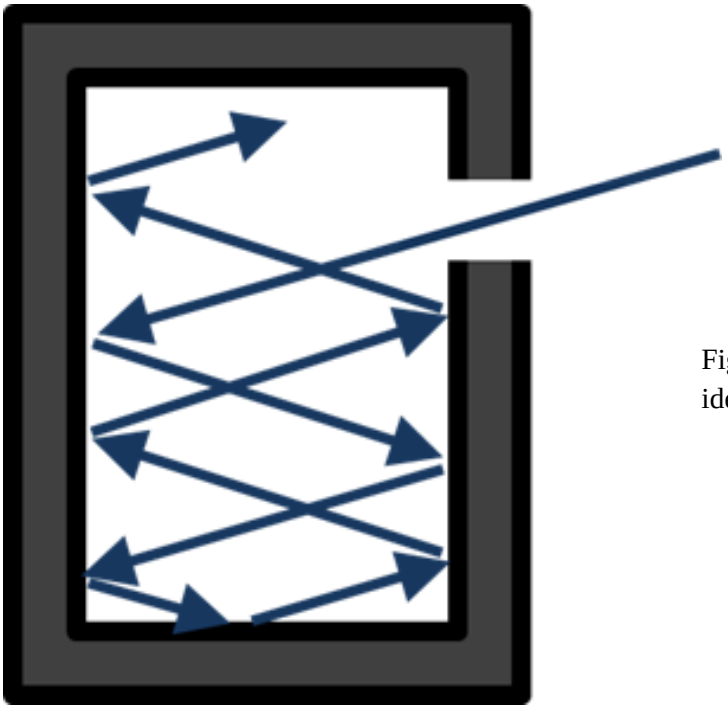

Figure 8: A close approximation of an ideal black body

Based on this concept, the emissivity of gold film varies between 0.02 and 0.03 as compared to that of a black body depending on the temperature and the thickness of the film. This also helps in calculating the wavelength of the radiation that would be applicable at a given temperature. Using this concept it was established that the radiation we would deal with a peak wavelength of about 3.0 µm and 80% of the wavelength would be under 7.0 µm at a temperature of 620^{o}C. This was calculated using Wien's Displacement Law[11]. According to Wien's Displacement Law:

Wavelength $\lambda = \frac{b}{T}$, where b is the Wien's Displacement constant which is equal to 2897768.551 nm.K and $T$is the absolute temperature of the emitting surface.

It was important to understand the performance of the gold film in this range of wavelength to find out its efficiency for the application we were looking at. It was also necessary to compare the performance of gold film radiation shield with other materials to understand the impact of this innovation. We decided to compare the performance with one of the most widely used materials for the purpose of thermal radiation shielding – steel plates.

Taking into consideration the temperature of 620°C for the sublimation source and the ambient temperature to be 25°C we found out that performance of one gold shield on quartz/Pyrex substrate was equivalent to 58 steel radiation shields. The conservation of heat with gold radiation shield can be seen in the figure below:

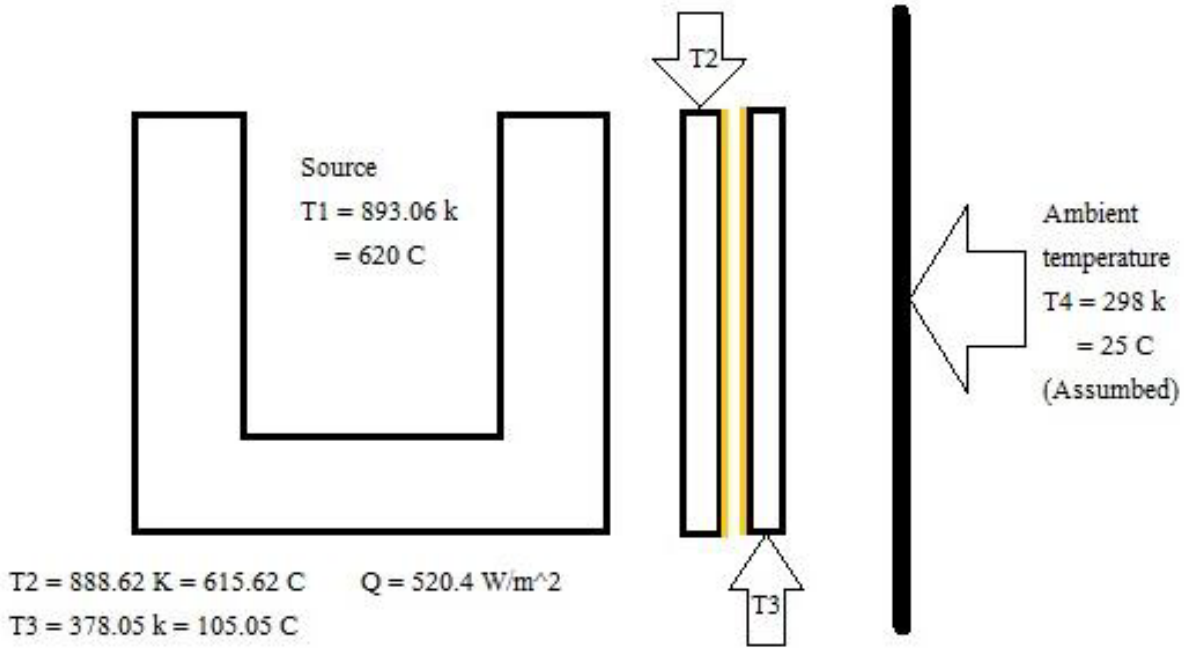

Figure 9: Conservation of heat using thin gold film on quartz/Pyrex substrate thermal radiation shields

Above stated values were calculated using the following equations and values:

$$\dot{Q} = \left(\frac{1-\varepsilon_1}{\varepsilon_1} + \frac{A_1 + A_2 - 2A_1F_{12}}{A_2 - A_1(F_{12})^2} + \left(\frac{1-\varepsilon_2}{\varepsilon_2} \right) \frac{A_1}{A_2} \right)^{-1} A_1 \sigma (T_1^4 - T_2^4)$$

Where,

Q = the heat of the system

ε_1 = Emissivity of emitting surface i.e. graphite source = 0.96

ε_2 = Emissivity of gold = 0.03

A_1 = Area of the emitting surface

A_2 = Area of the shield

$\frac{A1}{A2}$ = 1 (since both have the same surface area)

F_{12} = View factor that was taken as 0.9 [12]

$\sigma = 1.380653 \times 10^{-23}\ m^2\ kg\ s^{-2}\ K^{-1}$

Based on above stated calculations and study it was clear that it was a good option to be pursued for an industrial scale application. Appendix I shows the C program used for this calculation. Next step was to look for commercially available options and test them under extreme conditions. Before we look at the experimental procedure and results, it would be important to know other alternatives that were initially considered and their limitation that did not allow us to apply them. These alternatives and their drawbacks are discussed in the following chapters. In this chapter we will also look at the limitations of gold that must be overcome to use it for industrial scale application.

After looking at several commercially available thin film Gold mirrors, two samples were selected and acquired. These samples had to be tested and their performance evaluated before they could be used in an industrially viable setup. The following chapters describe the experimental approach, setup, results and evaluation to attain a good understanding of thin film Gold as an effective thermal radiation reflector.

CHAPTER 3: PROBLEM STATEMENT AND EXPERIMENTAL APPROACH

3.1 Early Approach and first Test Plan

Initially this project was aimed at designing of the radiation shields and optimizing the performance. The target was to optimize the parameters like film thickness for good reflectivity and best possible distance between successive films. But before getting into optimization of the design it was necessary to understand the effects of high temperature on the film of gold. Also, the time of each cycle was a major concern. Although gold is highly stable at high temperatures, exposing a metal to over 630^{o}C for 200 hour cycle might cause some changes.

It was decided to acquire thin film samples of Gold on quartz or Pyrex substrate. The first samples were ordered from Edmund Optics. These samples had a very thin film of gold on a substrate that was transparent quartz. The film thickness was not clearly known and the manufacturers were not willing to share the information. An approximate thickness of film was determined later to about 50 nm using White Light Interferometer and was confirmed using Ellipsometry that was performed by Jason Kepart at the CSUs Central Instrumentation facility.

3.2 Experimental Setup

For testing of this sample mirror, high temperature tube furnace was selected. This furnace has a metal body that holds a glass or ceramic tube in an inbuilt cylindrical channel. The channel is surrounded by heating coils that are in turn connected to an electronic controlled thermostat. The tube is insulated using a ceramic pipe or glass wool. For this experiment a quartz glass tube with glass wool insulation was used. The furnace control allowed various temperature and timer controls. Thus it was possible to control the temperature ramp up rate, length for which the temperature would be maintained and the cooling rate.

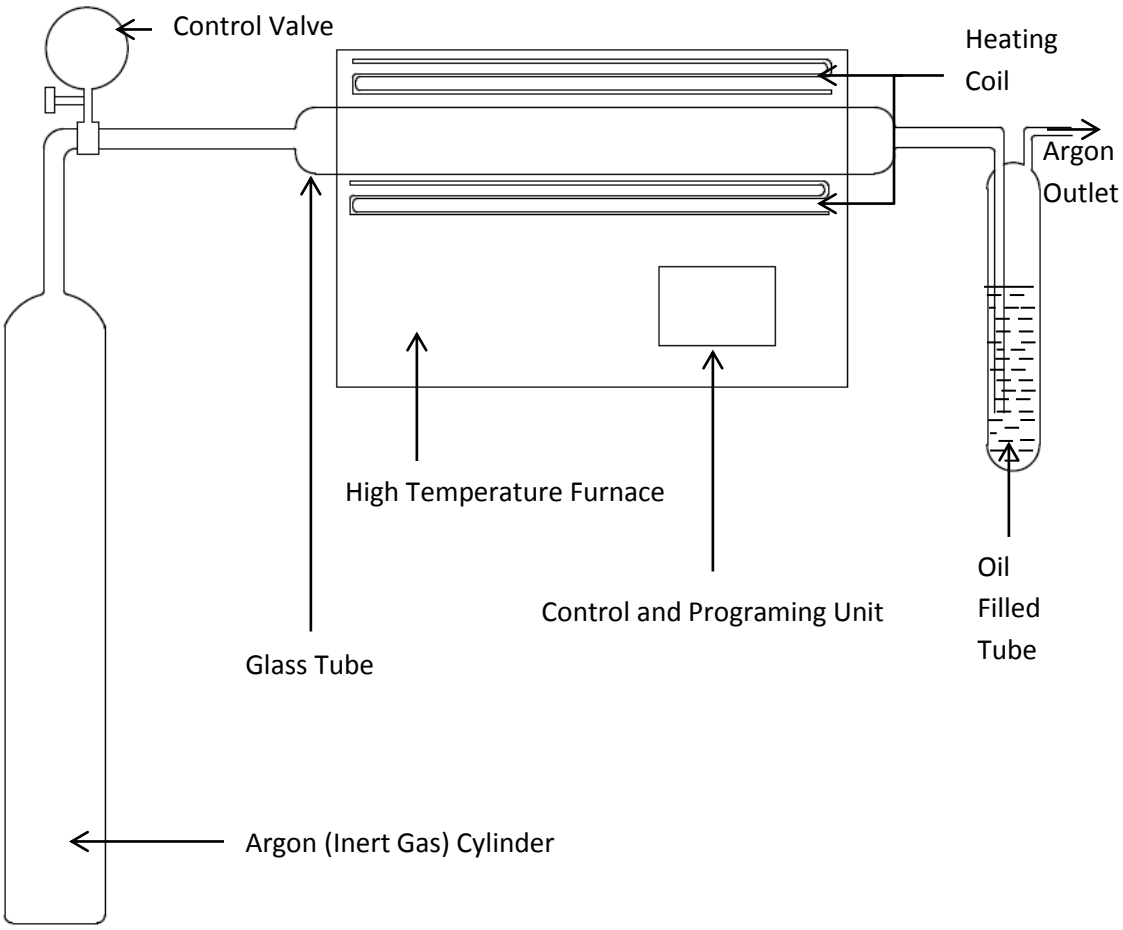

Figure 10: Schematic of Test Setup

Figure 11: High temperature tube furnace

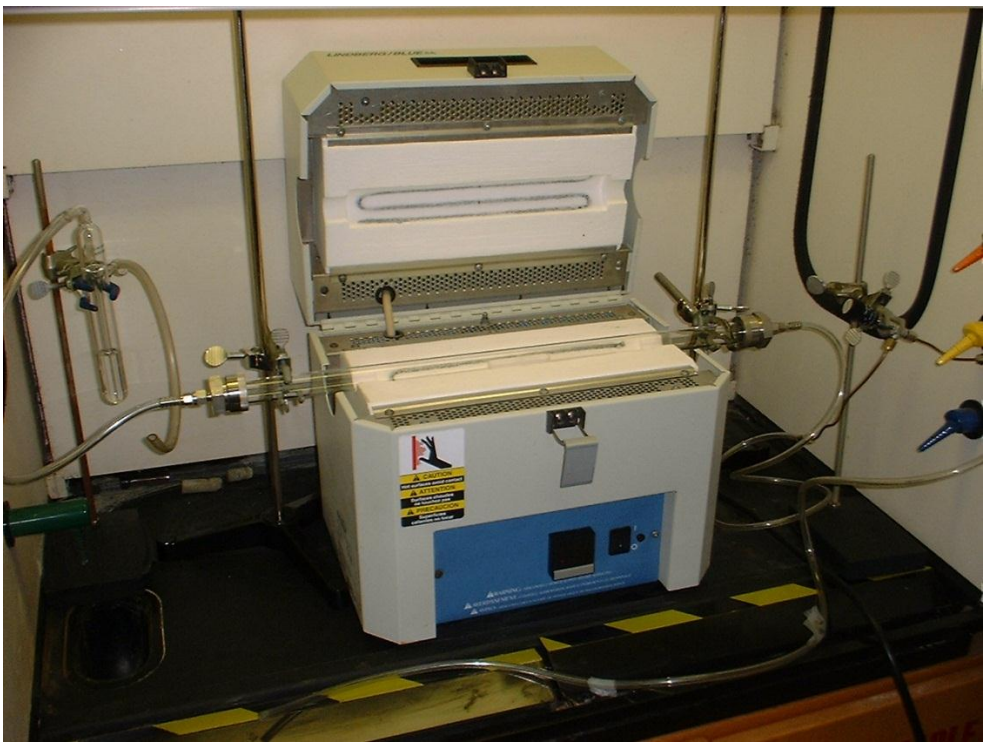

Figure 12: High temperature tube furnace showing interiors

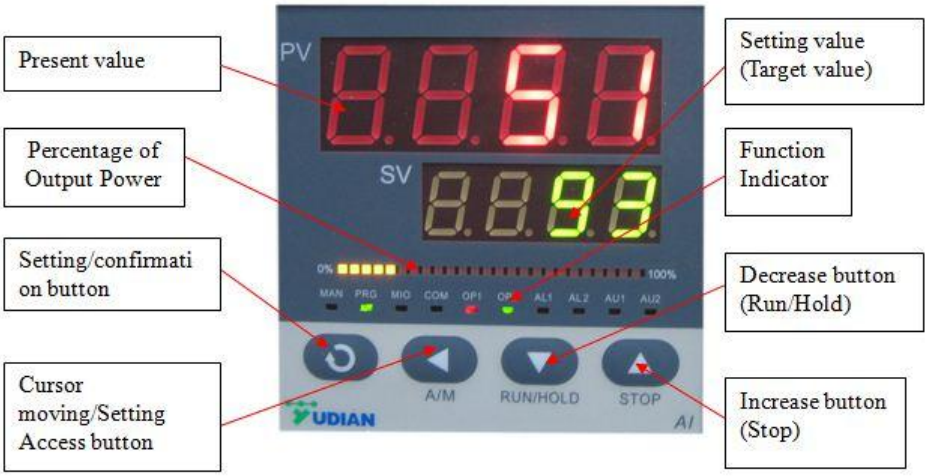

Figure 13: Typical programing and control unit with digital readout on a high temperature tube furnace

The actual shields would operate in vacuum and it would be important to simulate the conditions as close to actual operation as possible to estimate the effect of temperature on gold thin film mirror. For this purpose the furnace tube was flushed with argon gas to create an inert environment. This was done for several minutes before the heating cycle was initiated. The outlet end of the tube was extended into a test tube filled with high viscosity clear oil. The argon gas exiting the furnace tube was bubbled through this fluid. This serves a dual purpose. It helps to ensure that the argon gas is continuing to flow through the tube and keeps contaminant gases from entering the system from the outlet in case pressure of argon flowing reduces in the tube. The following figure shows the schematic of the test setup.

The sample gold film mirror was placed in the furnace on a ceramic plate. The temperature was ramped up at a very gradual rate of $3^{o}C$ per minute. At this rate it took the film and the internal environment about 3 hours and 30 minutes to reach the operating temperature of $620^{o}C$. As the argon gas continued to circulate through the furnace tube, this temperature was maintained for 200 hours which is the expected operating cycle time for this shielding mirror in actual operation. At the end of this 200 hours cycle, the furnace was programmed to shut down and allow the mirror to cool gradually at its own rate. Till the mirror reached room temperature again, argon circulation through the furnace tube was continued.

CHAPTER 4: MATERIAL ASPECT OF THE SHIELDS AND POTENTIAL SOLUTIONS

4.1 Overview of the Problem from Materials Perspective

Based on the literature search and preliminary mathematical evaluation, it was clear that thin film gold reflector was the best available option for application in a thermal sublimation source. However, literature search also revealed a very critical limitation to the use of these gold films. Although, chemically very stable even at high temperatures, physical phenomenon called thermal grooving caused by surface diffusion limits the use thin film of gold at high temperature[13]. This initially begins with formation of fine pin holes. Further, as the gases trapped between the film and the substrate begins to expand, they cause the film to burst and form larger holes. This is caused by problem with poor adhesion between the film and the substrate. When the temperature is further elevated, grain boundary grooving comes into picture which renders the film completely ineffective for application like reflector[13].

Physical deformation begins to take place at a fairly low temperature. Mean grain size starts increasing during moderate annealing of about 190^{o}C. This mean increase is from 0.2 µm to 0.5 µm as it is annealed in this temperature range [13]. Continuing annealing for upto 30 days at such temperature, pin holes start appearing which have an average size of 1 µm which are visible in optical microscope by transmitted visible light. Grain boundary grooving becomes prominent when the film is exposed to temperature of 340^{o}C for a period of 1 hour. This eventually leads to hole formation at 560^{o}C [13]. At about this temperature large bubbles, which are believed to be formed due to bursting of gases trapped between the film and substrate, begin to burst forming large holes. This blistering can form holes that can be as large as 20 µm in size [13]. As can be seen in the set of micrographs in figure 14, as temperature and exposure time increases there is a significant increase in film deformation. Formation of blisters is mostly because gold is insufficiently adhered to the surface of the substrate. While the film is being deposited some gases are trapped between the layers of the material since the film does not uniformly deposit and develop on the surface at once.

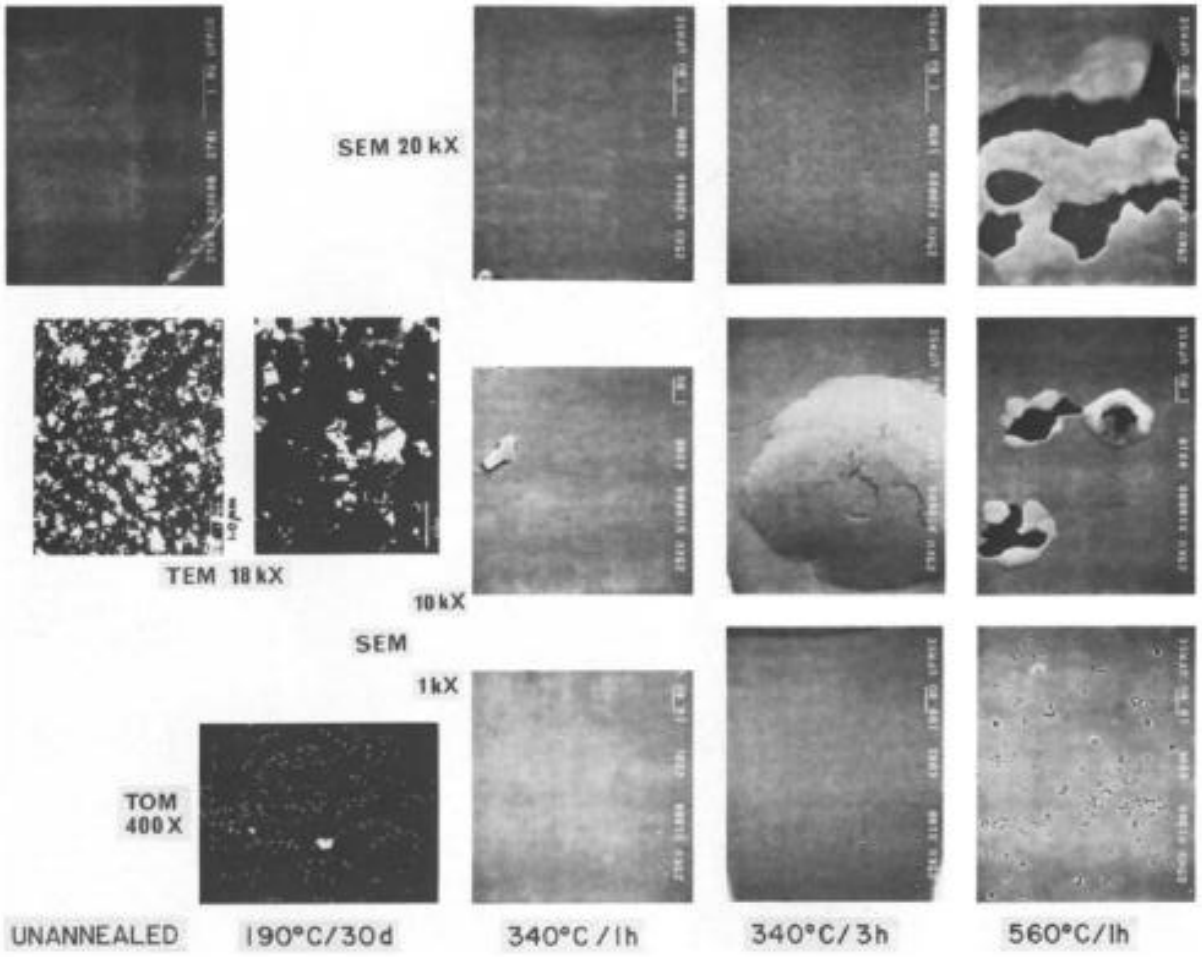

Figure 14: Micrographs of gold film exposed to various temperatures and time. Magnification increases from bottom to top [13].

This phenomenon of thermal grooving is quite common in metal thin films and is formally called island formation. It is called so due to the film breaking down to form island like structures on sufficient annealing. This has been observed in several other metals like aluminum, copper, silver, etc. Metal thin films show thermal grooving just before grain separation. If heating is further continued the grains separate at grain boundaries and agglomeration occurs [14]. Agglomeration is the phenomenon of creation of jumbled clusters or mass of varied parts. This occurs due to surface diffusion of thin films and difference in surface energies that act as the driving force. Island formation does not only occur at high temperatures. If a film is exposed to a comparatively lower temperature for a long time interval, the holes

that are formed expand and grow to break down the film. But the conditions that the gold thin films are to be exposed for reflector application, grain boundary grooving is the factor responsible for agglomeration.

It was now necessary to investigate the possible solutions to this so as to ensure that gold films would survive the temperature and exposure time. It must not only maintain the surface composure and consistency but also have good reflectivity before, after and during the exposure. There were several methods that were investigated but most of them had some kind of limitation that was not acceptable for our application. Ultimately, using an underlay of Indium, thus doping the gold film with a softer metal was found to be a good solution. All these possible solutions and their possible effects are discussed in further in this chapter.

4.2 Possible Solutions

There are several possible solutions that may be applied to avoid the problem of thermal grooving and the grain boundary separation that results from it. Some of the attempts made by other investigators in the past were analyzed. Most of them didn't meet the necessary parameters since it is not usual to utilize thin gold films for such high temperature application. Following are the solutions that were investigated:

- Using thicker gold films
- Using silicon oxide overlay
- Doping with sodium
- Doping with tin
- Doping with chromium
- Doping with indium

4.3 Review of All Possible Solution

In the following section we will look at the solutions that were investigated to avoid thermal grooving and island formation.

4.3.1 Using thicker gold films

The initial idea that first struck was to use thicker films of gold since that would require greater activation energy than the thin gold films to undergo grain boundary separation. In this case, it would have to be more like a foil of gold than a film. This would not only increase the cost exponentially but also require an entirely new set of study. This is because failure mechanisms in a plate of gold would defer from that in the case of film of gold.

4.3.2 Using silicon oxide overlay

Using a silicon oxide overlay is like sandwiching the gold film between a thick substrate of Pyrex or quartz and a thin superstrate of silicon oxide. It was supposed that the film of silicon oxide would hold the film together and keep it from undergoing deformation. Moreover, SiO has an emissivity in the infrared spectrum on a higher side (0.7 to 0.8).

A commercially available product was found to have the same characteristics and structure. A sample of this was acquired and a test plan was developed. The test details and the analysis is discussed at length in a later chapter.

4.3.3 Doping with Tin (Tin underlay)

Based on a publication that described the influence of thin layer of Tin underlay on stability of gold thin films, it appeared to be a good option to investigate. However, the details reveled that Tin sandwiched between Gold and SiO_2 substrate shows stabilizing effect due to SnO_2 formation on the free surface that prevents hillock and hole formation to minimize grain growth during isothermal annealing. However, this appears to be effective only between narrow temperature ranges of 300^{o}C to 500^{o}C. Our application was well 120^{o}C above this and so consideration of this as an option was eliminated[15].

4.3.4 Doping with other metals

Literature review was also carried out to investigate the effect of other metals like Copper, Vanadium and Titanium underlays on stability of gold films after isothermal annealing. Literature reveled that all these various films have a significant effect on stability of gold films up to the temperature of 500^{o}C after 1 hour of exposure. The Au/Cu composite films did not show great advantage in preventing hole formation in gold film. On the other hand Au/V and Au/Ti were insignificant to resist hillock formation. This is caused by an interplay between stress relaxation, capillarity force and oxidation behavior of underlay metals[16].Moreover, no study was found which suggested that these underlays play a prominent role in gold film stability at further elevated temperatures or for longer annealing times. Therefore these underlays were not considered as possible solutions.

4.3.5 Doping with Chromium (Chromium underlay)

In thin film Gold mirrors produced industrially mostly Chromium underlay is used as an adhesive sandwich layer between the SiO_2 substrate and Gold film. Chromium thus was expected to be more effective against island, hole and hillock formation than other options considered so far. For this purpose mirror samples were ordered from Edmund Optics that had an underlay of Chromium and was put under test. Details of the test result will be explained in the following chapters.

4.3.6 Doping with Indium (Indium Underlay)

As per the literature reviewed, Gold films with Indium underlays were the only ones that were successfully tested at temperature in excess of 500^{o}C. Experiments were conducted by R. E. Hummel *et al.* where 6% wt underlay of Indium was used for thin film of Gold. Observations showed no significant grain size growth or grain boundary grooving after annealing at 560^{o}C for 1 hour. Also, no pin holes were observed after heat treatment. This study did not measure the optical properties.

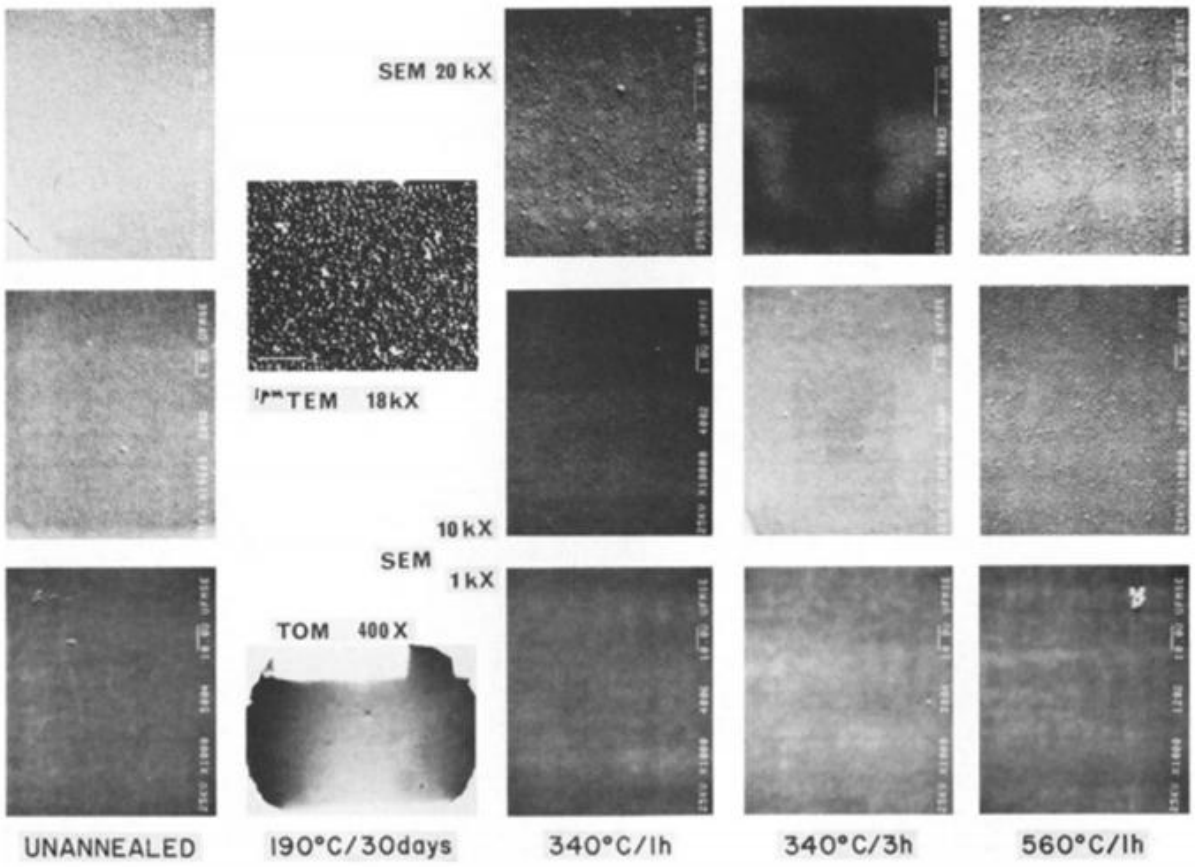

Figure 15: Micrographs of gold film doped with Indium exposed to various temperatures and time. Magnification increases from bottom to top[13].

CHAPTER 5: ANALYTICAL TECHNIQUES FOR GOLD FILM CHARACTERIZATION

5.1 Overview

Scanning Electron Microscope and White Light Interferometer was used to find out the film thickness and the mean surface roughness. Energy Dispersive X-ray Spectroscopy was used to understand the distribution of material on the film and UV spectrometer was used to measure the reflectance of the films in visible and infrared spectrum.

5.2 Scanning Electron Microscope Imaging

Scanning Electron Microscope or more popularly called SEM is an imaging and analysis method used for characterization of bulk specimens. It is among the most important and widely used electron-optical instrument used to investigate bulk specimen with 1 KeV to 50 KeV electron beam[17].

5.2.1 Principle and Operation

Electrons from a cathode electron source are accelerated by a voltage difference between cathode and anode that may be between 0.1 KeV to 50 KeV[18]. Primarily three kinds of cathodes are used to generate the electron beam – thermionic source, Schottky and field emission cathodes. Thermionic electron source is the most robust, economical and primitive kind of electron source that doesn't require ultra-high vacuum[19]. Another widely used material for such a source is Lanthanum Hexaboride (LaB_6)[20].A Schottky cathode is the predominant electron source technology used in present times for electron beam equipment. The only drawback is that it requires 4 orders high vacuum than a thermionic source to operate in[20].

An electron probe of 1-2 nm and 5-10 nm can be obtained for 20 KeV using a field emission or a thermionic source respectively. Smallest cross section of the electron beam by two or three electromagnetic lenses is used for demagnification. The electron probe scans the region of the specimen

through a raster scan. The recorded signals of secondary electrons (SE), back-scattered electrons (BSE) or specimen current (SC) are displayed on a Cathode Ray Tube (CRT) that is rastered in synchronization with the scanning probe[17].

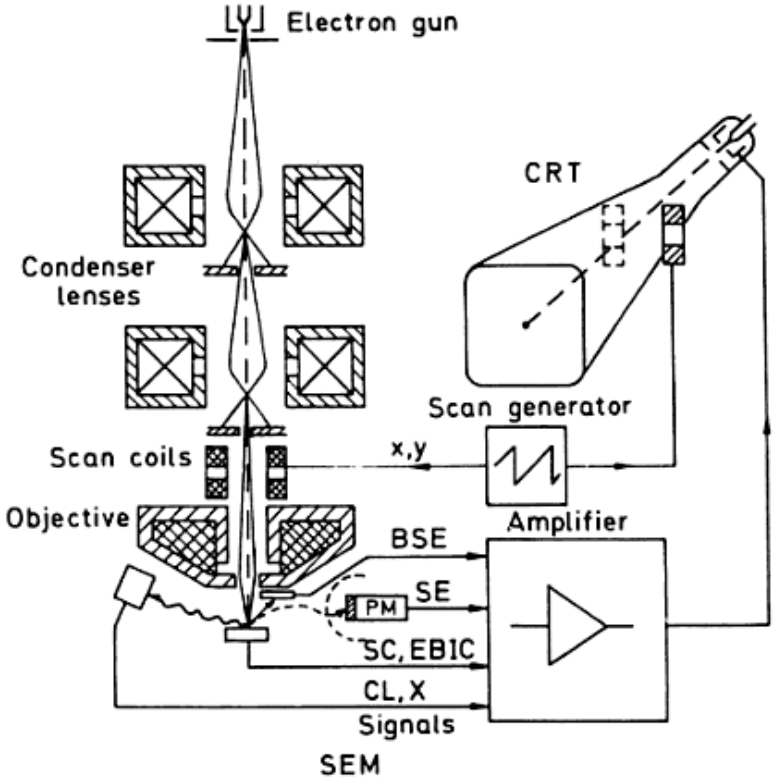

Figure 16: Schematic cross-section of a Scanning Electron Microscope[17]

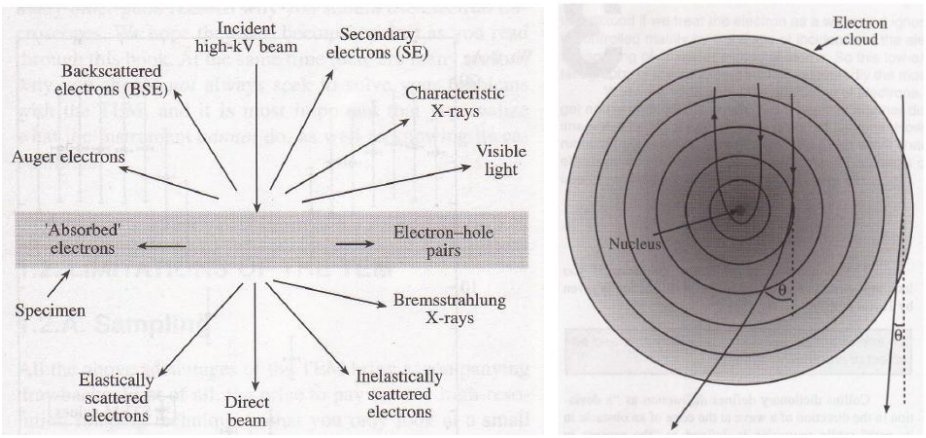

Figure 17: (Left) species of characteristic radiation availed from the specimen surface (right) mechanism of back-scatter electron generation

Some electrons from the incident beam interact with the specimen in which the energy is transferred to the atoms that cause the loosely bound outer electrons. The outer shell electrons of the specimen gain some energy but it is so low that only the electrons that escape from atoms extremely close to the surface can emerge and be detected. These are secondary electrons and are used for surface morphology. Some other beam electrons get defected so much due to the columbic interactions with the atom or to be more precise with the nucleus of the atoms that they emerge back from the surface. These are called Back-scatter electrons. The number of such electrons is directly proportional to the atomic number (Z) of the atoms in the specimen. Back-scatter electrons are useful in material characterization of the specimen but are not very useful to understand the surface morphology of the specimen[21]. There are many other signals that are generated some of which would be overviewed in the later part of this chapter.

5.3 Energy-Dispersion X-ray Spectroscopy

Energy-Dispersive X-ray Spectroscopy, popularly known as EDS, EDX or EDAX is an analytical technique used for elemental analysis or chemical characterization of known or unknown specimen. It utilizes the x-ray generated by interactions between the electrons of the specimen atom with the incident electron beam. It normally operates with an electron microscope and an x-ray detection coupled with a Multi-Channel Analyzer makes it an extremely powerful tool for material characterization.

An EDS system works on Bohr's atomic model for elemental analysis. An atom, according to Bohr's model has K, L and M shells that are associated with the energy level of the electron present in the atom. When an electron beam strikes the atom an electron from the first shell i.e. the K shell is knocked out. As a result of this, an electron from the next energy level which is the L shell, drops to the lower shell to stabilize that shell. But as this electron drops to a shell with lower energy level, the electron must release the excess energy that it possesses while it was in the higher shell. This energy is released in the form of x-rays and is unique for each shell of every element. The wavelength of the x-ray generated is a

function of the energy dispersed. This wavelength is absorbed by a detector that is used to characterize the elemental composition. Same principles apply to other higher shells.

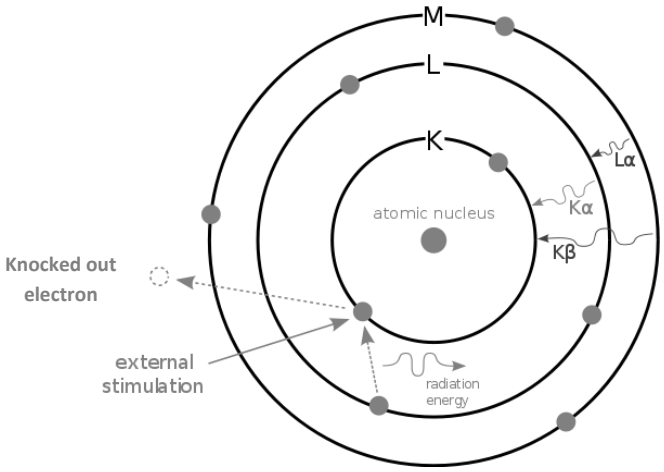

Figure 18: Bohr's model and mechanism of release of radiation during EDS analysis

The figure below shows how a standard EDS result appears. The Kα, Kβ, Lα, etc. show the energies associated with the drop of electron from each shell. For example, Kα shows that it is the energy released when an electron falls to the K shell from the next shell which is L shell. If the electron reached the K shell from a shell that is 2 energy levels higher it would be called Kβ.

In spite of this being an excellent technique for elemental analysis, like all other techniques, even this has some limitations. Energy dispersive X-ray spectroscopy cannot detect and thus cannot give a quantitative analysis of Hydrogen and Helium. The reason being that these 2 elements have only one K shell and therefore if one electron is knocked out of the shell there is no electron in a higher shell to replace it. Thus there would be no energy release in form of X-ray that can be detected.

The samples were analyzed using scanning electron microscopy (SEM) JEOL JSM 6500F field emission microscope equipped with a Thermo Noran energy-dispersive spectrophotometer (EDS) [22].

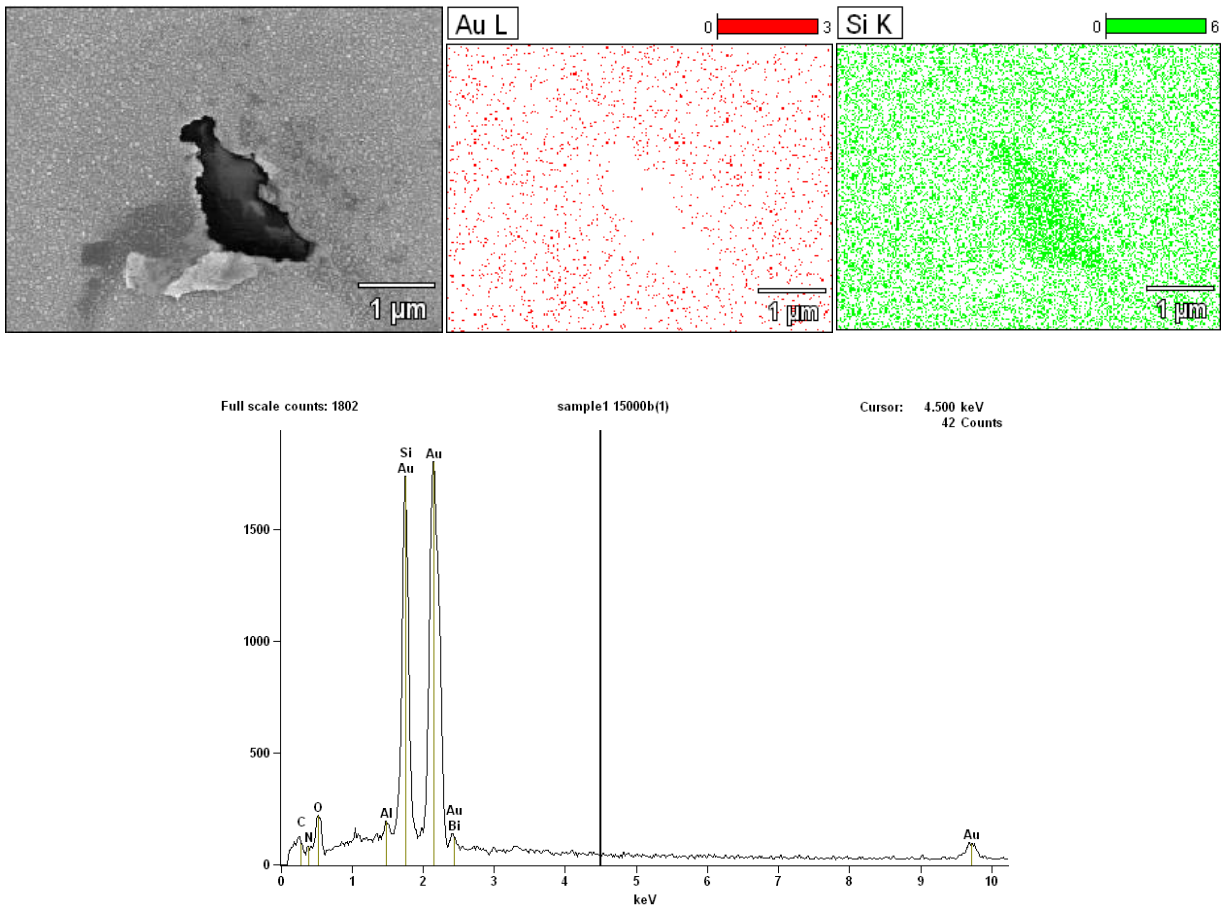

Figure 19: A typical EDS scan for an unknown Gold thin film sample on SiO substrate containing traces of Aluminum and Bismuth.

5.4 Scanning White Light Interferometer

A Scanning White Light Interferometer (SWLI)SWLI, also called coherence scanning interferometry (CSI) by the International Standards Organization (ISO), is a device for measuring the physical geometrical (3D) characteristics of an object using broad band white light . Fourier analysis (and other methods) are used to convert interference intensity data (fringes) to the spatial frequency domain, allowing production of an extremely accurate surface map captures intensity data at a series of positions along the vertical axis determining where the surface is located by using the shape of the white-light interferogram. The white light interferogram actually consists of the superposition of fringes generated by multiple wavelengths, obtaining peak fringe contrast as a function of scan position. In a SWLI system, an

imaging interferometer is vertically scanned to vary the optical path difference resulting in a series of interference patterns formed at each pixel in the instrument field of view. The data are stored digitally and processed in a variety of ways to produce Area (3D) results [23].

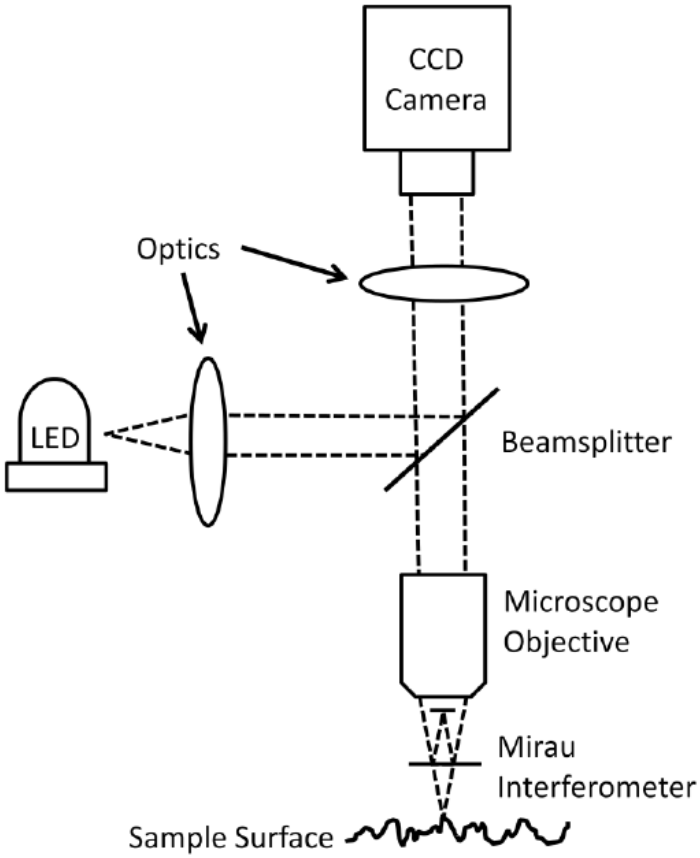

Figure 20: Schematic layout of a typical Scanning White Light Interferometer

A Charge-Couple Device (CCD) camera captures these fringes for software analysis. Several frames of intensity information for each point are obtained using which the software recreates the surface. The frames are then passed through an algorithm to convert these signals into height information. These kinds of microscope based white light interferometers are capable of measuring several types of surfaces ranging from ground and polished surfaces to steps and films[24].

Figure 21: Standard laboratory setup of a Scanning White Light Interferometer

The instrument used for this study was a Zygo, Scanning White Light Interferometer, Model 7300. The vertical (z) resolution is <1 Angstrom and the later resolution is dependent on the field of view and camera size. A 640 x 480 pixel camera was used.

5.5 UV-VIS-IR Spectrometer:

Spectrometer from CSU PV lab was used to measure the reflectance of the gold films in visible and infrared spectrum. This spectrometer has light input to cover a wide spectral range from visible and infrared wavelength. The light is then filtered through a high resolution monochromator before entering the sample chamber that is set for thin film samples. A highly sensitive PMT detector and an amplifier detect and amplify the signals that are collected by a computerized data acquisition system.

CHAPTER 6: TEST AND ANALYSIS OF MIRROR SAMPLES FROM OPTICAL COMPONENT MANUFACTURERS

6.1 Overview

There were various possible solutions to avoid problems associated with thermal grooving and island formation. The first two solutions that were tested were Gold film with Chromium underlay and Gold film with SiO overlay. The samples of Gold film with Chromium underlay were acquired from Edmund Optics while the ones with SiO overlay were ordered from Thor laboratories. These samples were tested using a High Temperature Tube Furnace as described in Chapter 3. After the test the samples were analyzed. Analysis included understanding surface morphology using SEM, qualitative material analysis using EDS, surface roughness measurement using SWLI and reflectivity measurement using spectrometer.

6.2 Visual Inspection

On visual inspection, these samples from Edmund Optics and Thor Laboratory had an extraordinarily flat surface with great reflectivity. They were completely spotless and had no visible texture. The images below show the surface of these samples before and after they were tested through the heating cycle.

The Edmund Optics shows a clear deformation after the sample went through an annealing cycle of 200 hours at 620^{o}C. The black lines visible on the sample before the test are from a paper that was kept in front of the mirror. The purpose of this paper was to ensure that the reflection of the lines would make the visual reflectivity of the surface clearer. As it can be noticed here that the mirror had very good reflectivity before the test but after the heating, the film broke down and completely lost the reflective characteristics.

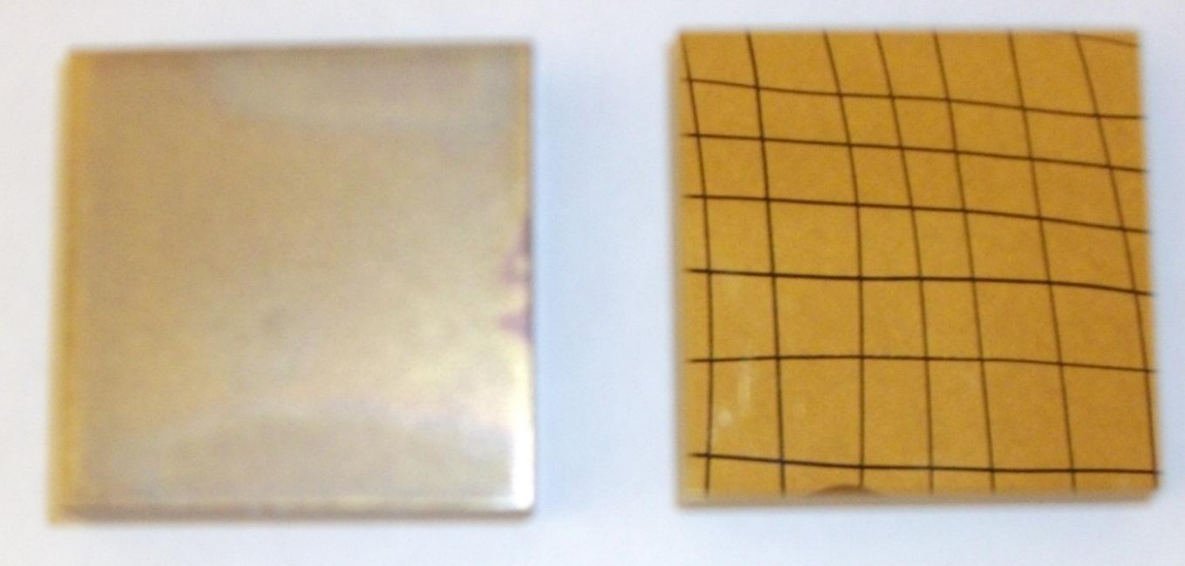

Figure 22: Mirror samples from Edmund Optics: to the left is the image of the sample after test and to the right is the one before test. The black lines visible on the mirror are from a piece of paper that was placed in front of the mirror while taking this picture. Its purpose is to clearly show the difference in reflectivity of Gold mirror before and after testing. Noticeable is the fact that no reflection is seen after heating the mirror.

The images in figure 23 show reflectivity of samples from Thor Laboratories that had an overlay of SiO on top of Gold film. Thing to be noted here is that these samples originally appeared very similar to the Gold mirrors from Edmund Optics. They had to be sputtered with Graphite to avoid charging while performing SEM and EDS scan.

Looking at these samples we notice that the consistency of the film was maintained after the test. However, there were some patches on the surface that were created after annealing them. These patches required some attention and were analyzed using other methods. There was not much that could be determined by just visual inspection of these mirrors. Although, the film retaining consistency did give a reason to be optimistic but at the same time unusual patches on the surface did raise some questions.

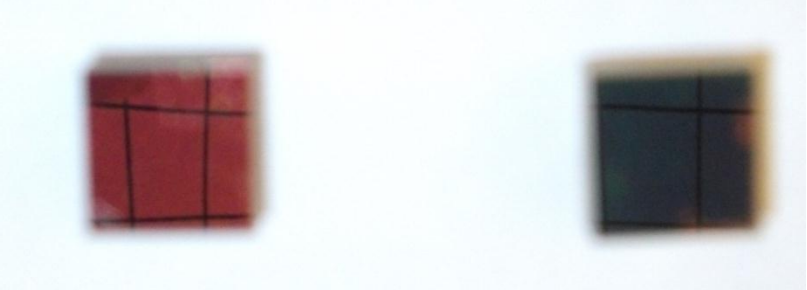

Figure 23: Mirror samples from Thor laboratory: to the left is the image of the sample after test and to the right is the one before test.

6.3 Reflectivity Measurements using Spectrometer:

After running the high temperature annealing test for 200 hours and visually inspecting the samples, reflectivity of the mirrors in Visible and Infrared spectrum were measured. Reflectivity of the mirror before and after the test was the metric, based on which the performance of the mirrors could be evaluated. Following graphical plots represent the reflectivity of these mirrors in both visible and infrared spectrums.

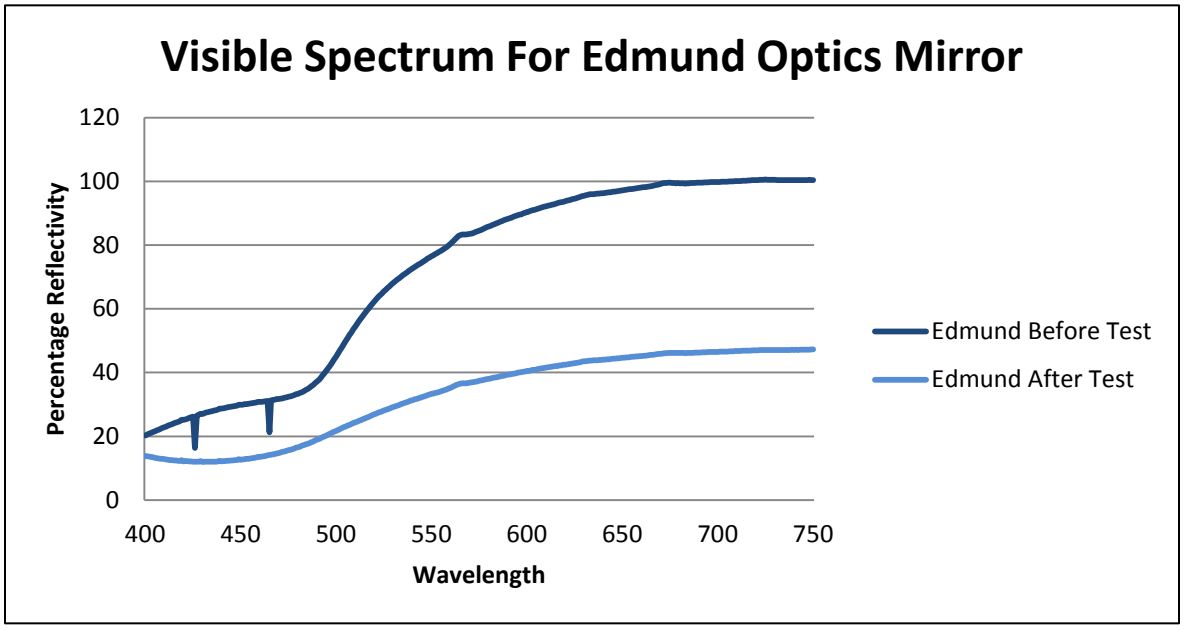

Figure 24: Plot of percentage reflectivity v/s wavelength (nm) for Edmund Optics sample in Visible Spectrum before and after annealing

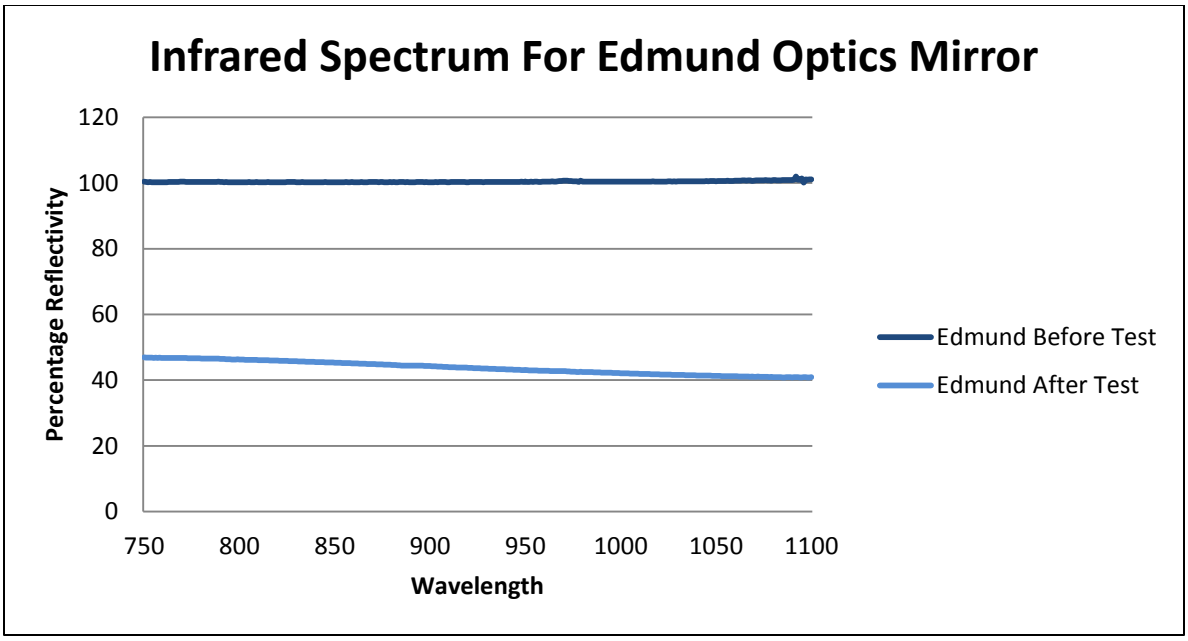

Figure 25: Plot of percentage reflectivity v/s wavelength (nm) for Edmund Optics sample in Infrared Spectrum before and after annealing

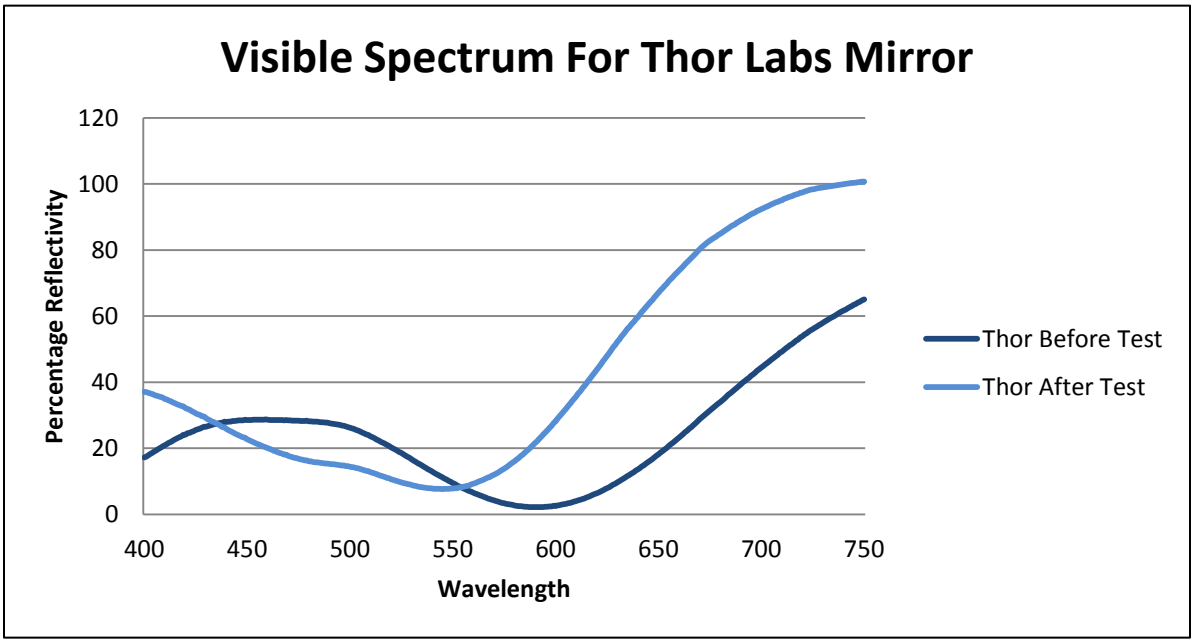

Figure 26: Plot of percentage reflectivity v/s wavelength (nm) for Thor Labs sample in Visible Spectrum before and after annealing

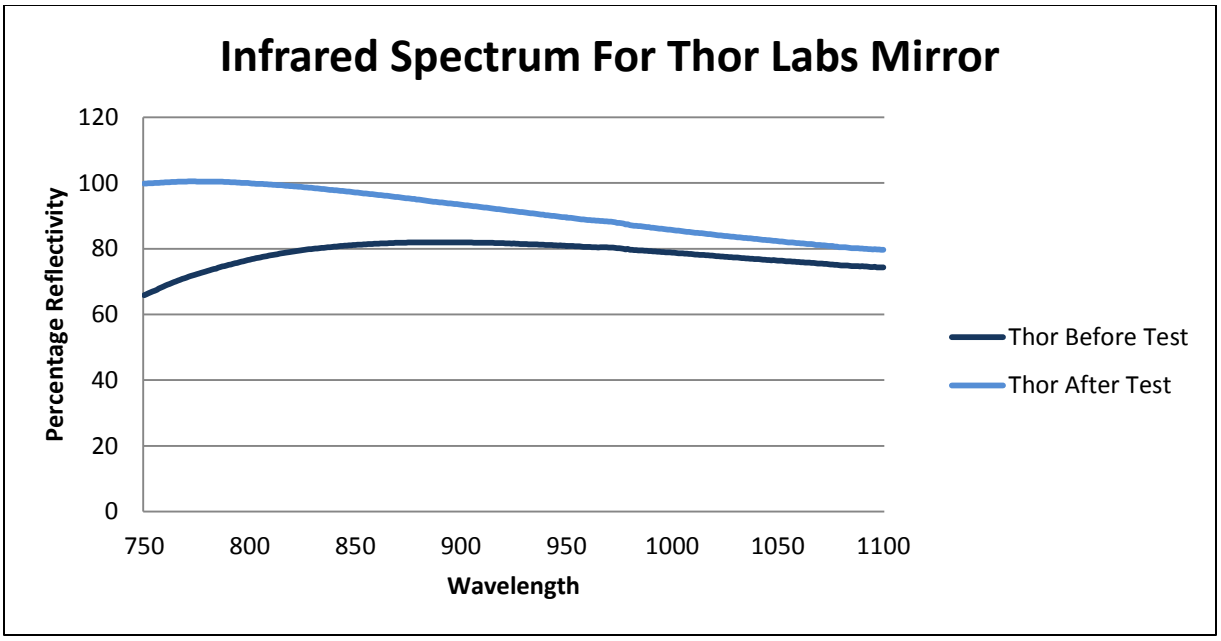

Figure 27: Plot of percentage reflectivity v/s wavelength (nm) for Thor Labs sample in Infrared Spectrum before and after annealing

As it can be seen, the samples from Edmund Optics clearly did not qualify for any consideration. This mirror saw a major fall especially in the infrared spectrum from nearly 100% reflectivity to under 50% reflectivity after only one cycle of 200 hours.

Thor Laboratory samples on the contrary saw an improvement in the reflectivity after they were annealed. However, the reflectivity in the region of infrared spectrum, where it mattered the most, the reflectivity started to decrease. After the wavelength of about 850 nanometers, the reflectivity decreases to almost 80%. This is in spite of the film showing improvement of about 10% from before the annealing test was conducted. This definitely gave a reason to consider these as a possible alternative but there was a necessity to understand other things like patches formed on the surface before running these films though another cycle.

6.4 Microscopic Imaging and Evaluation

To understand the change in surface morphology and texture, electron microscope and optical microscope images were studied. These helped understand the performance of both the mirrors.

6.4.1 Microscope Images of Edmund Optics Samples

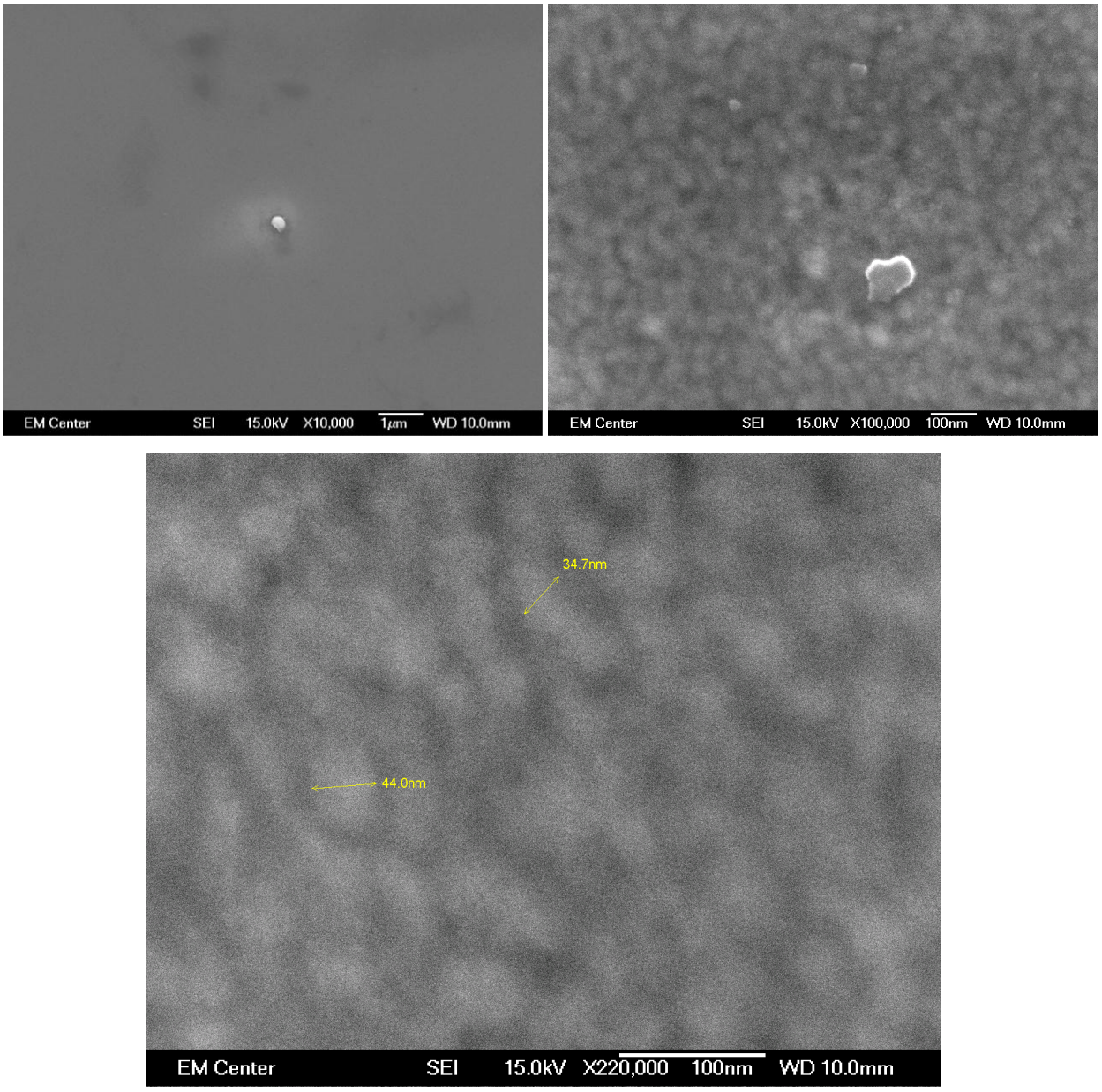

Figure 28: Image of sample from Edmund Optics using a Scanning electron Microscope (Top left) at 10000x magnification (Top right) at 100000x magnification and (Bottom) at 220000x magnification before annealing

As it can be noticed in the microscope images above, the Gold film from Edmund Optics had absolutely no texture. It was extremely uniform and quite spotless. Even at magnification as high as 220000x the film had very high consistency. However, the following SEM images of the same sample after an annealing cycle of 200 hours at 620^{o}C showed significant changes.

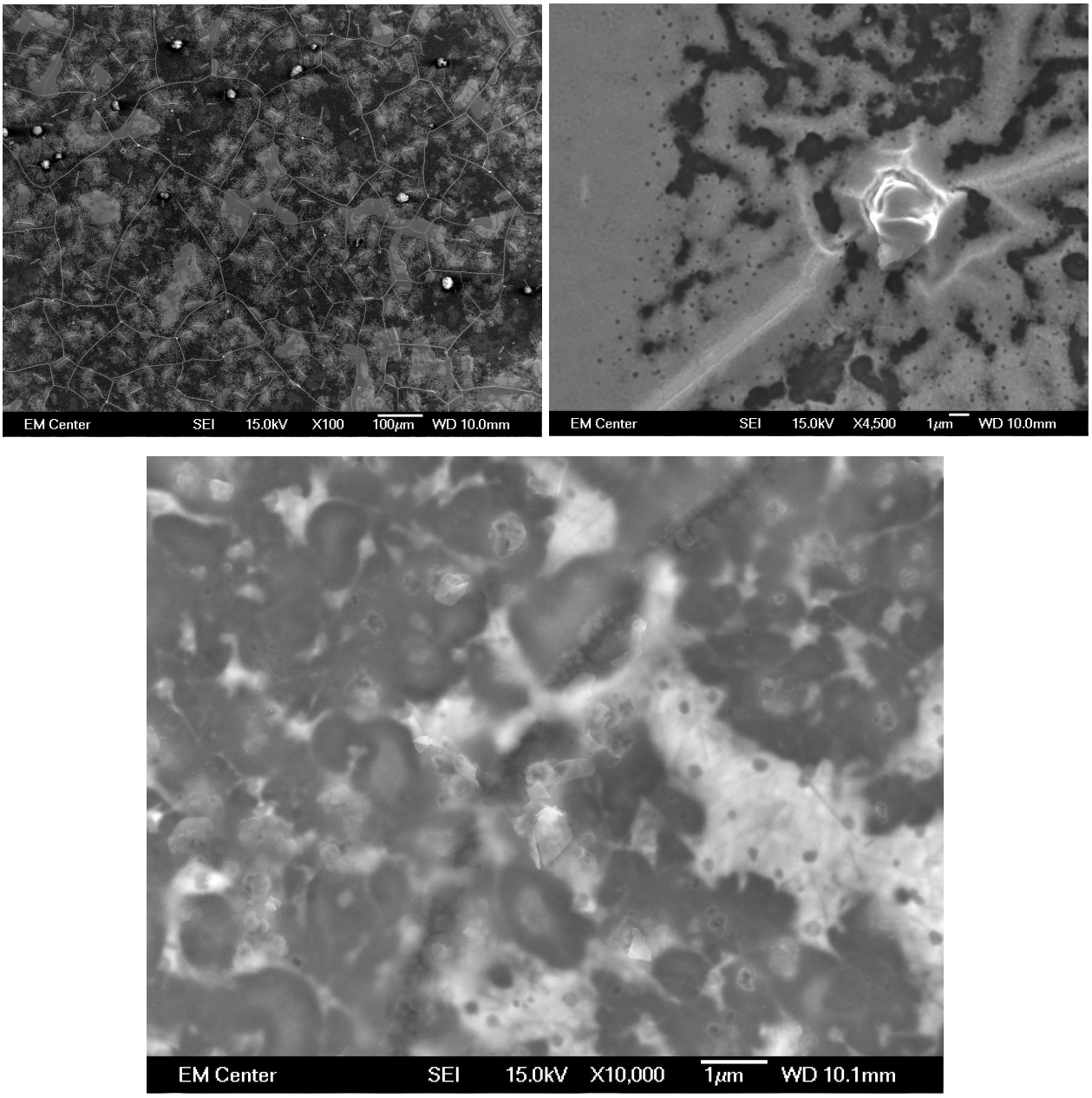

Figure 29: Image of sample from Edmund Optics using a Scanning electron Microscope (Top left) at 100x magnification (Top right) at 4500x magnification and (Bottom) at 10000x magnification after annealing.

Comparison between the microscope images before and after annealing for a Gold film mirror sample from Edmund Optics clearly showed signs of thermal grooving and island formation. Visual inspection showed the disintegration of the film which was confirmed through these SEM images. Also, it is important to know that further magnification after 10000x was not practical for the film after it was annealed since there was not enough conductivity. The SiO_2 substrate started to charge up if any further magnification was attempted. This also proved that breaking down of film had exposed the substrate completely.

6.4.2 Microscope Images of Thor Laboratory Samples

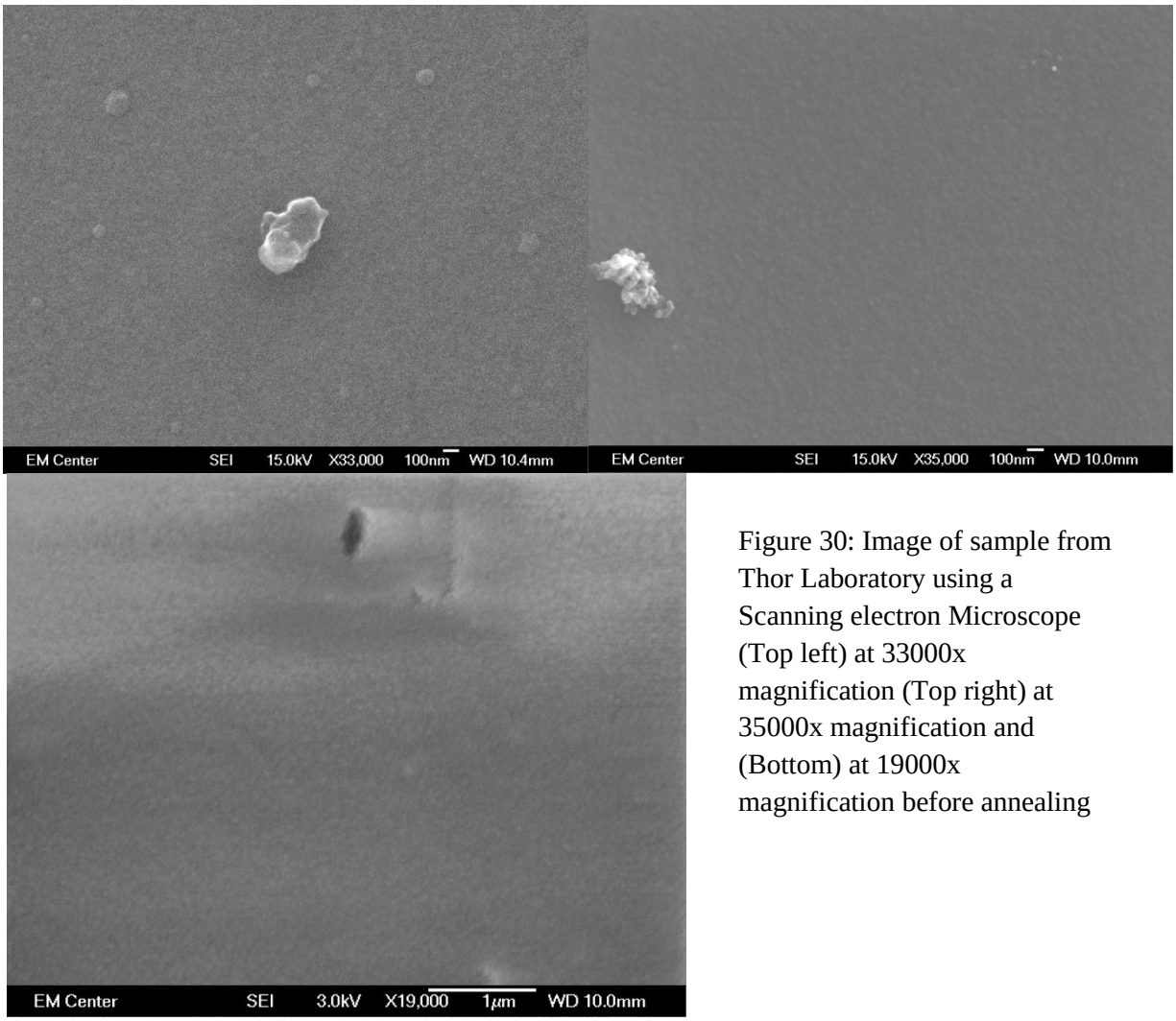

Figure 30: Image of sample from Thor Laboratory using a Scanning electron Microscope (Top left) at 33000x magnification (Top right) at 35000x magnification and (Bottom) at 19000x magnification before annealing

Once again, the sample showed a very uniform surface with almost no texture. There were a very few particles that were scattered over the surface of the sample. These particles were probably protrusions of SiO_2 that developed during fabrication of these mirrors. But they are too tiny and too few in number to make any significant difference to the characteristics of the mirror.

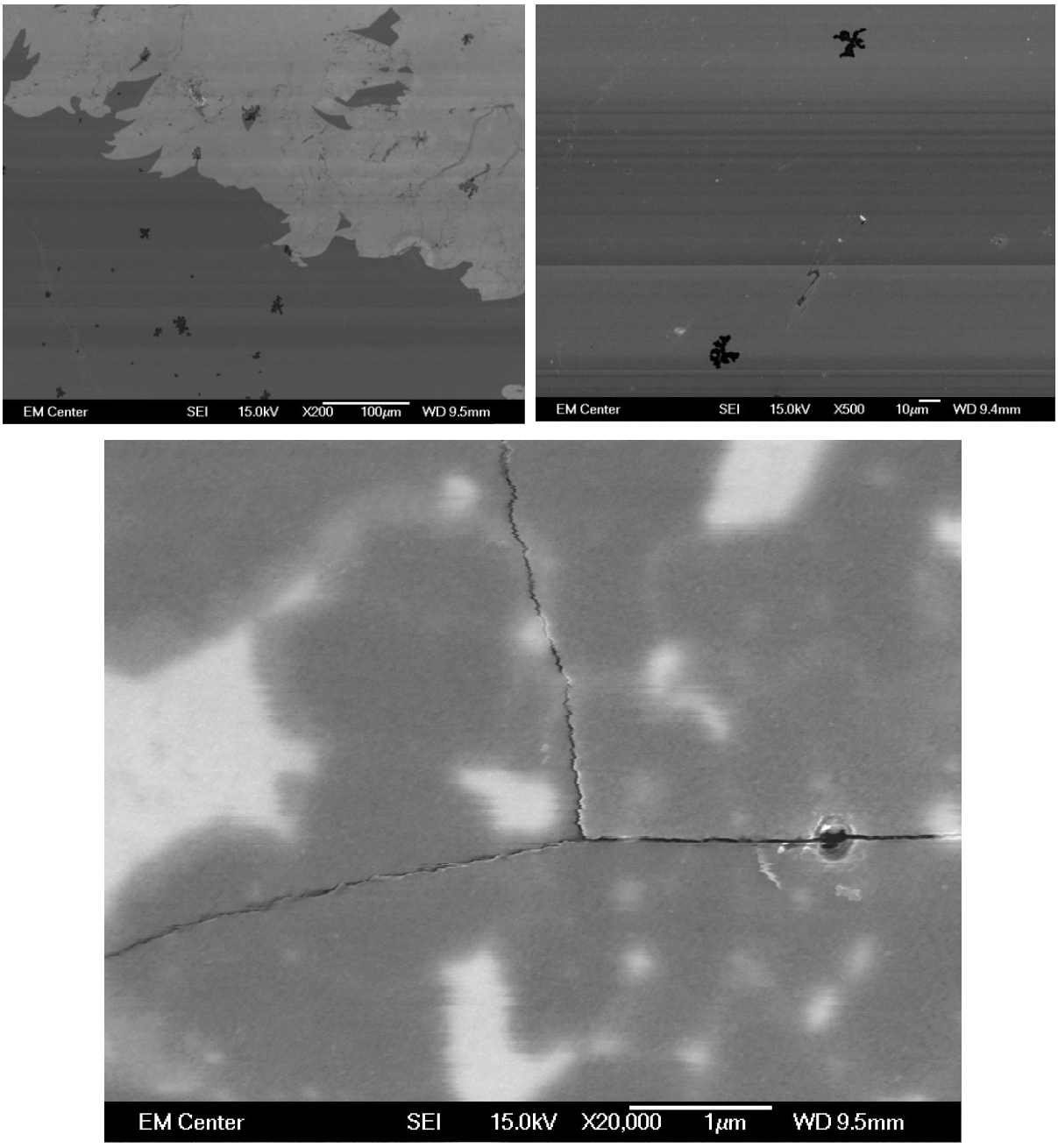

Figure 31: Image of sample from Thor Labs using a Scanning electron Microscope (Top left) at 200x magnification (Top right) at 500x magnification and (Bottom) at 20000x magnification after annealing.

Similar to the case of samples from Edmund Optics, the magnification in case of annealed samples was limited due to charging of the surface. Patches observed during visual inspection were looked at under higher magnification that can be seen in the first image at the top left. The patch appeared as if it was a case of peeling of the film or loosing adhesion with the substrate. Further magnifying to about 20000x showed that there were signs of brittle cracking. It seemed to be a case where the temperature caused an effect similar to glass tempering to the SiO overlay.

6.5 EDS Results for Samples After Test

EDS analysis was carried out to understand the constitution of these films and also to understand the distribution of material in these Gold films.

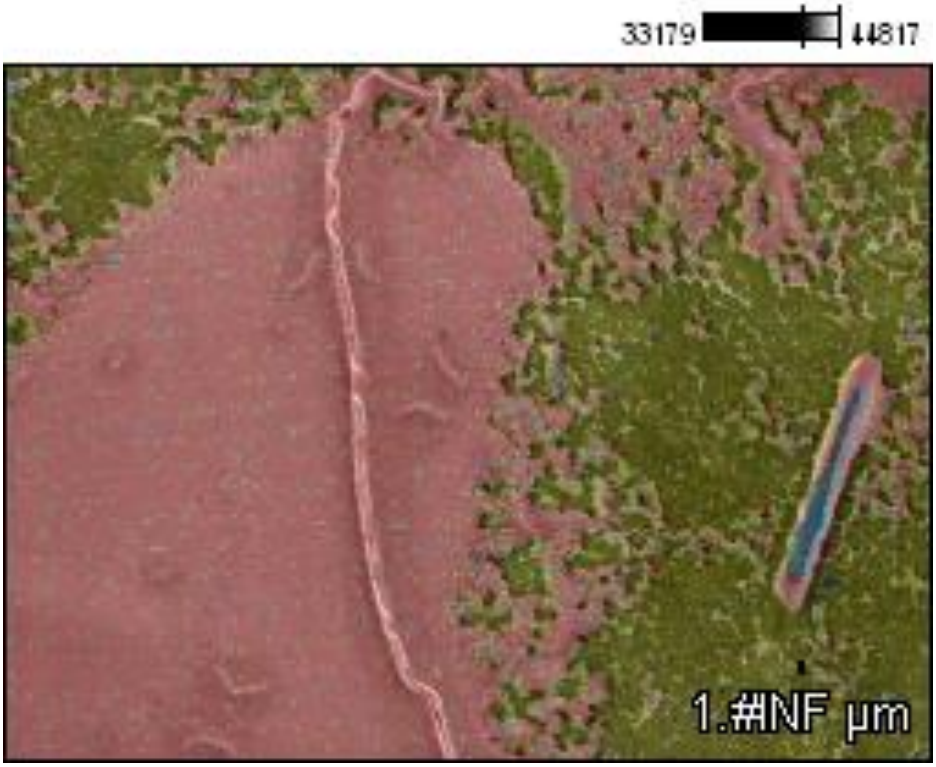

Accelerating Voltage: 15.0 kV

Figure 32: EDS scan of a random region on the surface of annealed Edmund Optics mirror at 1500x magnification. This image is from EDS analysis in SEM showing different phases in different colors.

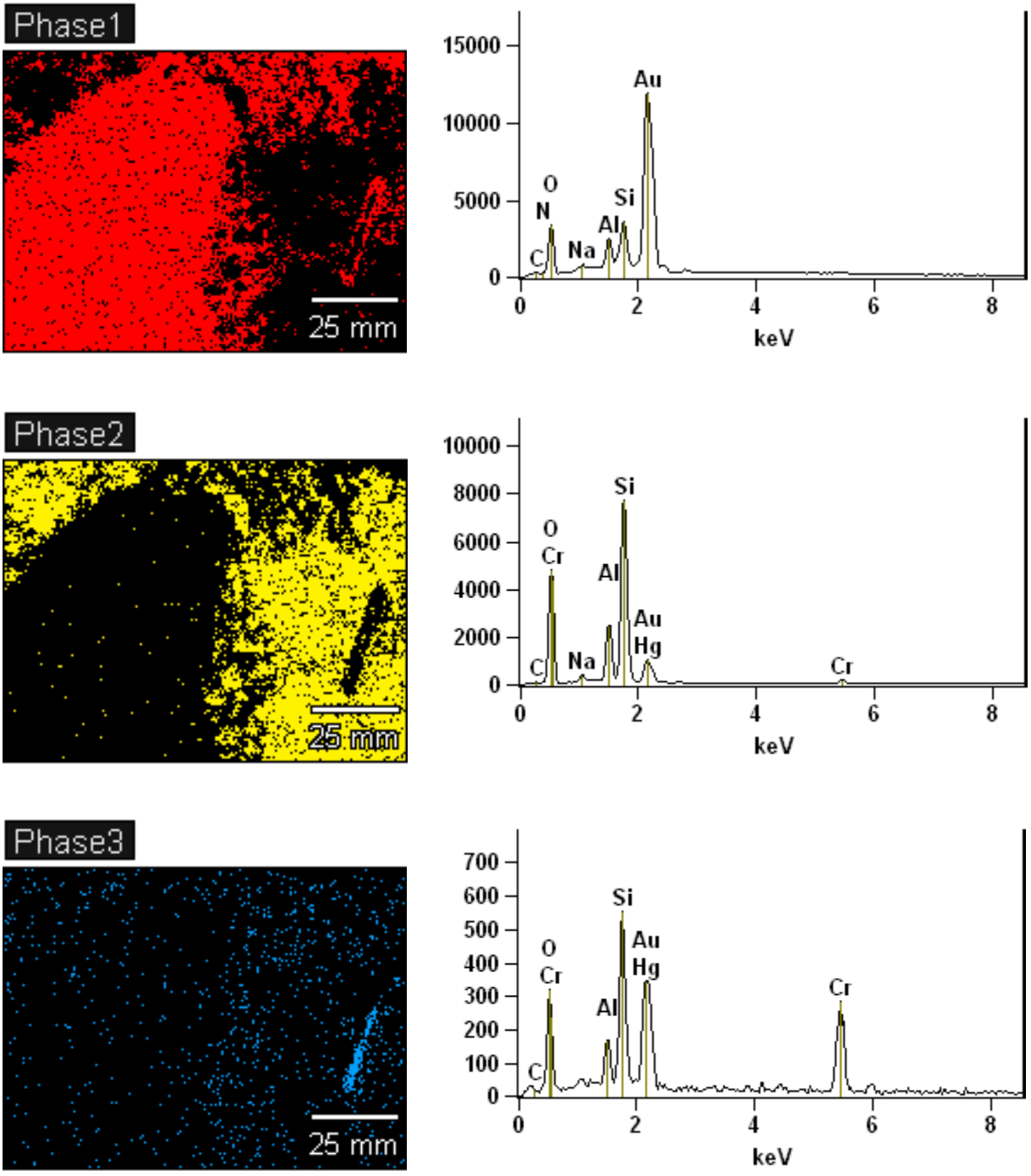

Figure 33: EDS scan showing various phases in the region shown in figure 32. The phase 1 shows Gold dominant region, phase 2 shows Silicon Oxide region which is the substrate and phase 3 shows Chromium rich region.

The EDS scans confirm island formation in the Gold film on the sample from Edmund Optics. Distinct Gold and SiO_2 dominant regions can be seen here. Phase 3 shows a fairly scanty but uniform distribution of Chromium which confirms its use as an adhesive underlay. Other elements such as Mercury, Aluminum and Nitrogen could potentially be contaminants since their presence is not dominant and did not show up as a separate phase. Sodium seen in phase 1 could be from the SiO_2 substrate that can have a small amount of Sodium.

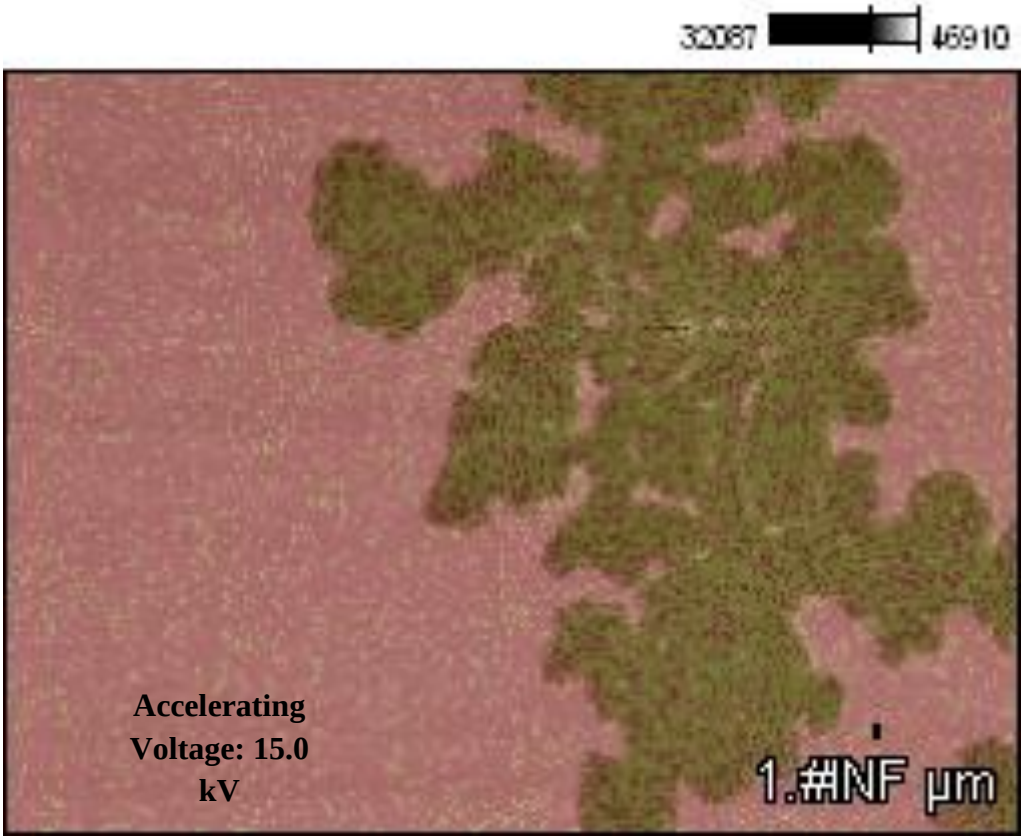

Figure 34: EDS scan of a random region on the surface of annealed Edmund Optics mirror at 1500x magnification. This image is from EDS analysis in SEM showing different phases in different colors.

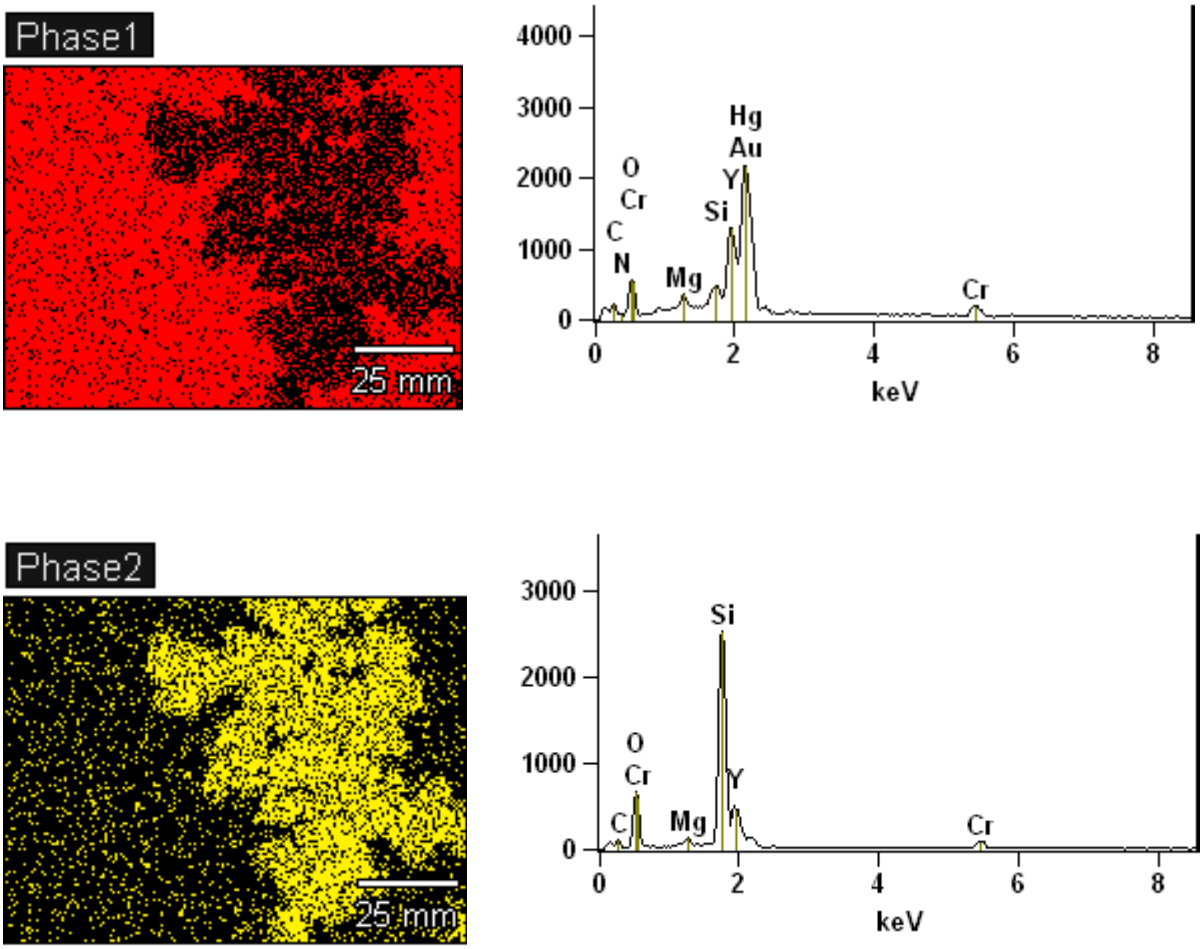

Figure 35: EDS scan showing various phases in the region shown in figure 34. The phase 1 shows Gold dominant region while phase 2 shows Silicon Oxide region which is the substrate and the overlay

EDS scan shows difference in material distribution when the unusual patches on the surface of the film from Thor Laboratory are analyzed. Distinct regions of Gold and SiO_2 dominant regions can be seen here. Both phases show a very scanty but uniform distribution of Chromium which confirms its use as an adhesive underlay in this sample as well. Other elements such as Mercury, Aluminum, Nitrogen, Magnesium and Yttrium could potentially be contaminants since their presence is not dominant and did not show up as a separate phase.

6.6 SWLI Surface Roughness Measurements for Samples After Test

6.6.1 SWLI roughness measurement for samples from Edmund Optics

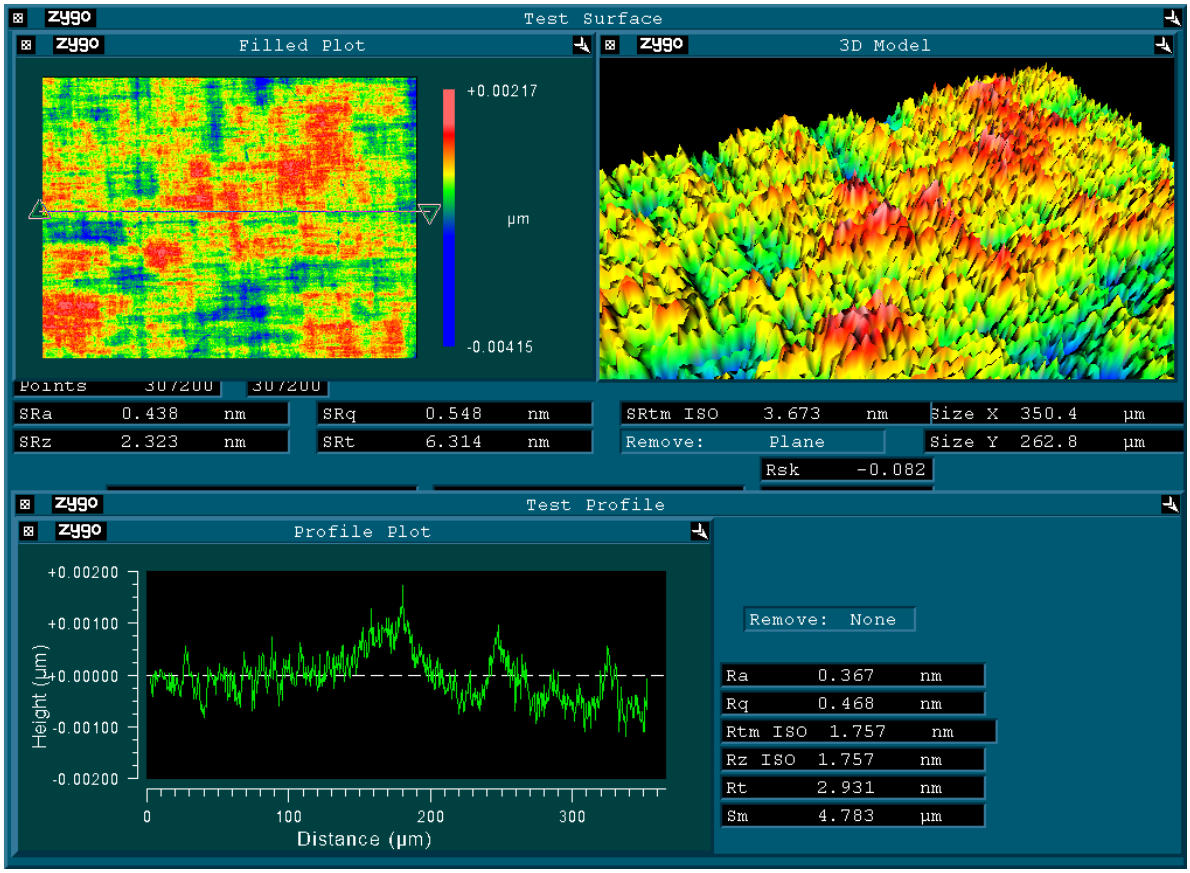

Figure 36: SWLI scan of Edmund Optics mirror before annealing

The above image is from a White Light Interferometer scan taken for an Edmund Optics sample before it was annealed. Top left window (filled plot) shows the top view of the surface while the top right window (3D Model) shows an isometric view of the surface. Bottom left window displays the roughness of the surface at the section that is highlighted by a line that is visible in the filled plot window. The mean roughness of this film as can be seen in the field named “SRTm ISO” (Root Mean Square) is 3.679 nm.

The image below is a similar image from the same sample after annealing. The texture of the surface in this scan can be related to the SEM image seen in figure 31. After annealing the root mean

square roughness increases from 3.679 nm to a comparatively mammoth value of 5182.197 nm. This means that the roughness increased on this mirror by about 1400 times after it was annealed.

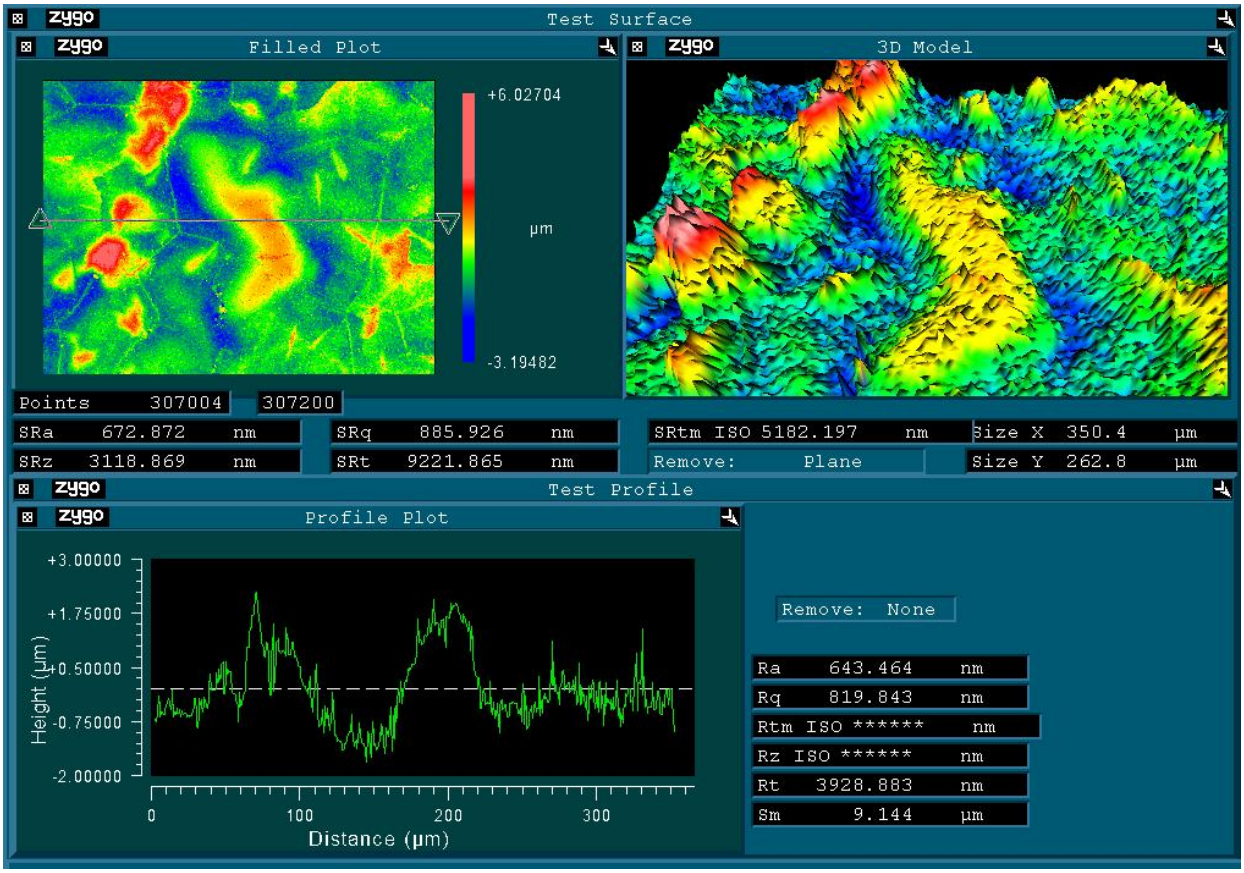

Figure 37: SWLI scan of Edmund Optics mirror after annealing

6.6.2 SWLI roughness measurement for samples from Thor Laboratory

Figure 38 below shows the surface scan of a sample from Thor Laboratory before annealing. This was scanned at a magnification of 10x. Figure 39 is a scan of the surface of same sample after annealing at 100x magnification. The root mean square roughness here may be misleading. A vertical section is monitored on the surface in figure 38 while a horizontal surface section in figure 39. This was because the scan of the surface before annealing did not show any significant roughness and therefore to get an idea of the actual roughness such a section was selected. Figure 40 shows a scan of the unusual patch that had a dendrite type structure that can be related to dark spots seen in figure 31 top right image.

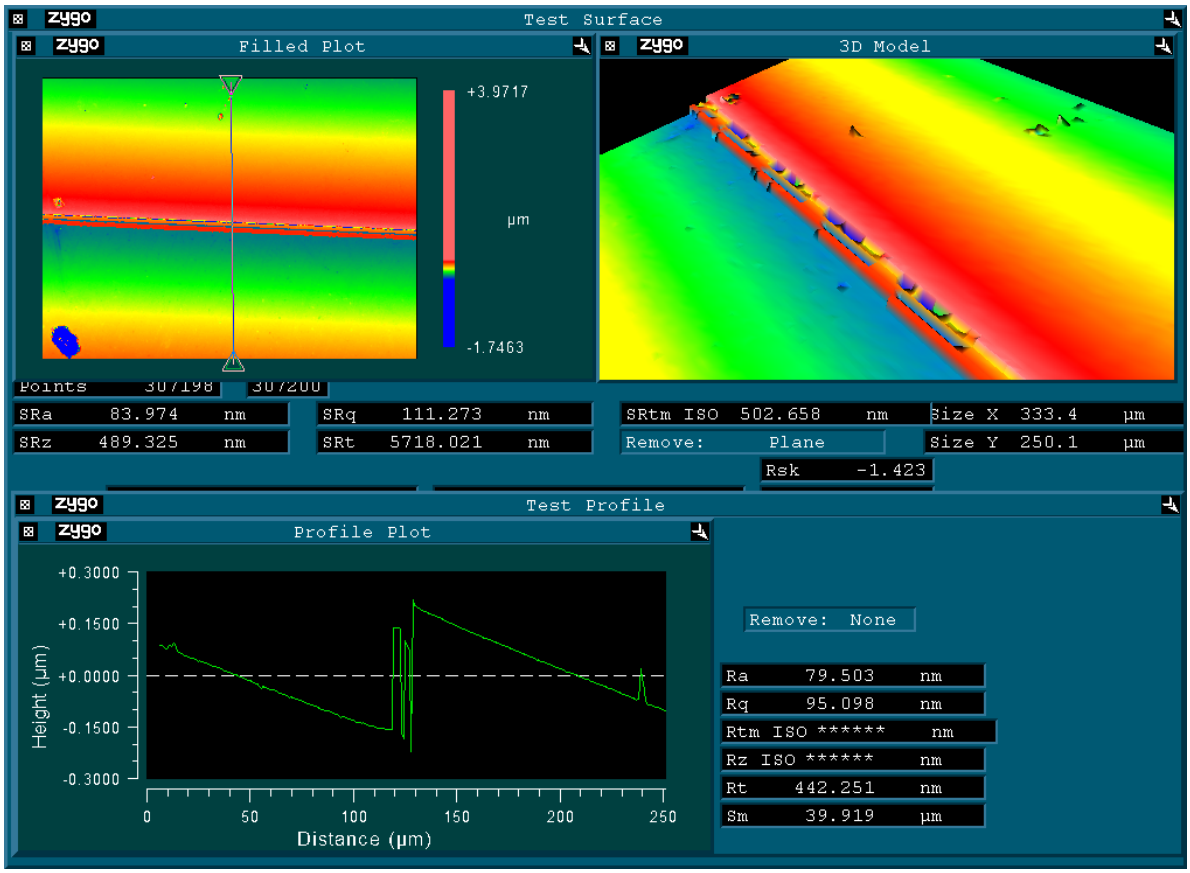

Figure 38: SWLI scan of Thor Laboratory mirror before annealing

The scan below shows that after annealing there is not only some amount of deformation in the film but also there is a deformation in the SiO overlay. It seems to be the crack initiation point cause by tempering induced in the SiO film due to high temperature. Other larger regions that show an awkward patch as if the film is peeling off can be seen in figure 40 that represents the scan of the surface at 10x. It can be related to the top right SEM image in figure 31. It can clearly be seen that the surface at the patch is rising above rest of the surface indicating loss of adhesion between the film and the substrate. This could be due to expansion of trapped gases under the film.

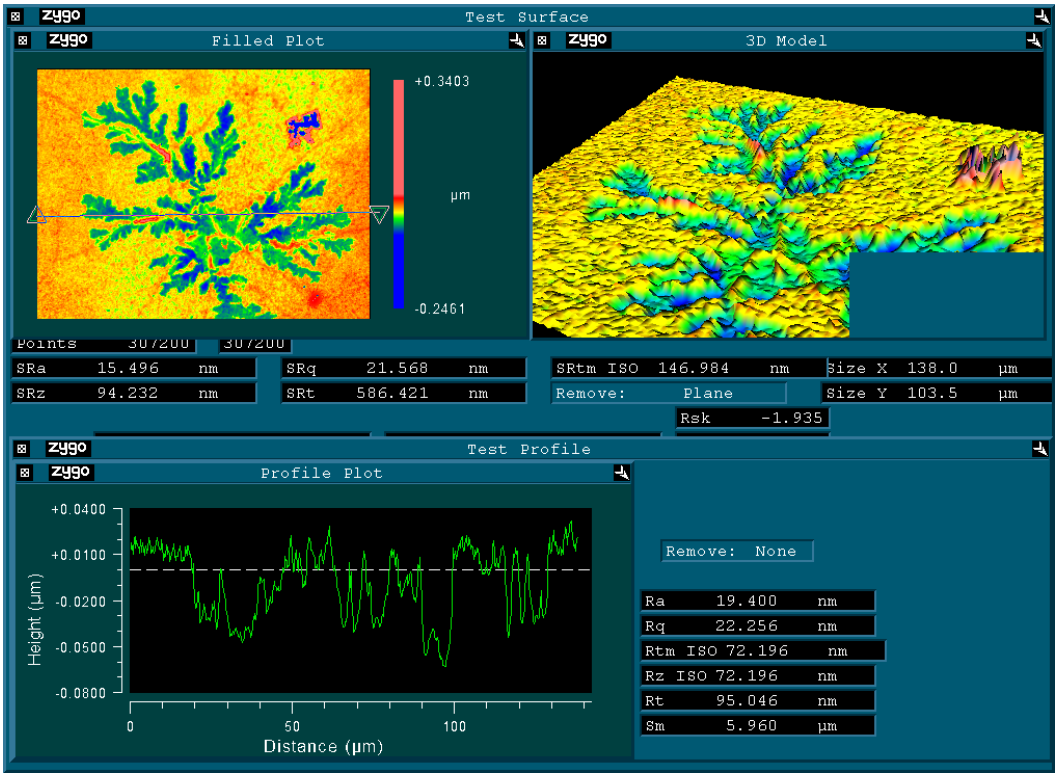

Figure 39: SWLI scan of Thor Laboratory mirror after annealing

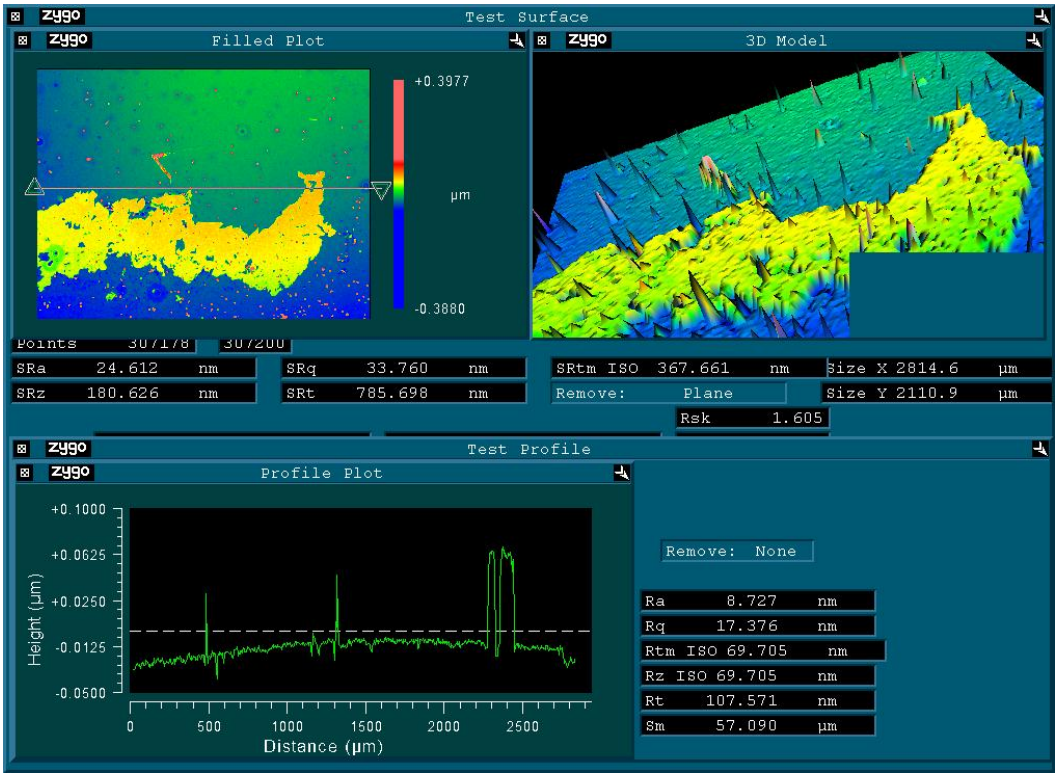

Figure 40: SWLI scan of Thor Laboratory mirror after annealing

6.7 Conclusion Derived from Analysis of First Phase Experiments

The two samples that were acquired from optical component manufacturers – Edmund Optics and Thor Laboratory failed to meet the requirement to act as the basis of a successful radiation shielding mirror. These represented 2 out of the 3 possible solutions. The first sample from Edmund Optics had an underlay of chromium which failed to keep the film from breaking down and forming islands. On the other hand the sample from Thor Laboratory did look promising in the beginning but its analysis suggested otherwise. It not only had poor reflectivity in the infrared spectrum but also had several defects at the microscopic level. This suggested that it was not a very reliable solution either. Next step would be to replace the Chromium underlay with Indium and test these samples. Such films have shown promising results in electronic circuit application. However, the entire literature search revealed that most of the study of Gold films with Indium underlay looked at the electrical properties and no optical studies were performed in the literature. Also, no manufacturer was found who would supply such mirrors. Therefore, it was decided that new samples would be custom fabricated and tested for performance. Details about preparation of these samples and their analysis are described in the next chapter.

CHAPTER 7: TEST AND ANALYSIS OF MIRRORS CUSTOM FABRICATED AT CNL

7.1 Overview

The first phase of experiments brought the study to a conclusion that the first two anticipated solutions to avoid thermal grooving and island formation were not applicable at such a high temperature. To explore the prospect and effect of the third solution it was necessary to prepare the samples rather than purchasing from the available range in the industry. The facility at University of Colorado Boulder called Colorado Nanofabrication Lab was used to fabricate such samples.

7.2 Colorado Nanofabrication Lab

The Colorado Nanofabrication Lab (CNL) is an open user facility at the University of Colorado on the Boulder campus engineering department. This facility is supported by National Science Foundation and is one of the 14 members of the National Nanotechnology Infrastructure Network (NNIN). Out of several available equipments for nanofabrication and characterization are a few thin film deposition systems.

For deposition of Gold and Indium, a 3-boat thermal evaporator was used. This had a bell jar with a cryogenic pump connected to it. There were three boats that could be connected to the electrical power source. Only one out of these three could be operated at a time but can be switched without breaking vacuum. Usually tungsten boats with alumina coating are used in such evaporators. Gold and Indium do not readily alloy with alumina and therefore this boat was used. The bell jar had a rotating disk on which the sample substrate would be mounted. A shutter allowed immediate covering and uncovering of the substrate while depositing, thus help avoid over deposition. The bell jar was equipped with a crystal monitor. The digital readout connected to this monitor gave precise information about the thickness of material deposited up to 1 nm precision.

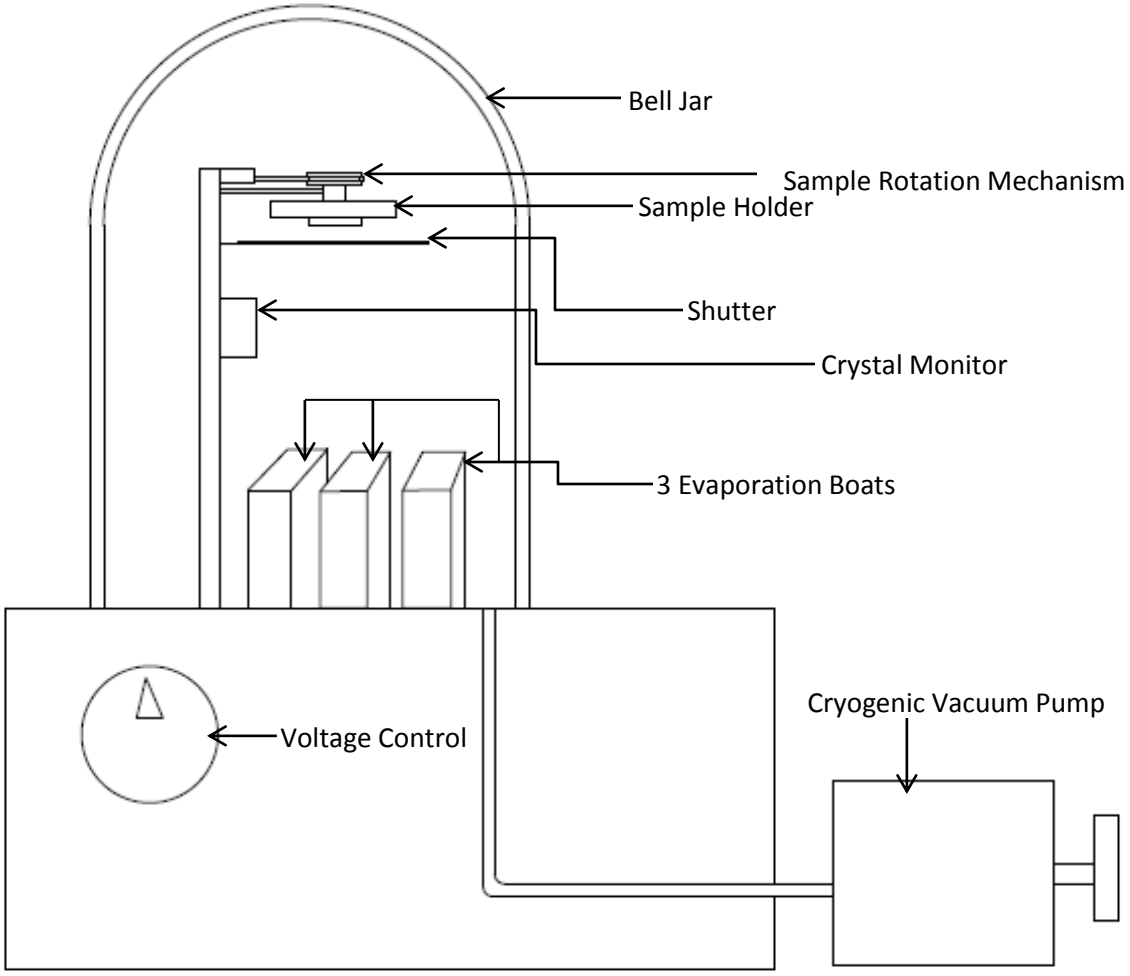

Figure 41: Schematic of Vacuum Thermal Evaporator at Colorado Nanofabrication Lab, CU Boulder

For the substrate, round quartz glass with a 1.5 inch diameter were purchased from McMaster-Carr. These glass substrates were thoroughly cleaned using iso-propanol and distilled water to get rid of all contaminants. They were also ultra-sonic cleaned before they were used for Indium and Gold deposition.

7.3 Sample Specifications and Preparation

Reference from "Thermal grooving, thermotransport and electrotransport in doped and undoped thin gold films" by R. E. Hummel *et al.* revealed that using 6% Indium underlay for specified quantity of Gold helps avoid thermal grooving, grain boundary separation and island formation. Temperature and

time of the experiments performed were way lower than the intended values of this study, they could still be related and were taken as the base for this experiment.

The first sample was prepared with 1000A^{o} of Gold that had 6% underlay of Indium. To understand the effect of Indium better, another sample was prepared that had 50% Indium for 800 A^{o} Gold film. These were tested and as expected the film with 6% underlay of Indium showed highly promising results. To see if the performance could be further improved and parameters optimized it was decided that another sample be prepared with a slightly higher proportion of Indium and a thicker Gold film. For this purpose a third sample was prepared with 2000A^{o} of Gold that had 7.5% underlay of Indium. All these samples after annealing at the same 620^{o}C for 200 hours were analyzed. The observation from this experiment and its analysis are described in the following part of this chapter. As a random experiment to check the effect of gold deposition on a glass substrate without any underlay, a 500 A^{o} Gold deposition was also attempted. This experiment showed that without an underlay of Indium, Gold could not adhere well to the glass substrate. It created a very patch film that was not uniform and majority parts of the substrate were had no gold film.

Thus it was also proved that it was essential to have a thin underlay of a softer material to allow a successful deposition of gold.

7.4 Visual Inspection of the Samples

As in case of previous two samples, samples with 6% Indium and 7.5% Indium also had an exceptionally fine surface with good reflectivity on visual inspection. They were spotless and texture free. However, the sample with 50% Indium gave a very different appearance. The following images show the surface of thin film Gold reflectors before and after they were annealed.

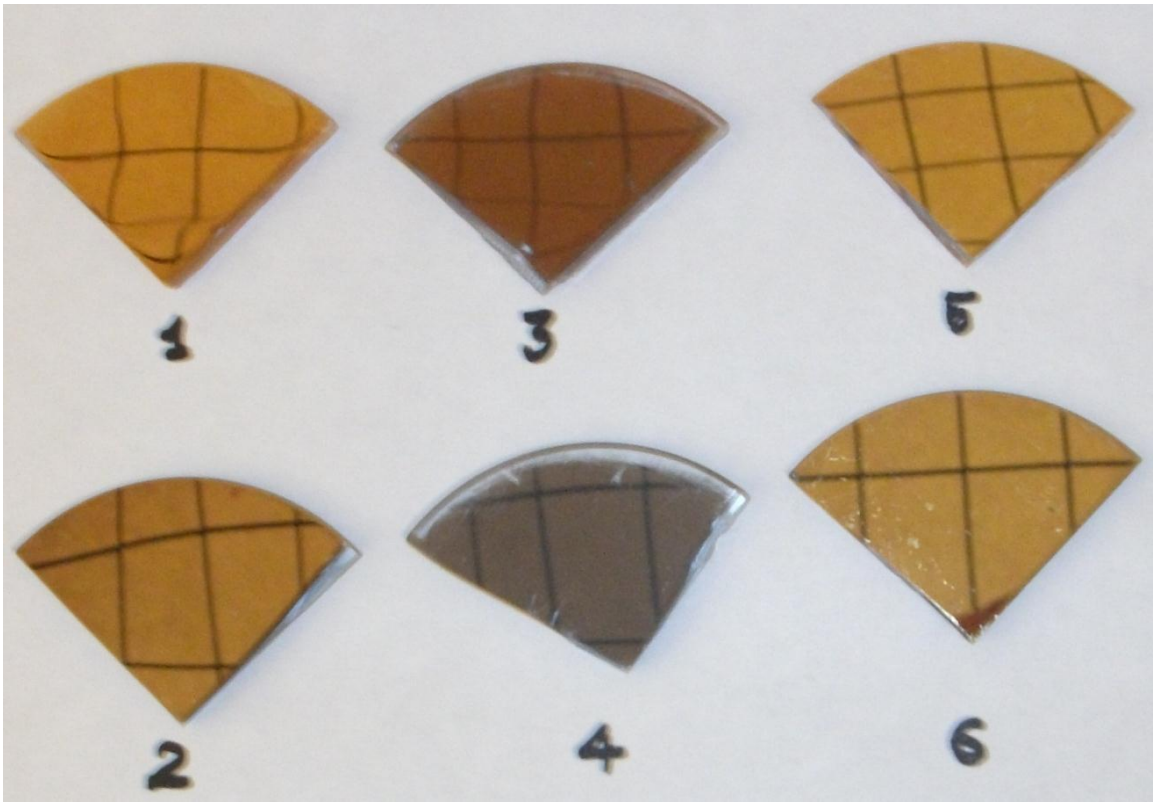

Figure 42: Samples prepared at CNL – (2) 6% In/1000A^{o} Au before annealing (1) 6% In/1000A^{o} Au after annealing (4) 50% In/800A^{o} Au before annealing (3) 50% In/800A^{o} Au after annealing (6) 7.5% In/2000A^{o} Au before annealing (5) 7.5% In/2000A^{o} Au after annealing

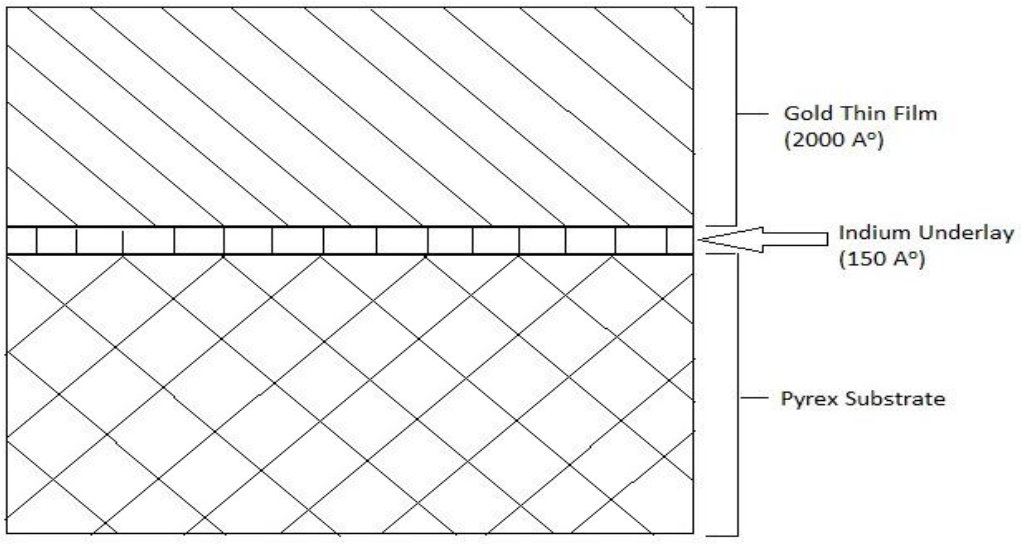

Figure 43: Schematic of Gold film with Indium underlay (7.5% Indium under 2000A^{o} of Gold) [Not to scale]

Important thing to be noticed here is the fact that none of the films showed any distortion or deformation as far as visual inspection is concerned. The black lines show the reflectivity of these films in visible light spectrum. It is clear that the films even after 200 hours of exposure to extremely high temperature maintained the composition and did not break down. No signs of thermal grooving, grain boundary separation or island formation are remotely noticeable. This observation made it clear that Indium definitely had a distinct and positive effect on gold film at the temperature and time they were tested for.

The same analytical methods as in case of mirrors from Edmund Optics and Thor Laboratory were repeated for the set of these three samples. Reflectivity of the mirror before and after the test was on the top of the metric, based on which the performance of the mirrors could be evaluated.

7.5 Reflectivity Measurements using Spectrometer

Following graphical plots represent the reflectivity of these mirrors in both visible and infrared spectrums.

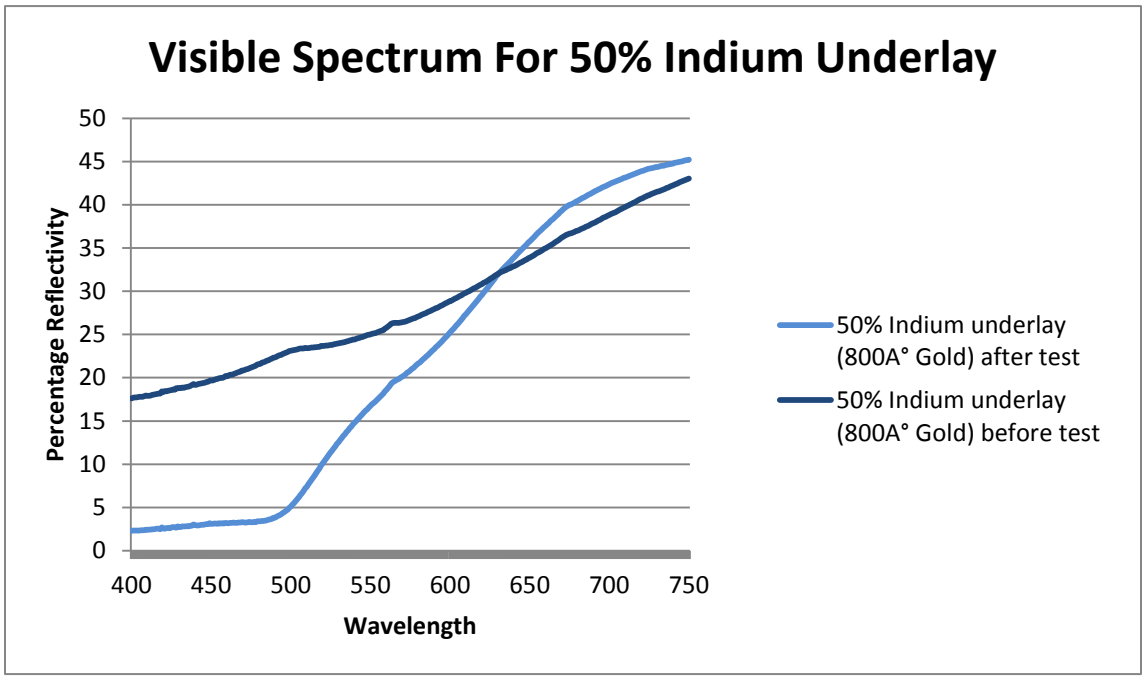

Figure 44: Plot of percentage reflectivity v/s wavelength (nm) for 50% Indium under 800A^{o} Gold sample in Visible Spectrum before and after annealing

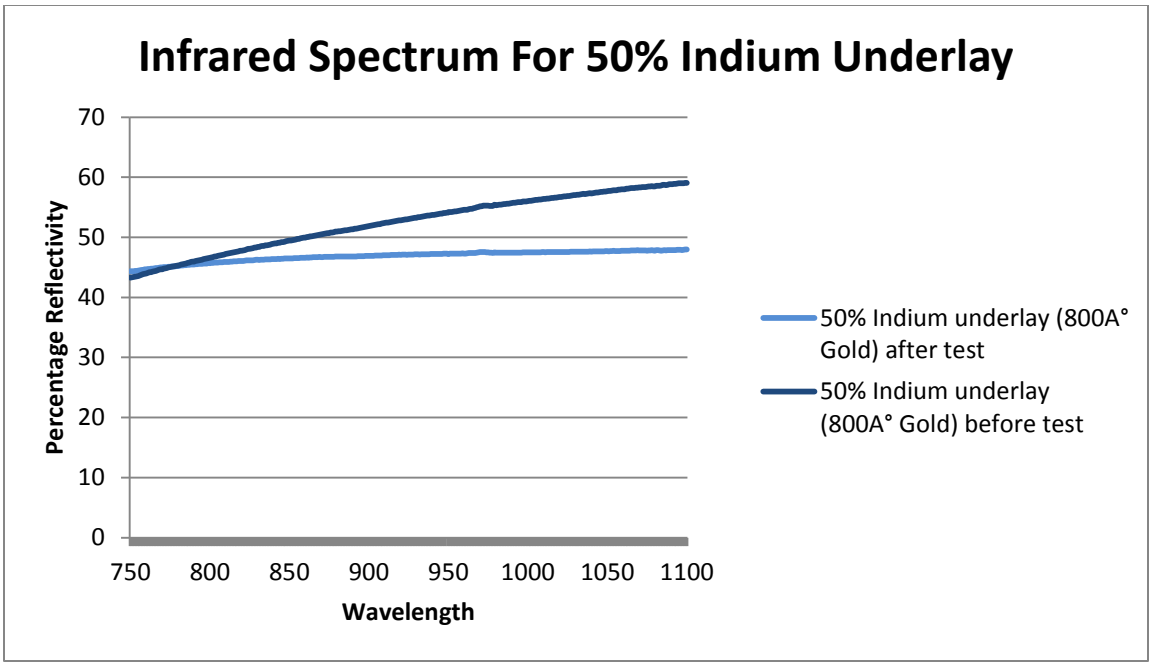

Figure 45: Plot of percentage reflectivity v/s wavelength (nm) for 50% Indium under 800A^{o} Gold sample in Infrared Spectrum before and after annealing

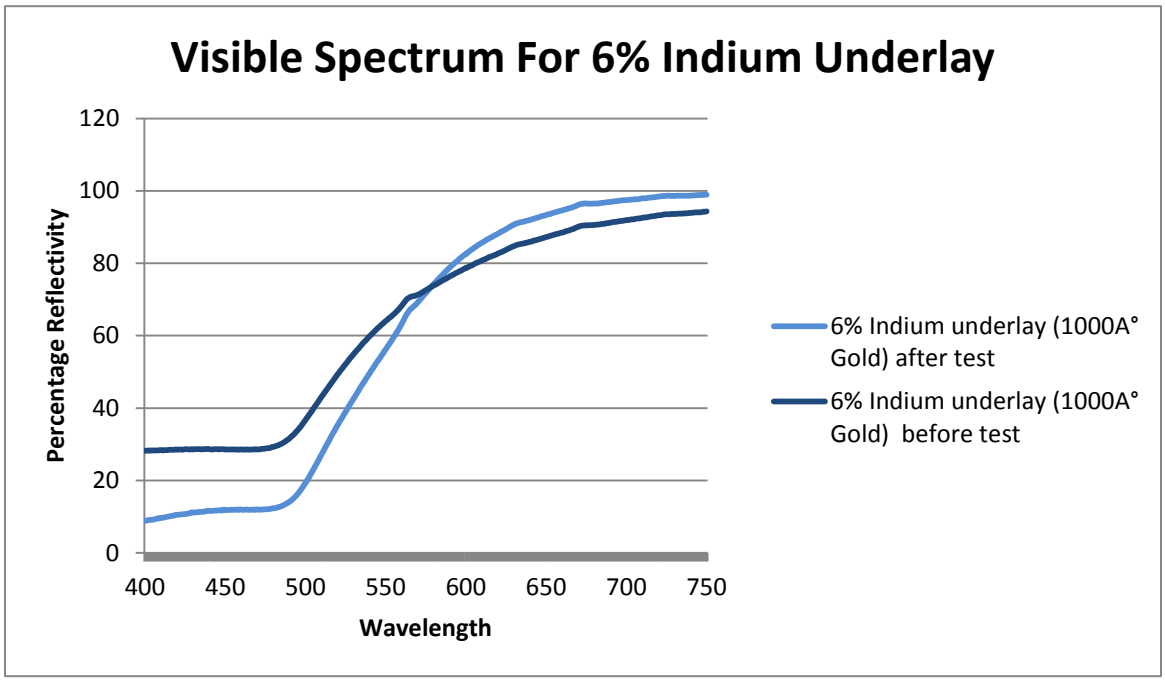

Figure 46: Plot of percentage reflectivity v/s wavelength (nm) for 6% Indium under 1000A^{o} Gold sample in Infrared Spectrum before and after annealing

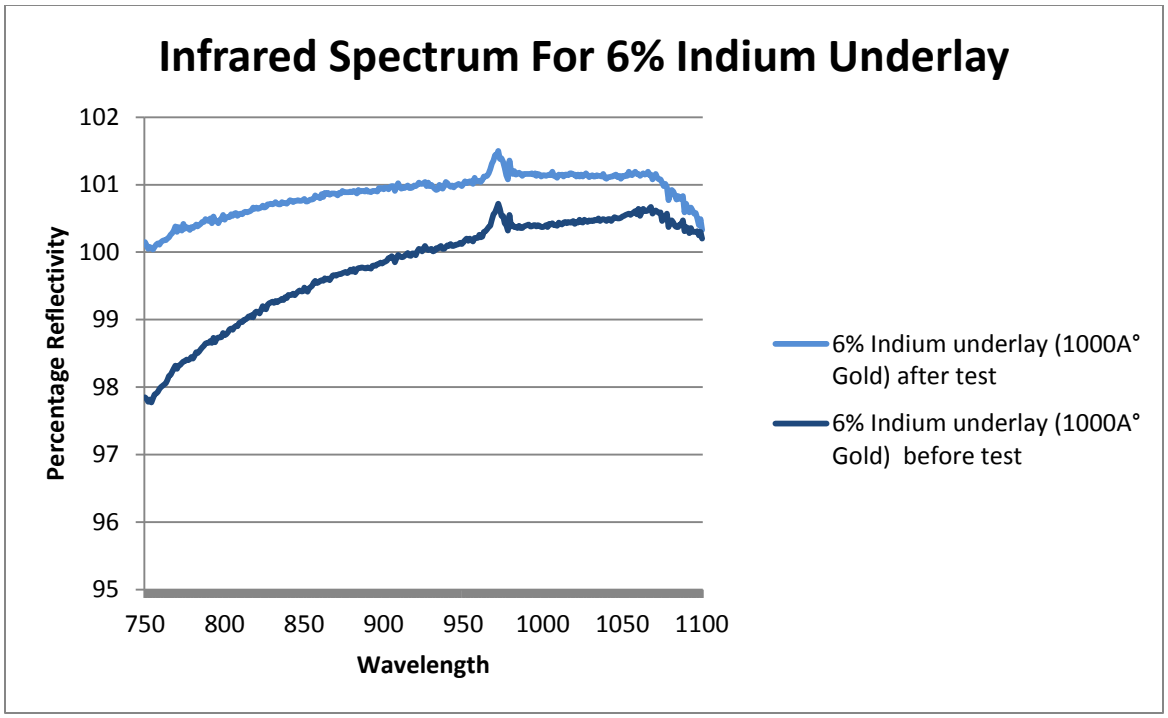

Figure 47: Plot of percentage reflectivity v/s wavelength (nm) for 6% Indium under 1000A^{o} Gold sample in Infrared Spectrum before and after annealing

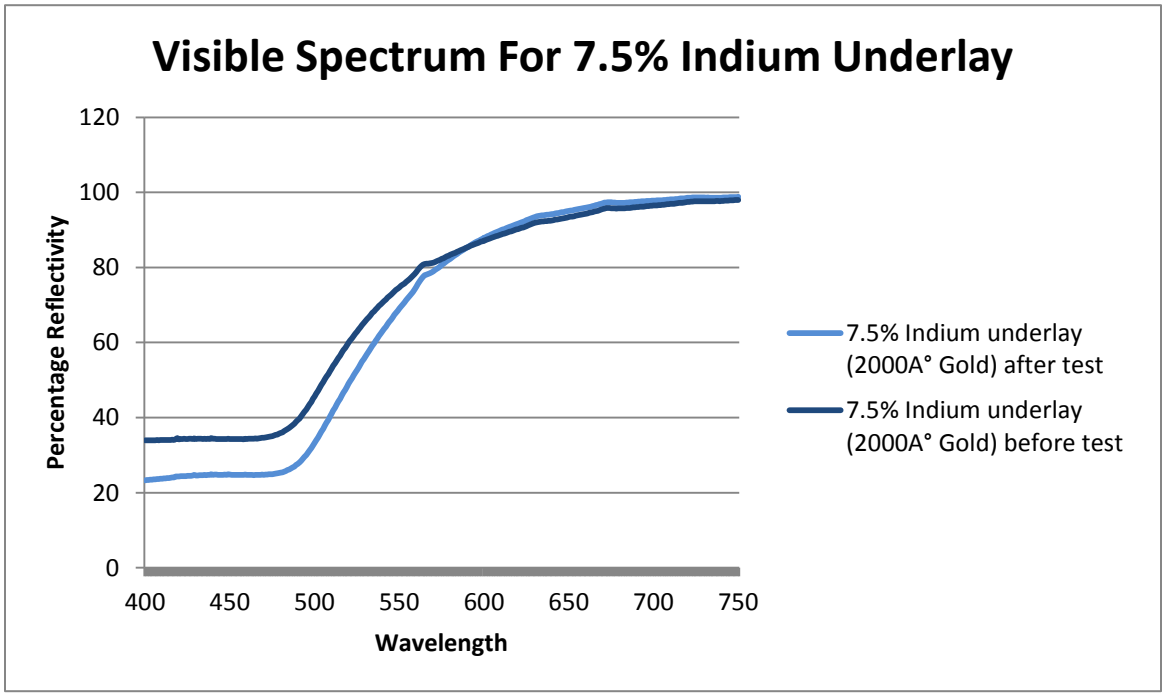

Figure 48: Plot of percentage reflectivity v/s wavelength (nm) for 7.5% Indium under 2000A^{o} Gold sample in Infrared Spectrum before and after annealing

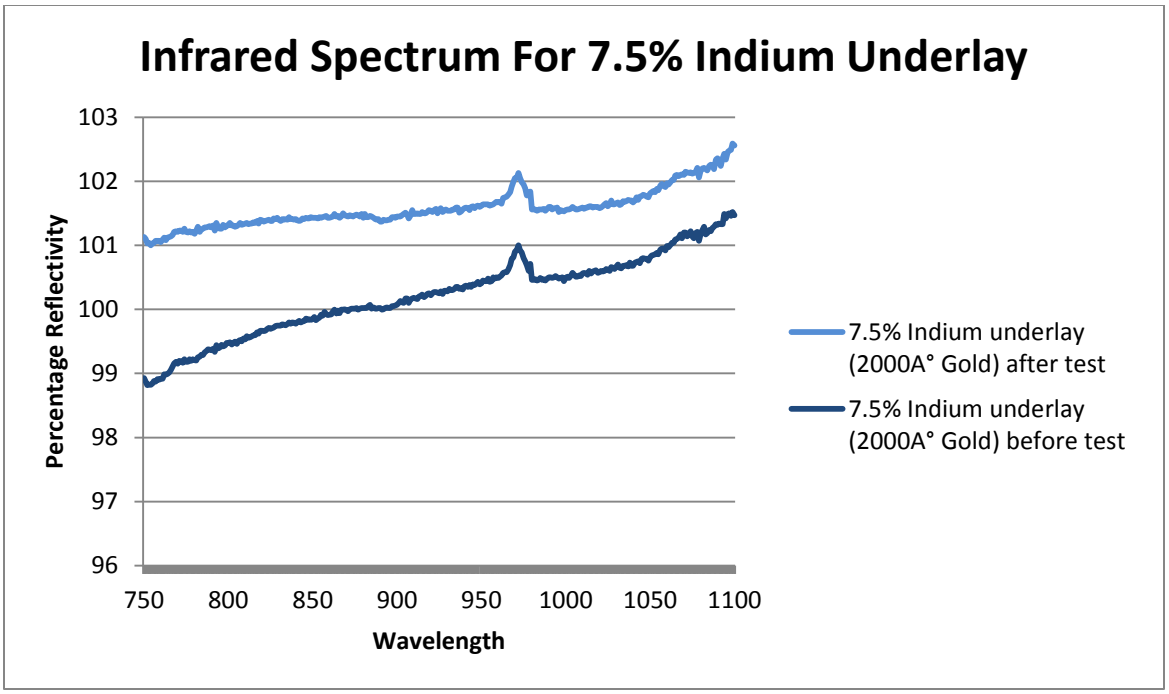

Figure 49: Plot of percentage reflectivity v/s wavelength (nm) for 7.5% Indium under 2000A^{o} Gold sample in Infrared Spectrum before and after annealing

Looking at the graphical plots of the reflectivity measurement, a striking similarity can be noticed. For the samples with 6% Indium and 7.5% Indium, the reflectivity improved by about 10% in infrared spectrum after they were annealed. Sample with 50% Indium had low reflectivity which showed that excess Indium has a negative effect on performance of the shields. Both 6% Indium and 7.5% Indium mirrors show over 100% reflectivity. These values are more than 100% because the reflectors that were used to calibrate the spectrometer had a lower reflectivity than these mirrors[25]. As a result, the reflection measured by the spectrometer gave a value that exceeded 100%. Based on these observations, samples with 6% Indium and 7.5% Indium were great contestants for further research. However, following analysis also shows details about the mirror that had 50% Indium content. Purpose of including the analysis of this sample is to give a clear comparison and better understand the behavior if Indium doped Gold films in high temperature.

7.6 Microscopic Imaging and Evaluation

To understand the change in surface morphology and texture that might have caused the performance of one sample to fall and other two to improve, electron microscope and optical microscope images were studied. These helped understand the performance of all three mirrors.

7.6.1 Microscope Images of Film with 50% Indium/800 A^{o} Gold

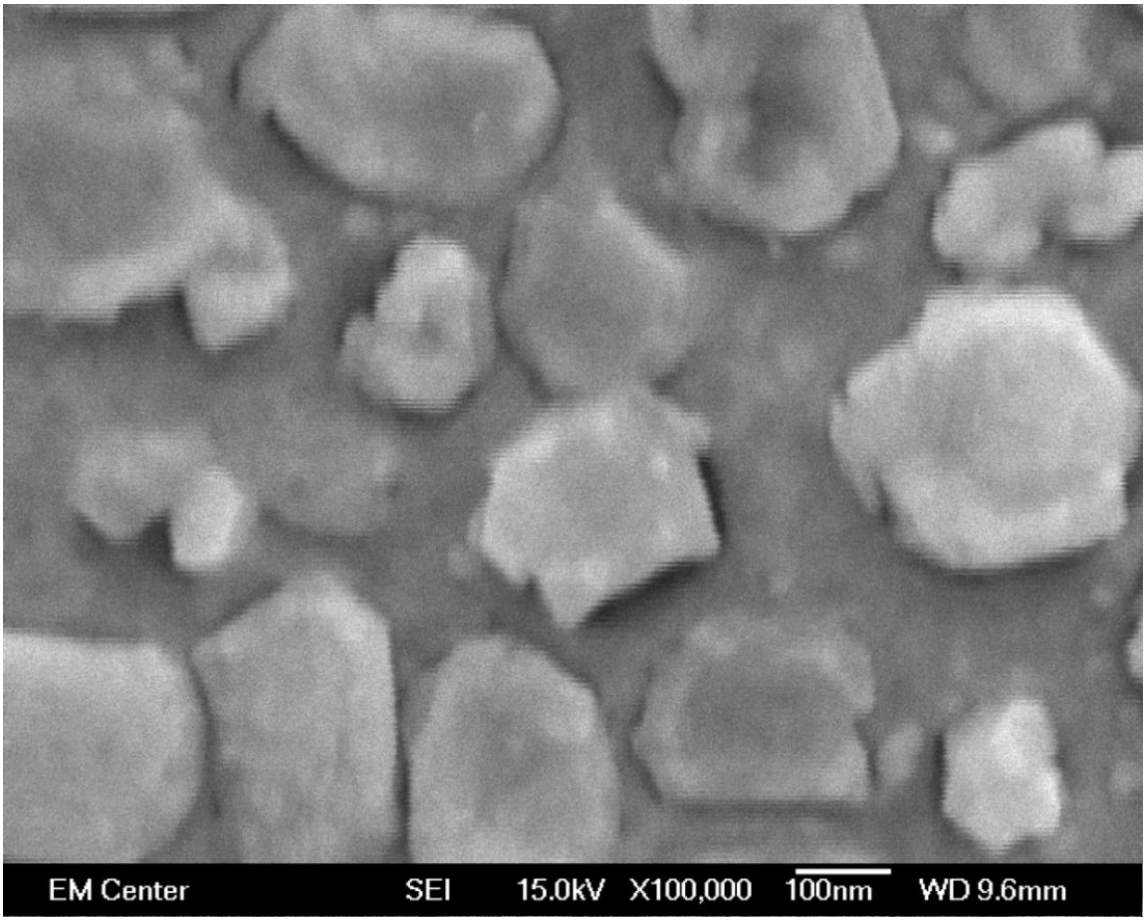

Figure 50: Image of the sample with 50% Indium under 800A^{o} Gold film before annealing

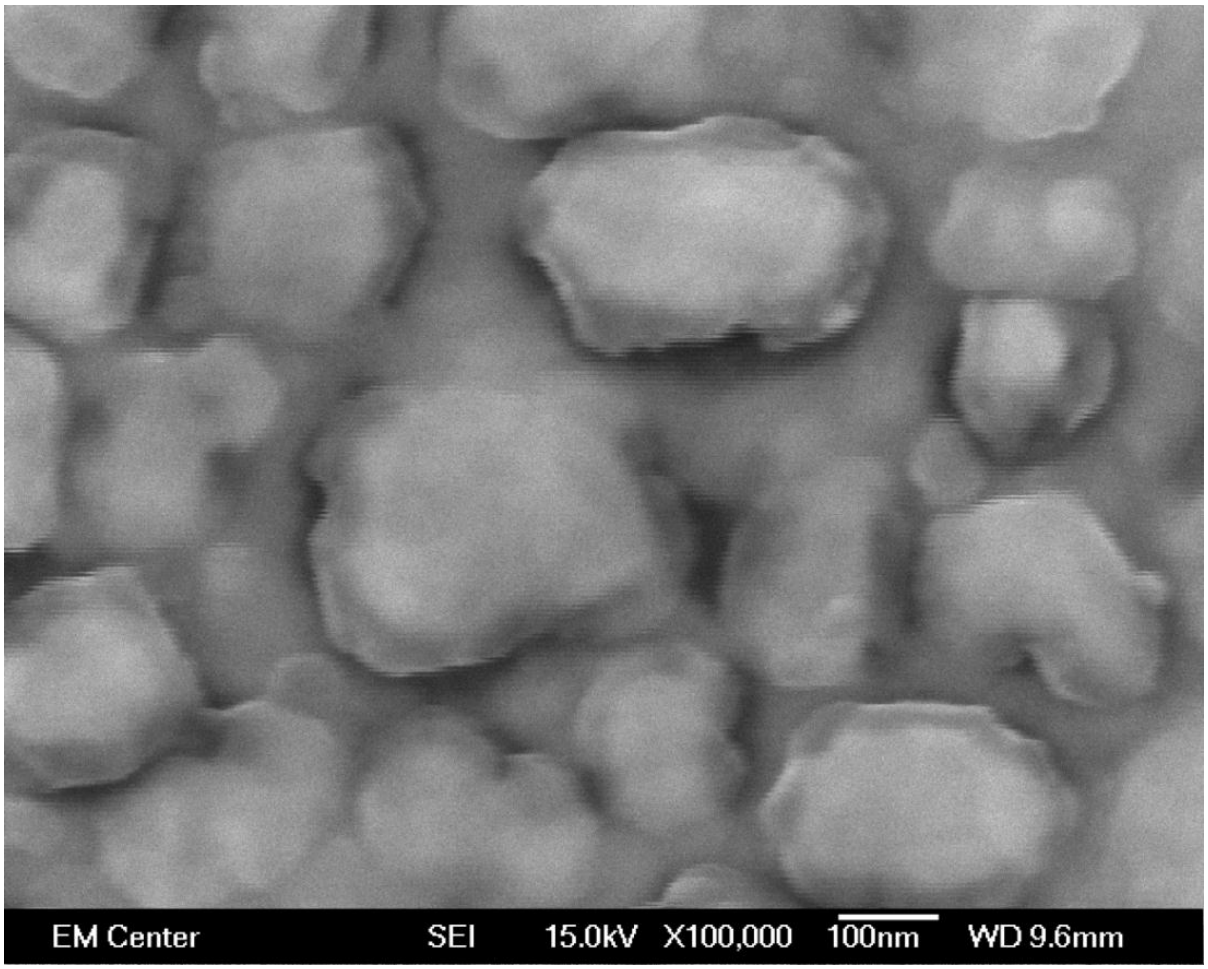

Figure 51: Image of the sample with 50% Indium under 800A^{o} Gold film after annealing

As it can be seen, there is no major difference in the film noticeable at even 100000x magnification. This does not answer the question that what made the performance of this film fall after annealing. But it does hint towards the fact that having Indium underlay does help maintain the physical composition and characteristics of thin gold film.

7.6.2 Microscope Images of Film with 6% Indium/1000 A^{o} Gold

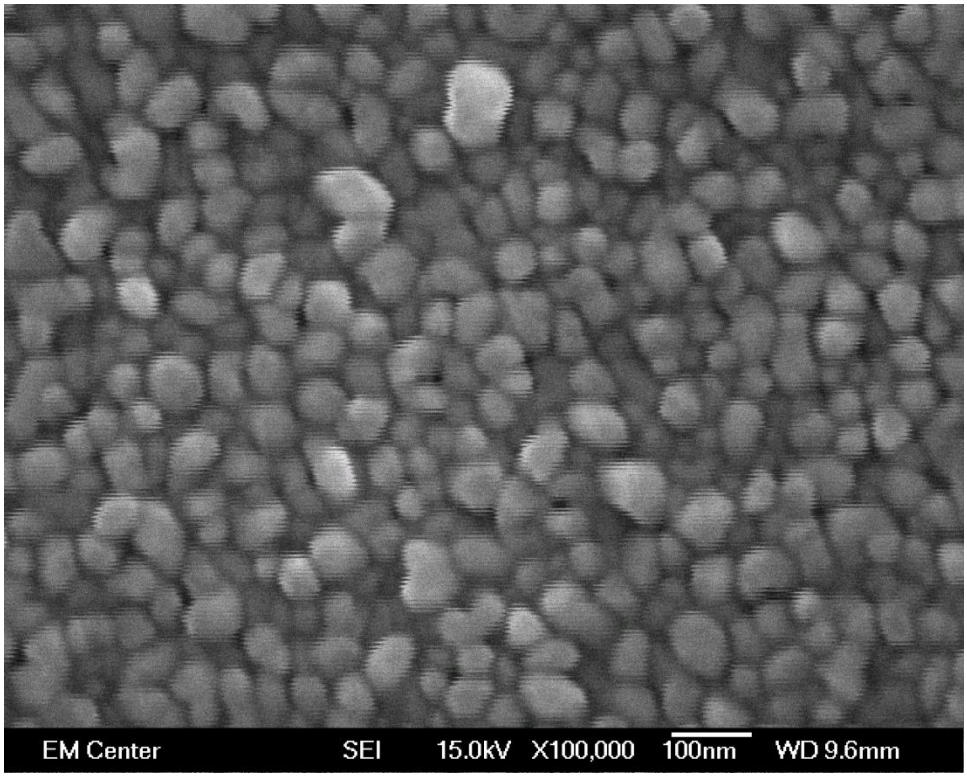

Figure 52: Image of the sample with 6% Indium under 1000A^{o} Gold film before annealing

In case of these films there is a definite change in the morphology of the sample after annealing. The precise mechanism of occurrence here is not understood. The solubility of Indium in Gold is known to be just under 6%[13].This is very close to the proportion of Indium against gold in this film. That is the only explainable cause for the change in morphology as it is observed here. More important observation here is that although there is a change in the morphology of the film, there is no sign of breaking down of the film or separation in the grain boundary.

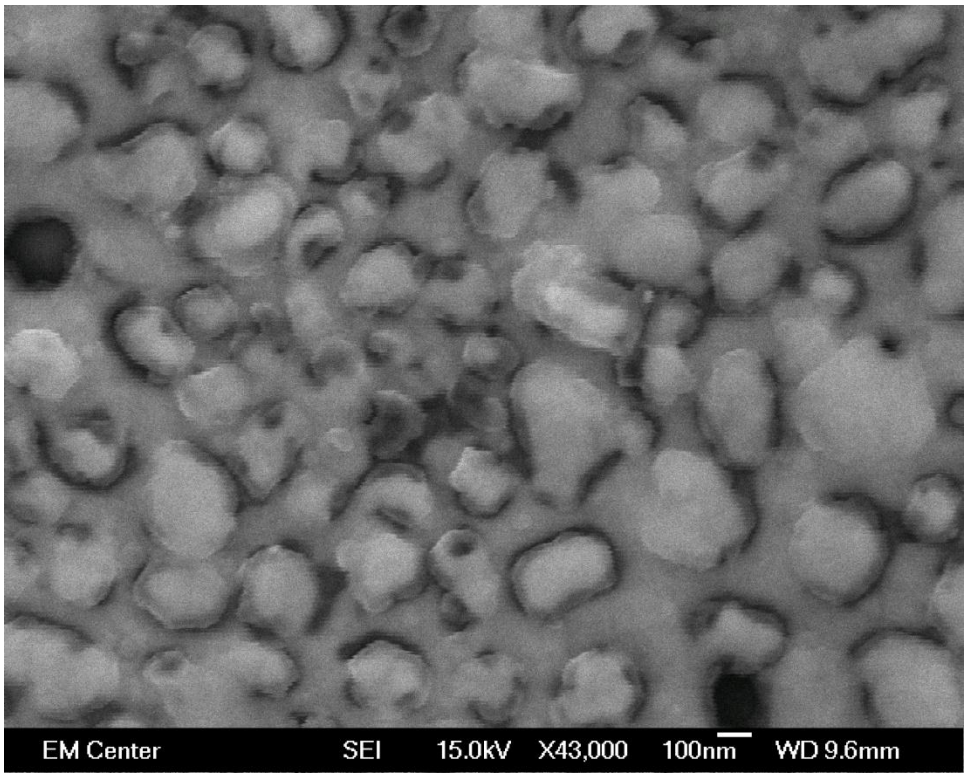

Figure 53: Image of the sample with 6% Indium under 1000A^{o} Gold film after annealing

7.6.3 Microscope Images of Film with 7.5% Indium/2000 A^o Gold

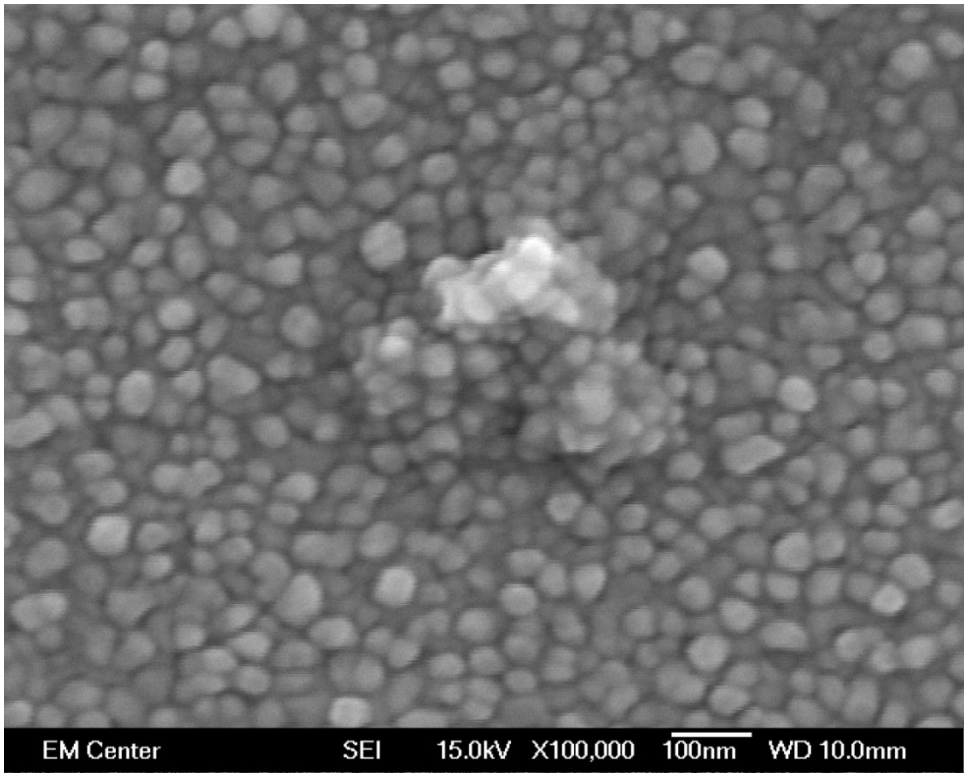

Figure 54: Image of the sample with 7.5% Indium under 2000A^o Gold film before annealing

These two films (before and after test) show extremely high resemblance. Both these films can easily be related. Except formation of a few pin holes, there is nearly no change in the morphology or texture of the film when observed through a SEM at 100000x magnification. The reason could be greater thickness of Gold on top of Indium. The layers underneath might have a changed morphology similar to what was observed in the 1000 A^o Gold film with 6% Indium after annealing. But since there is greater amount of gold creating a thicker film, it does not show up in the top layer. This could also well be the reason for better reflectivity of these films. Comparatively a lower Indium Oxide content on the surface which does not have a very good reflective properties may be the reason for better performance of these films.

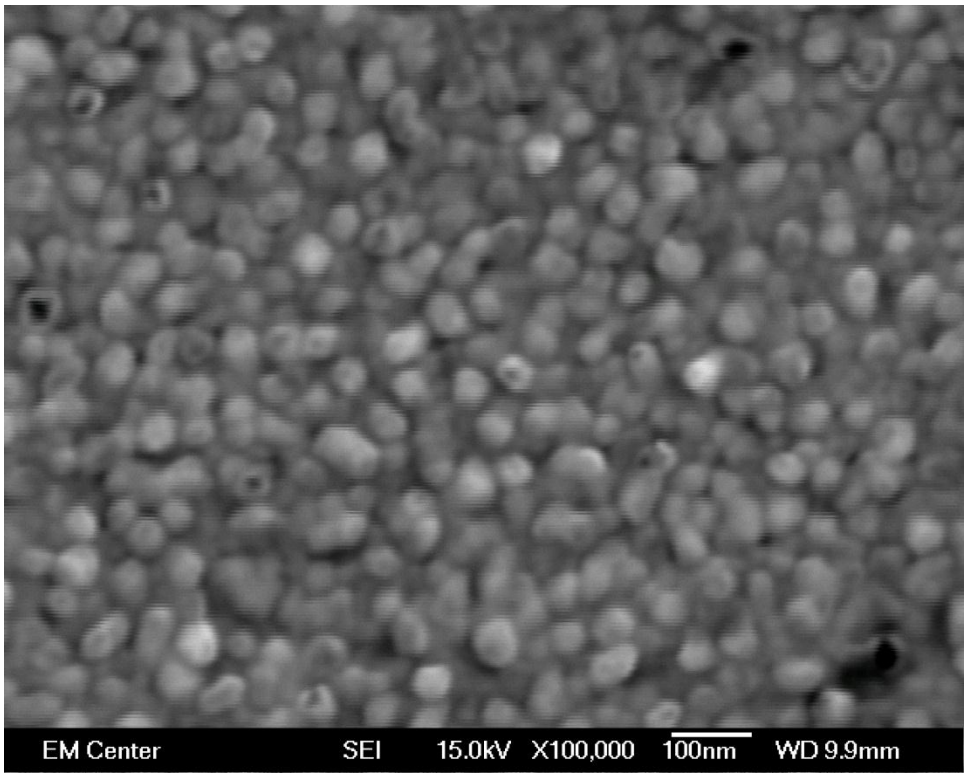

Figure 55: Image of the sample with 7.5% Indium under 2000A^{o} Gold film after annealing

As can be observed from the SEM images 7.5% Indium under 2000A^{o} of Gold film has less change after annealing than the 6% Indium with 1000 A^{o} of Gold. This shows that it is a close to optimum combination for the film thickness and underlay percentage. This observation is supported by other characterization methods like EDS and SWLI.

7.7 EDS Results for Samples Before and After Annealing

7.7.1 EDS scan of sample with 50% Indium under 800A^{o} of Gold

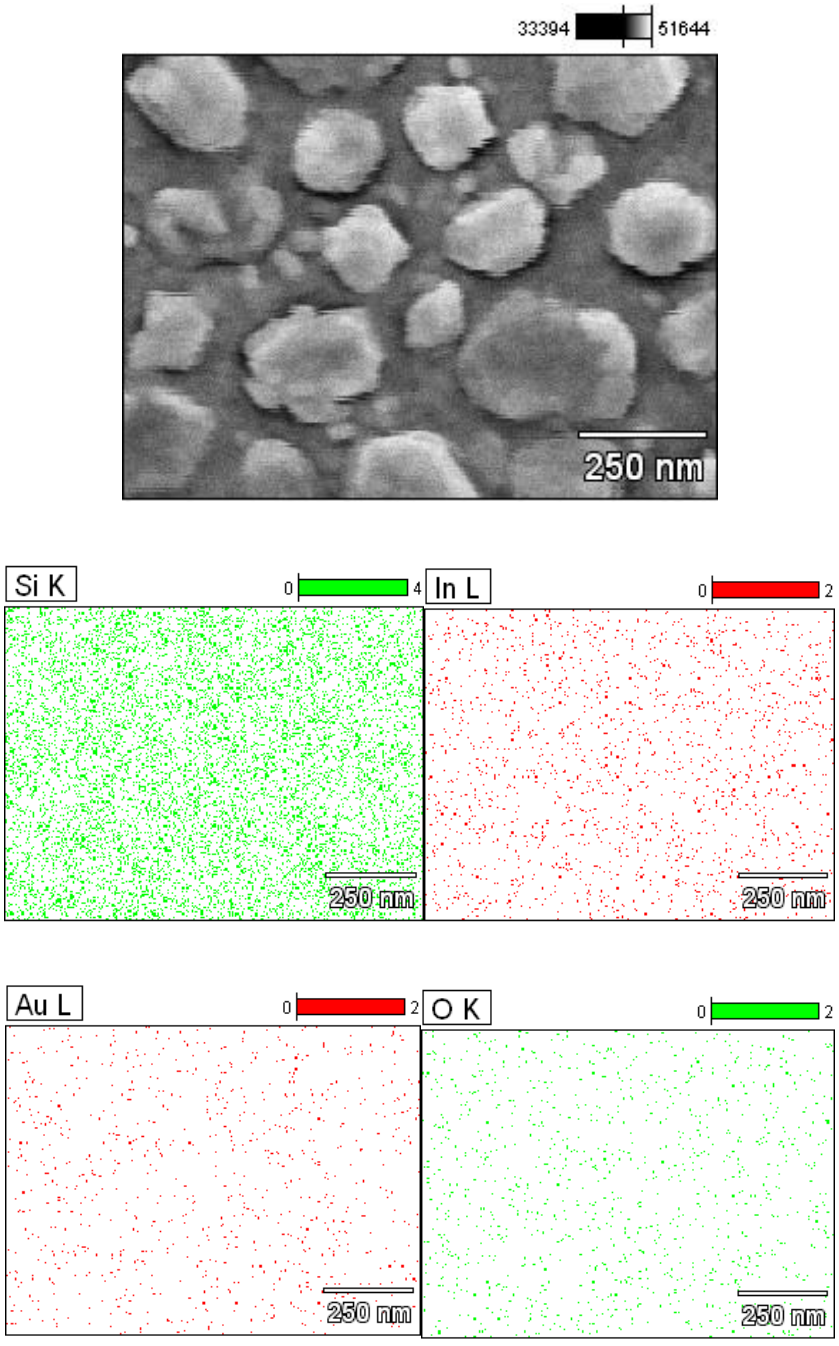

Figure 56: (Top) SEM image of region scanned (Bottom four) EDS material map of sample with 50% Indium under 800A^{o} of Gold before annealing (Acc. Voltage: 15.0 kV)

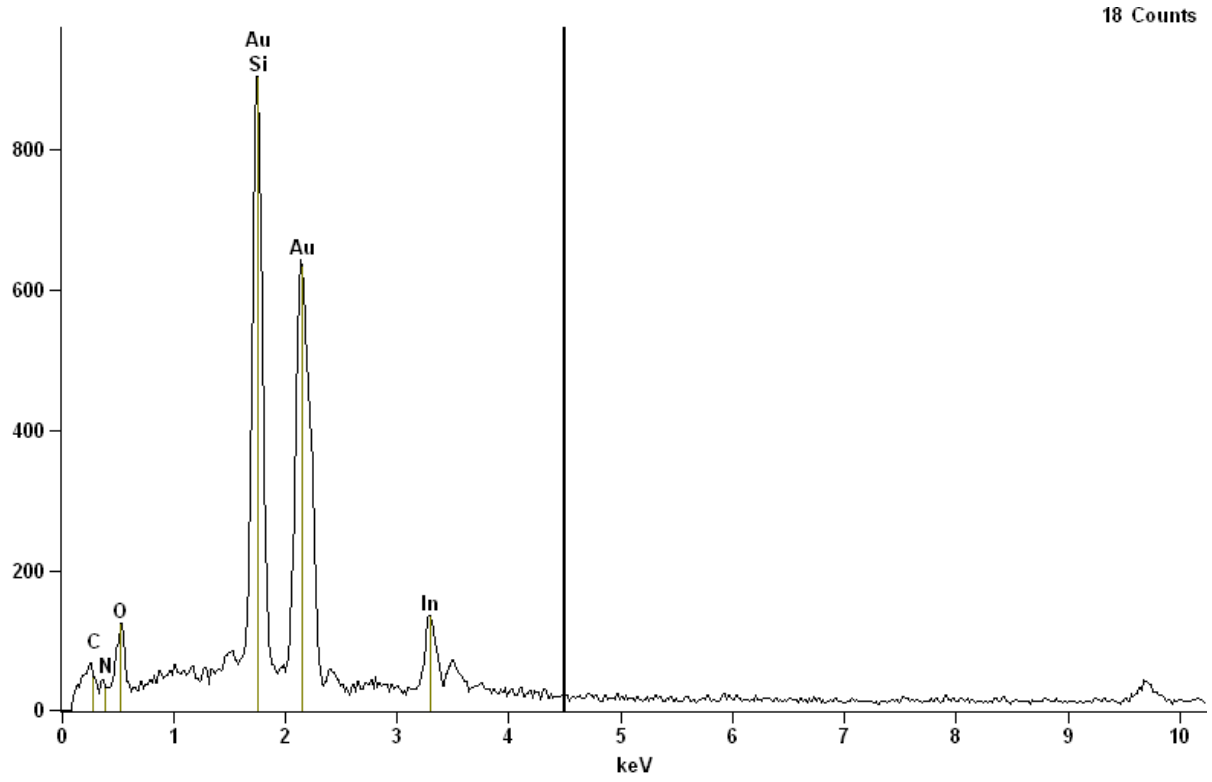

Figure 57: EDS scan of sample with 50% Indium under 800A^{o} of Gold before annealing (Acc. Voltage: 15.0 kV)

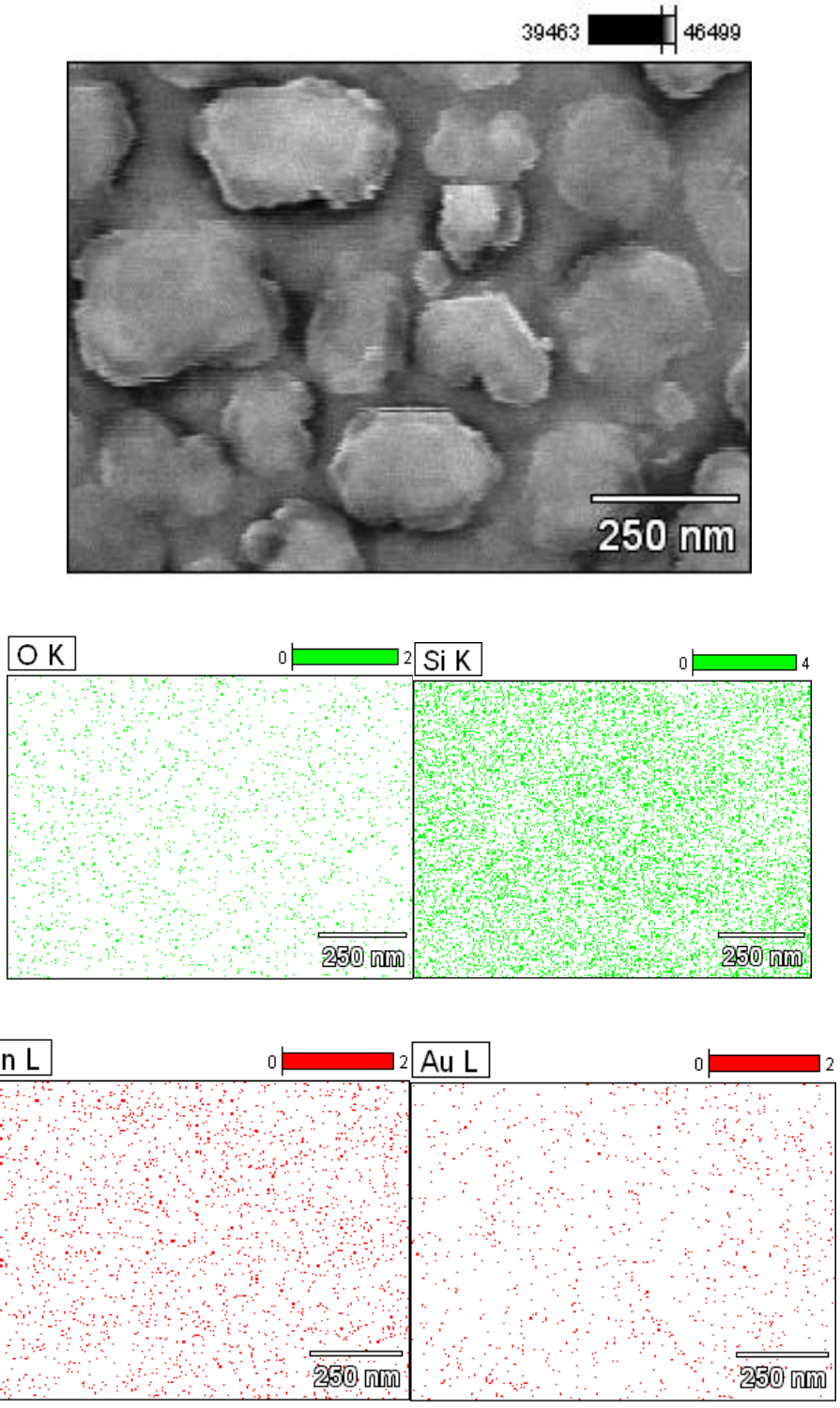

Figure 58: (Top) SEM image of region scanned (Bottom four) EDS material map of sample with 50% Indium under 800A^{o} of Gold after annealing (Acc. Voltage: 15.0 kV)

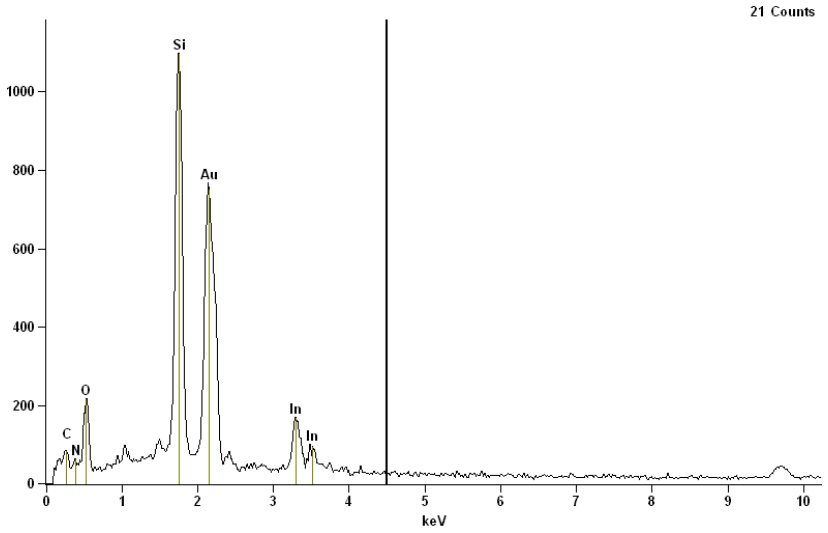

Figure 59: EDS scan of sample with 50% Indium under 800A^{o} of Gold after annealing (Acc. Voltage: 15.0 kV)

As can be seen in the EDS plots above, Gold does not entirely cover the Indium layer. Indium is exposed to ambient environment and can oxidize. Also, Silicon Oxide visible here, may not necessarily imply that the film is breaking down and exposing the substrate. Accelerating voltage used here is fairly large and the electron beam may be penetrating though the top layer of Gold and Indium. So the Silicon Oxide that can be seen may still be under the layer of Gold and Indium thin film.

7.7.2 EDS scan of sample with 6% Indium under 1000A^{o} of Gold

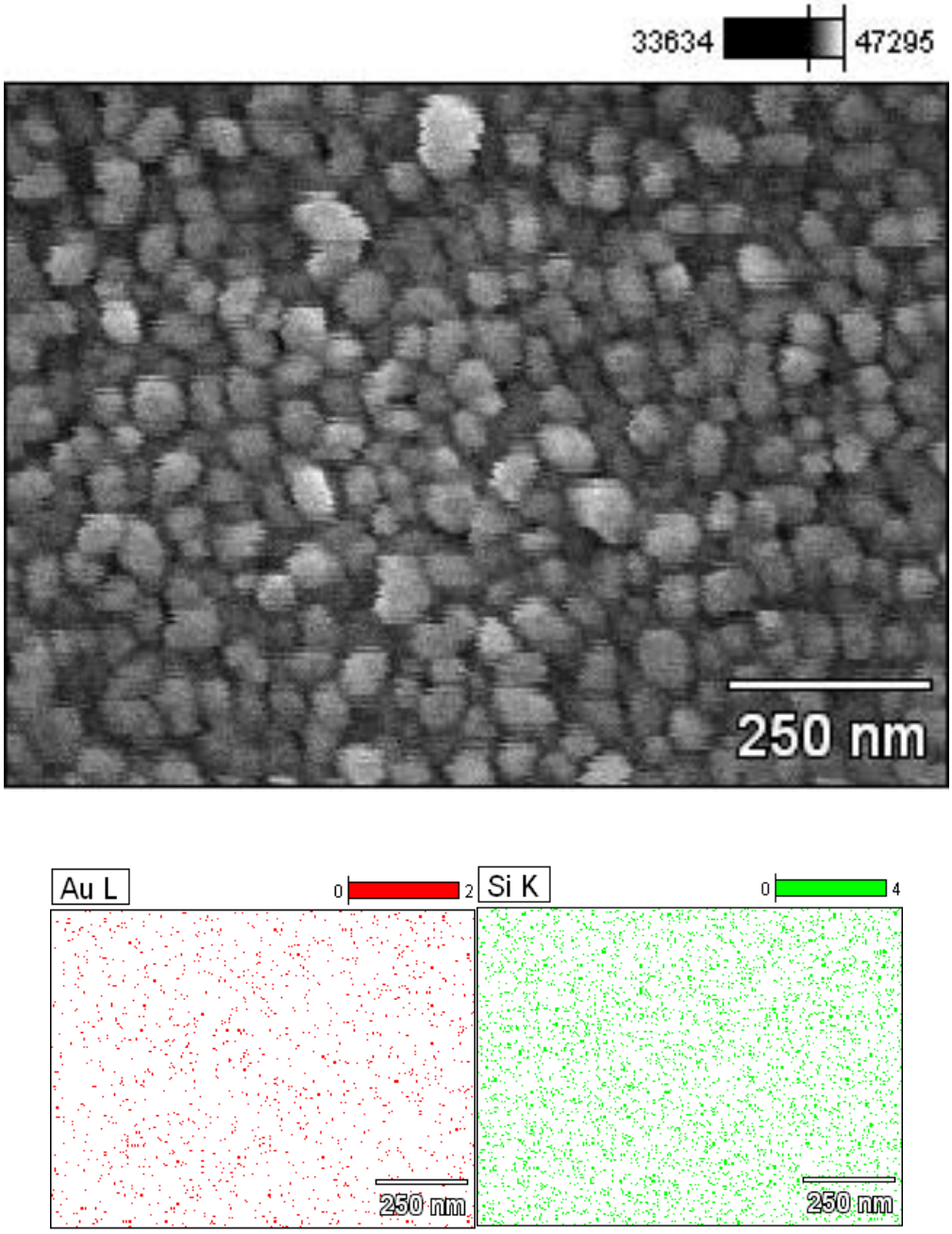

Figure 60: (Top) SEM image of region scanned (Bottom two) EDS material map of sample with 6% Indium under 1000A^{o} of Gold before annealing (Acc. Voltage: 15.0 kV)

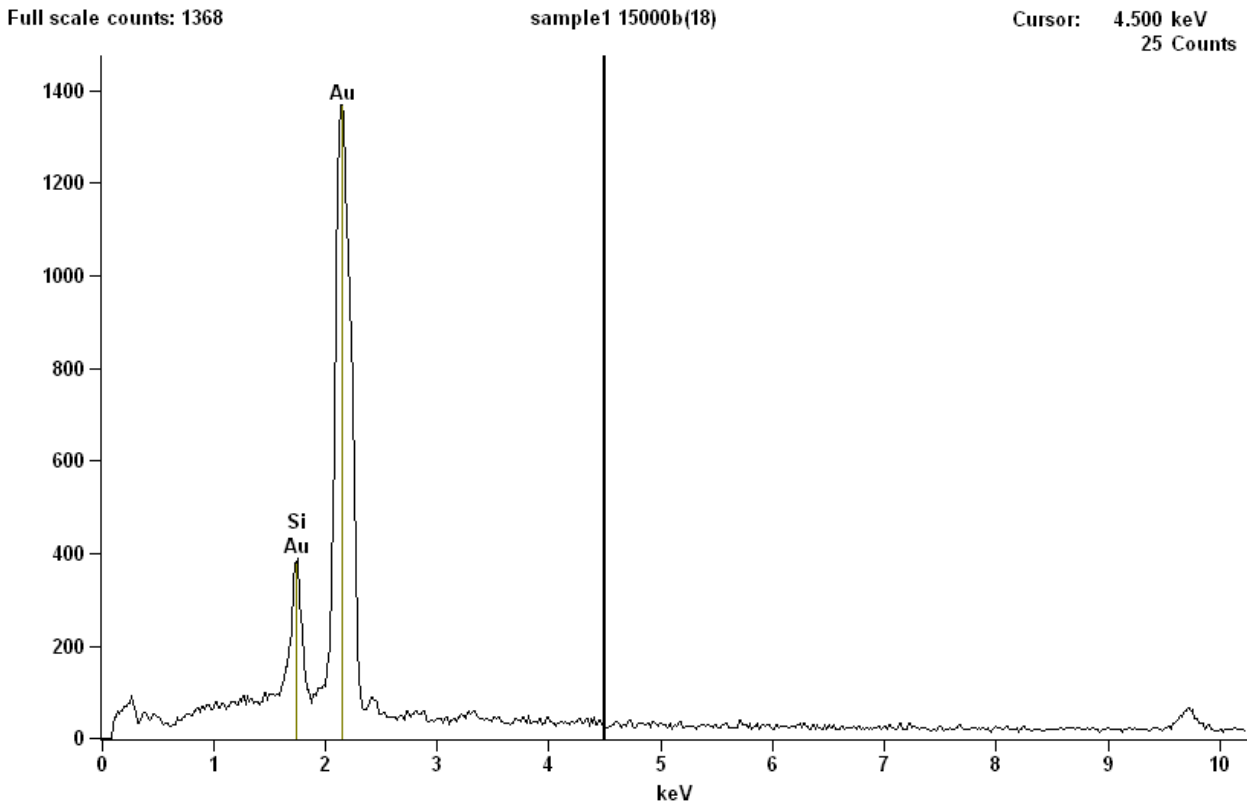

Figure 61: EDS scan of sample with 6% Indium under 1000A^{o} of Gold before annealing (Acc. Voltage: 15.0 kV)

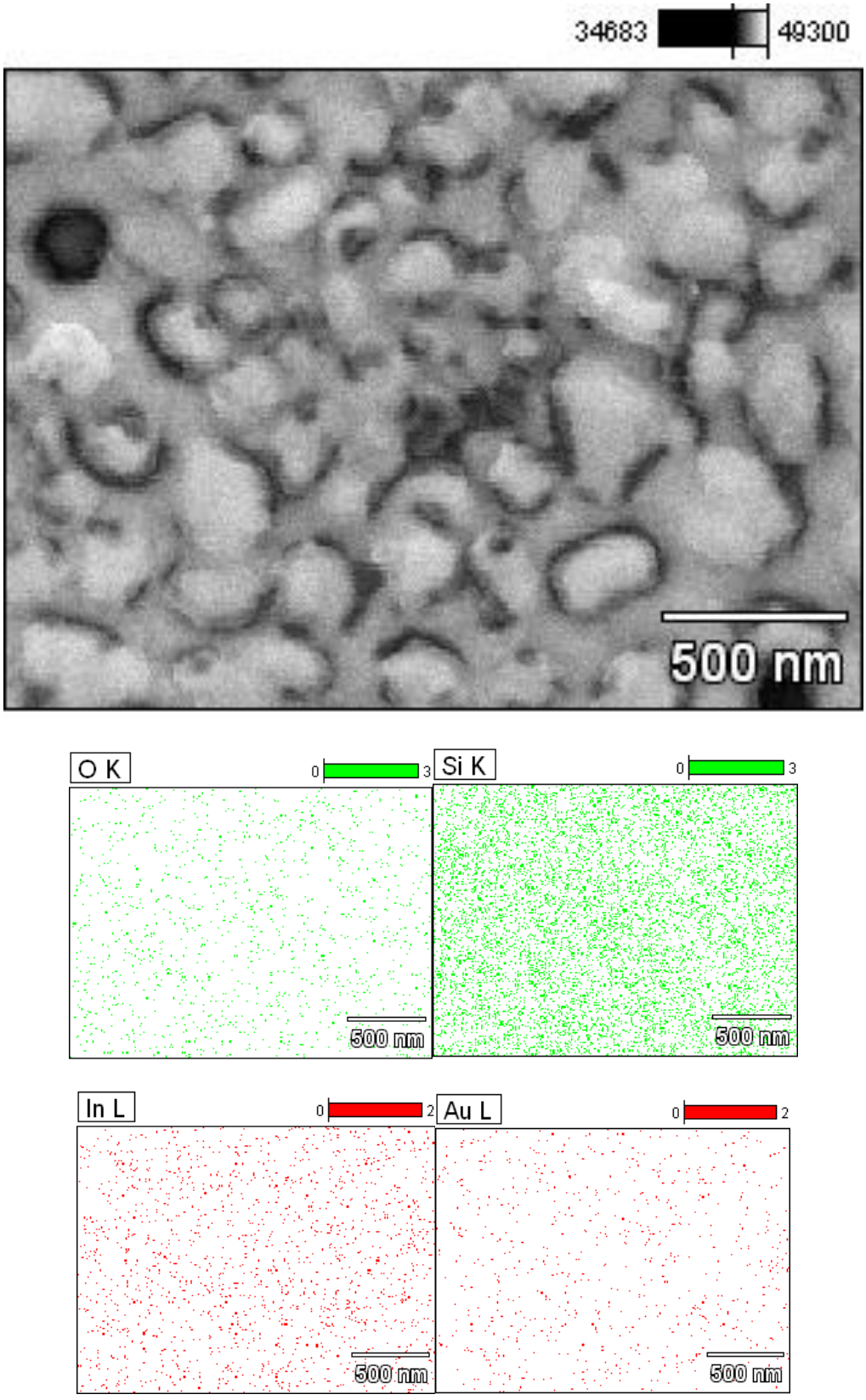

Figure 62: (Top) SEM image of region scanned (Bottom four) EDS material map of sample with 6% Indium under 1000A^{o} of Gold after annealing (Acc. Voltage: 15.0 kV)

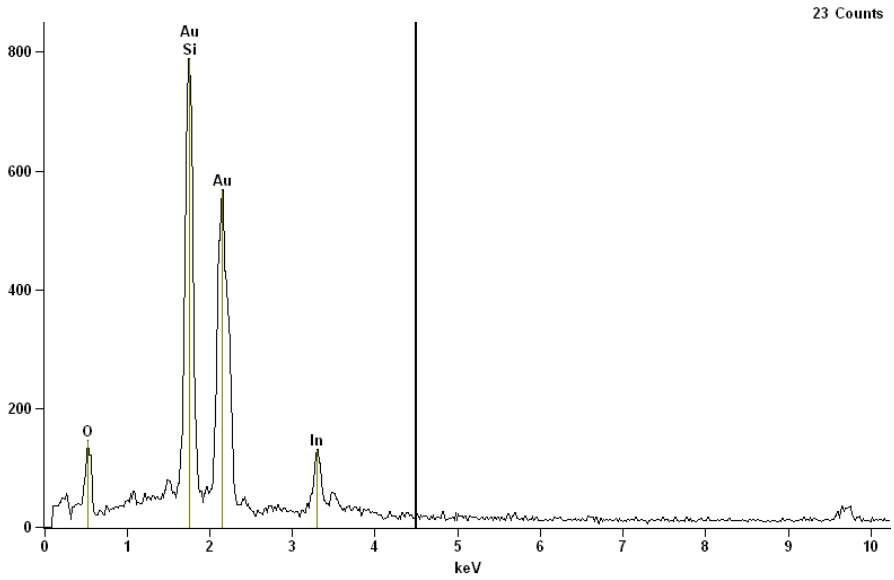

Figure 63: EDS scan of sample with 6% Indium under 1000A^{o} of Gold after annealing (Acc. Voltage: 15.0 kV)

Looking at the EDS scan of the second sample before annealing suggests that Gold film has a very uniform and stable cover over Indium underlay. EDS does not detect any Indium before it was annealed. After it was annealed, EDS could detect contents of Indium. This observation supports the observation made thorough SEM where annealing caused Indium to alloy with Gold and form a solid solution. As it is known, Indium has about 6% solubility in Gold and that is the proportion of Indium in this film. Silicon is detected from the substrate. Oxide visible in the scan after annealing can be either from SiO_2 substrate or from the formation of Indium Oxide at the surface or both. Although an attempt was made to simulate vacuum using Argon environment, presence of small amount of Oxygen cannot be eliminated. Due to this, the presence of Indium Oxide cannot be completely ruled out.

7.7.3 EDS scan of sample with 7.5% Indium under 2000A^{o} of Gold

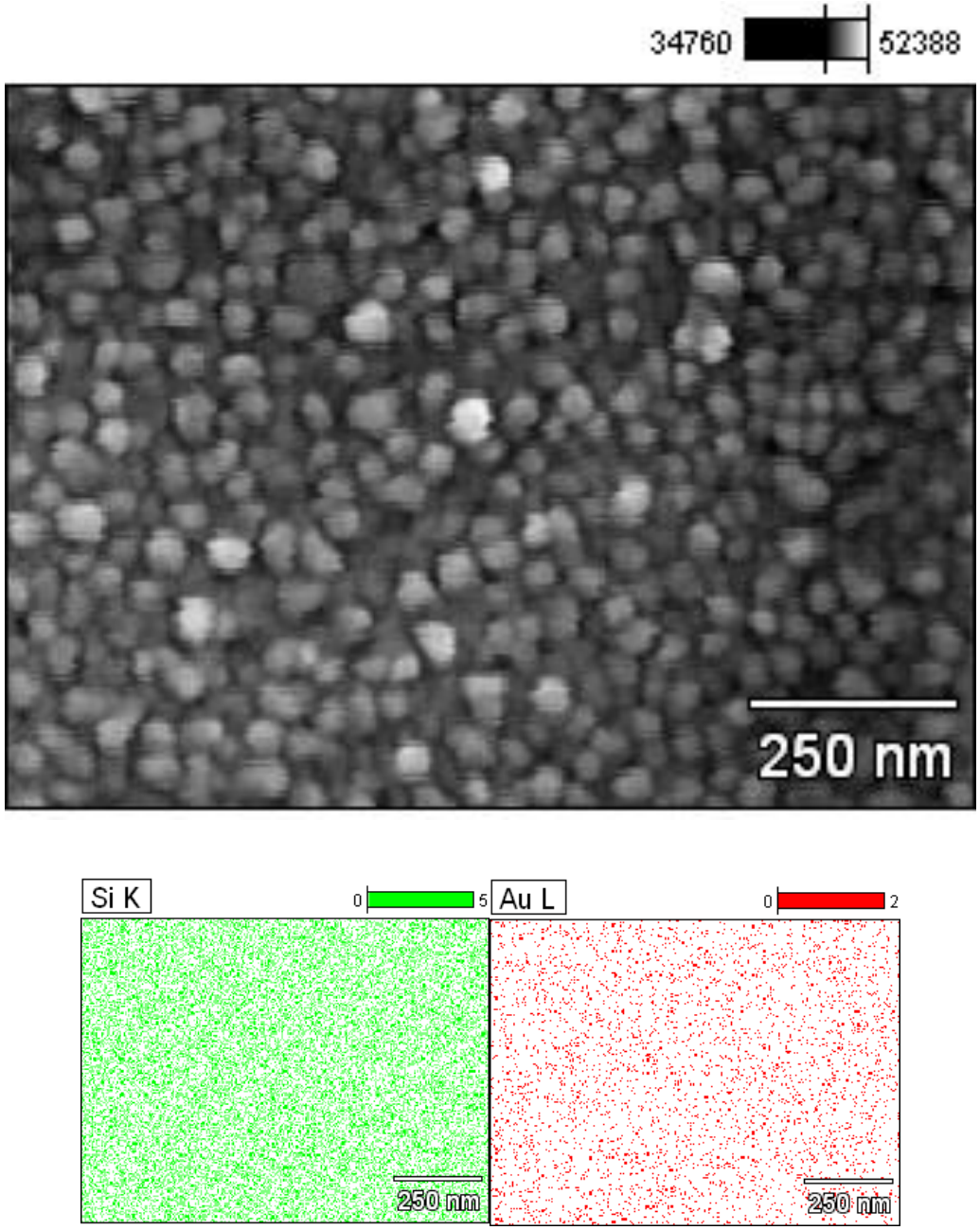

Figure 64: (Top) SEM image of region scanned (Bottom two) EDS material map of sample with 7.5% Indium under 2000A^{o} of Gold before annealing (Acc. Voltage: 15.0 kV)

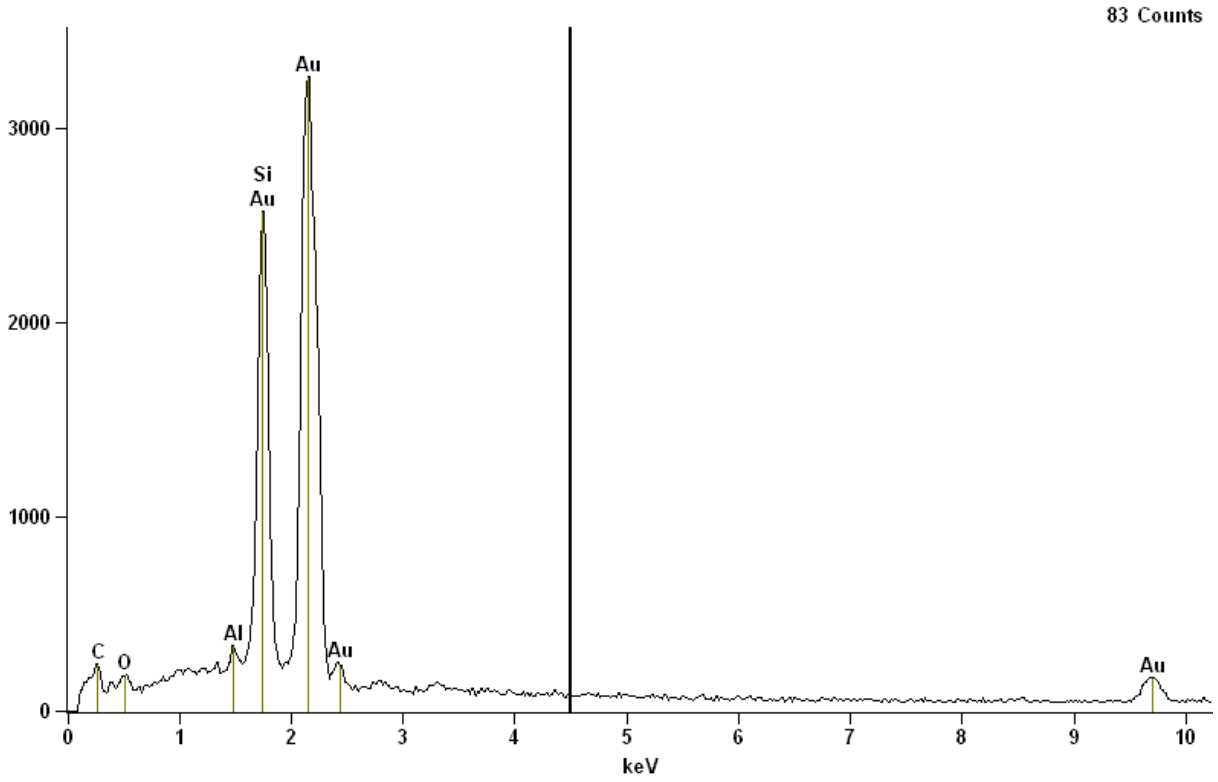

Figure 65: EDS scan of sample with 7.5% Indium under 2000A^{o} of Gold before annealing (Acc. Voltage: 15.0 kV)

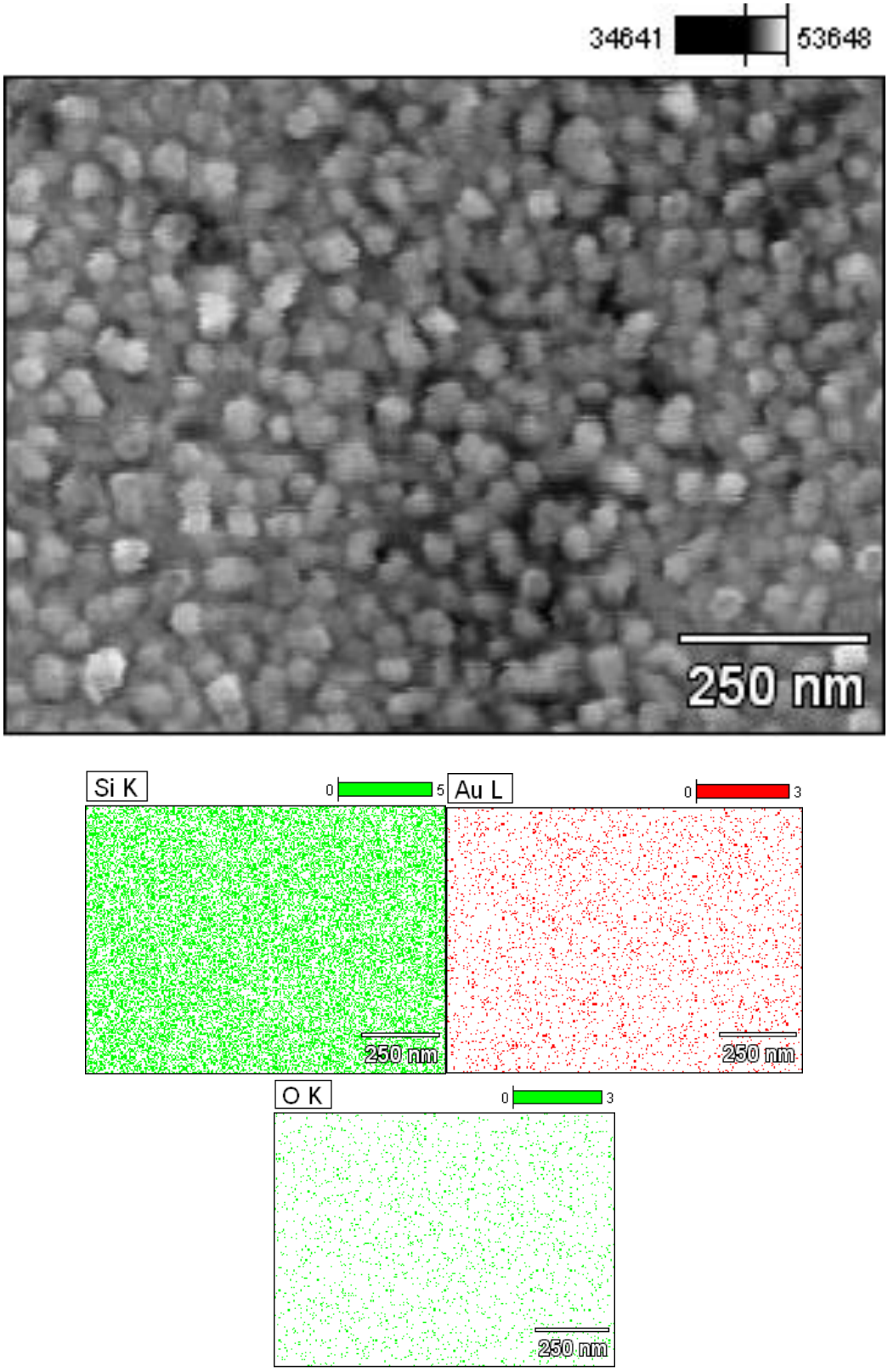

Figure 66: (Top) SEM image of region scanned (Bottom three) EDS material map of sample with 7.5% Indium under 2000A^{o} of Gold after annealing (Acc. Voltage: 15.0 kV)

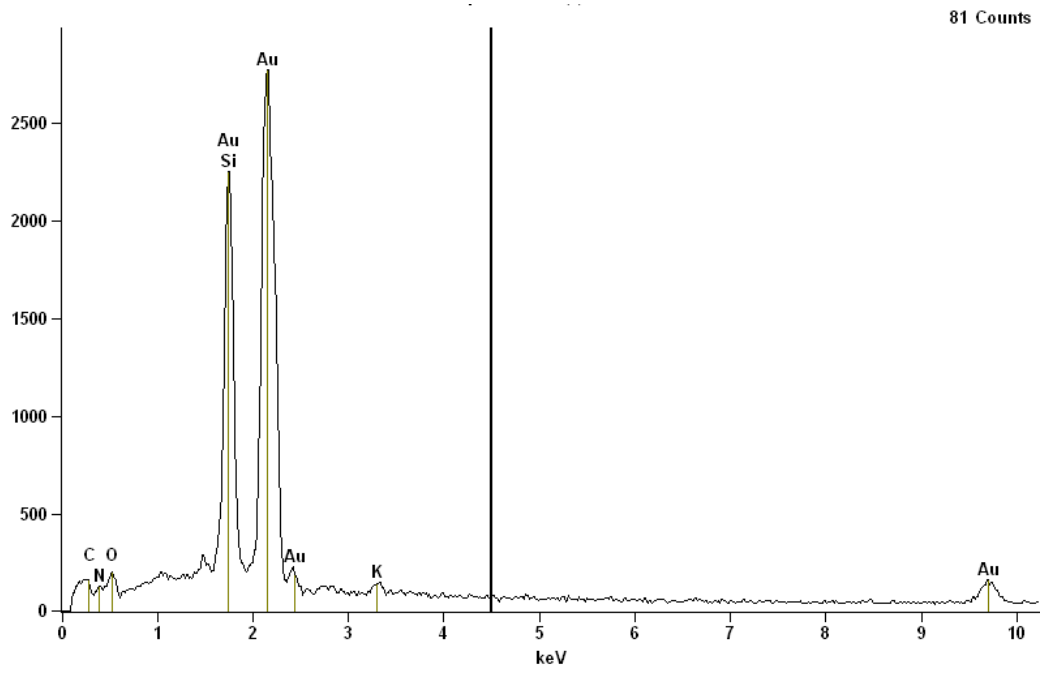

Figure 67: EDS scan of sample with 7.5% Indium under 2000A^{o} of Gold after annealing (Acc. Voltage: 15.0 kV)

The third sample with 7.5% Indium and 2000A^{o} seems to be the best performing sample. SEM suggested that there was nearly no physical deformation. Except a few pin holes all else seems to be same in case of before and after annealing. Moreover, even EDS suggest similar results. There is almost no change in the EDS results from before and after the mirrors were annealed. No Indium is detected in either of the scans showing that the film is seeing nearly no change at the surface. Alloying of Indium and Gold occurs at the layers underneath and doesn't affect the surface. Although these layers underneath allow the film to be exposed to high temperature without losing the composition.

7.8 SWLI Surface Roughness Measurements for Samples Before and After Annealing

7.8.1 SWLI roughness measurement for samples with 50% Indium under 800 A^{o} Gold

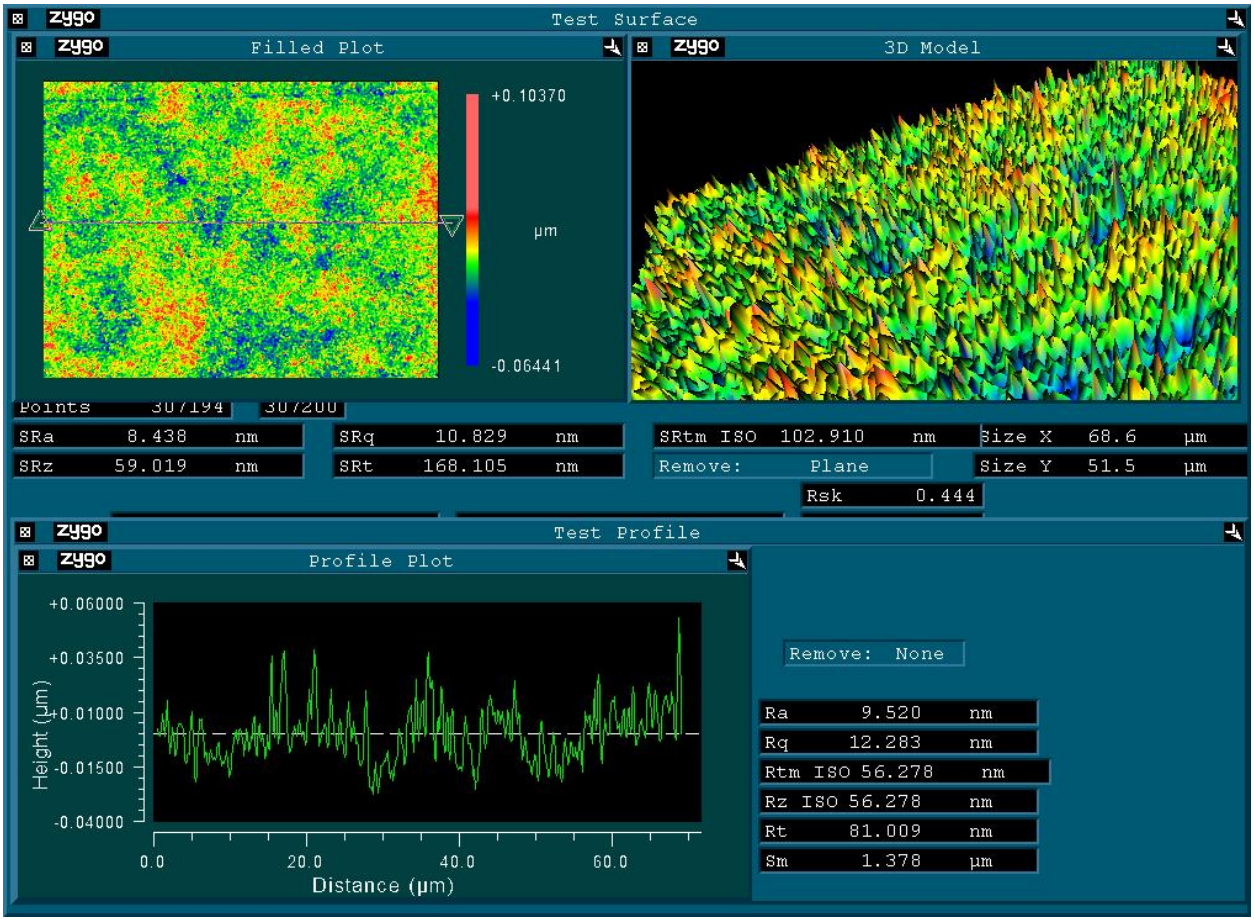

Figure 68: Image of SWLI roughness measurement for samples with 50% Indium under 800 A^{o} Gold before annealing

Using SWLI the surface roughness can be measured. The mean roughness here for the first sample with 50% Indium under 800A^{o} Gold is 102.910 nm before annealing and sees almost no change after it is exposed to high temperature. However, it is important to notice that although the change is negligible but the value itself is much higher as compared to the other two cases.

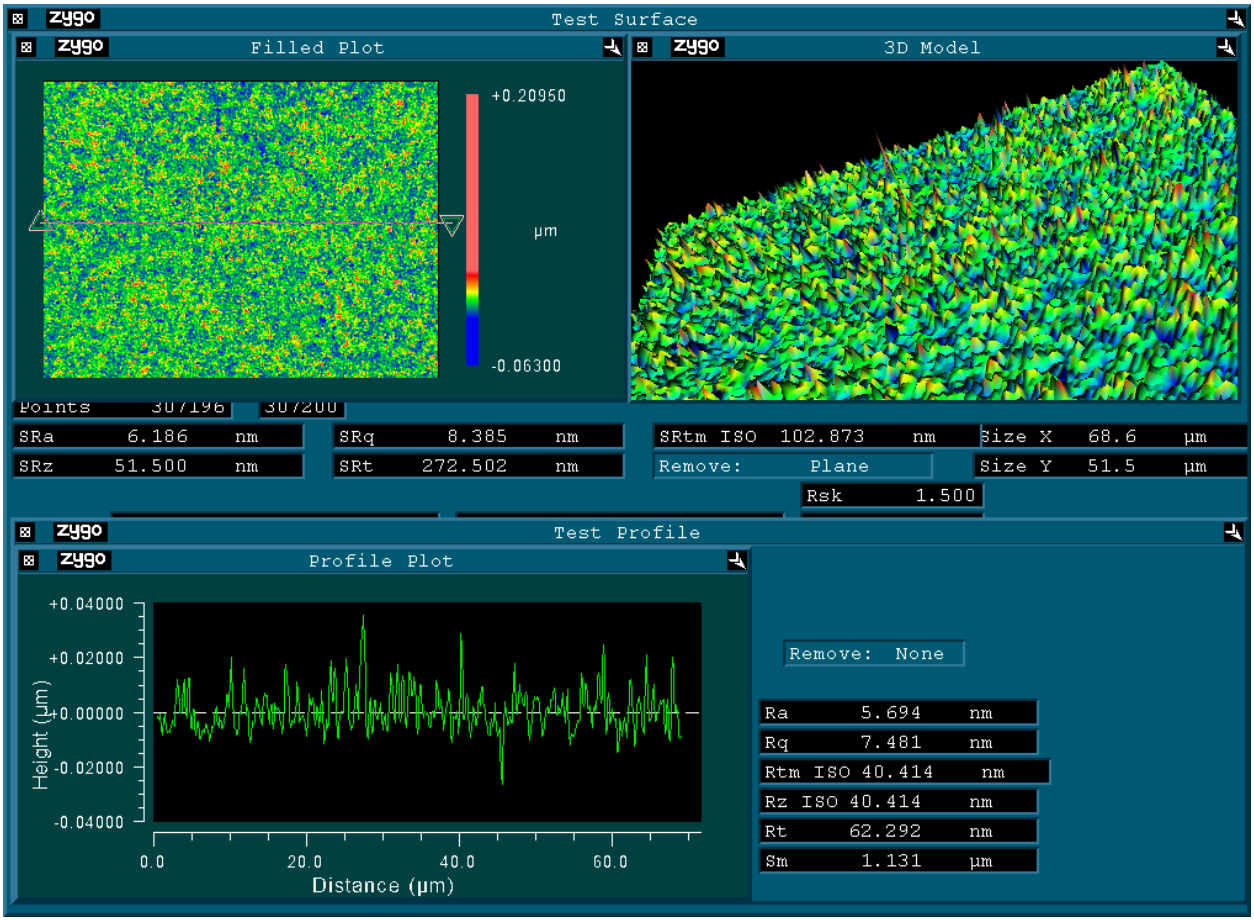

Figure 69: Image of SWLI roughness measurement for samples with 50% Indium under 800 A^{o} Gold after annealing

7.8.2 SWLI roughness measurement for samples with 6% Indium under 1000 A^{o} Gold

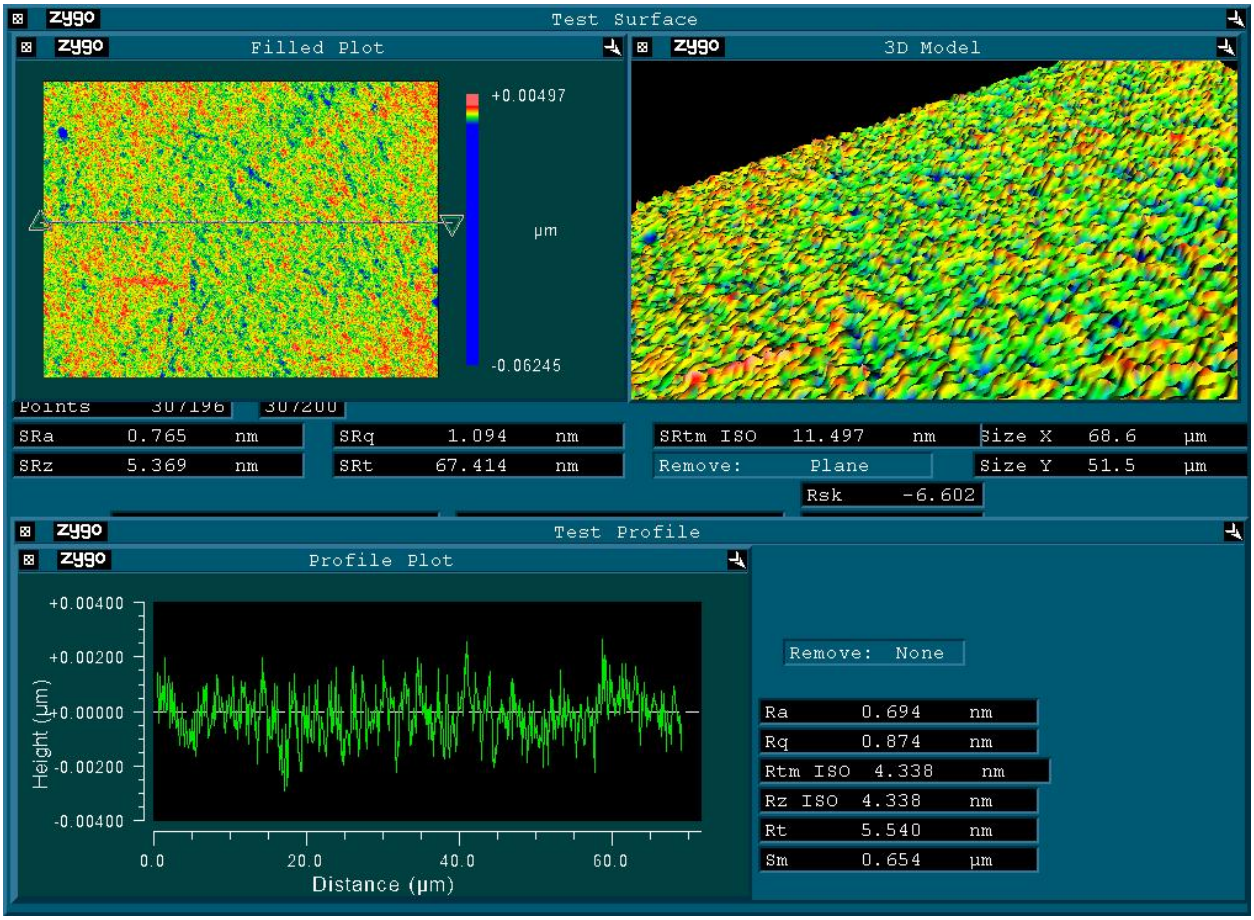

Figure 70: Image of SWLI roughness measurement for samples with 6% Indium under 1000 A^{o} Gold before annealing

The mean roughness increases from 11.497 nm to 48.065 nm with the sample that contained 6% Indium with a 1000A^{o} Gold film. So there is a significant change but it must be considered that in spite of the change by over almost 4 times, the sample still has a much lower surface roughness as compared to the first sample. This is another indication that this proportion of Indium is around the optimum amount for fabrication of thin Gold films for high temperature application.

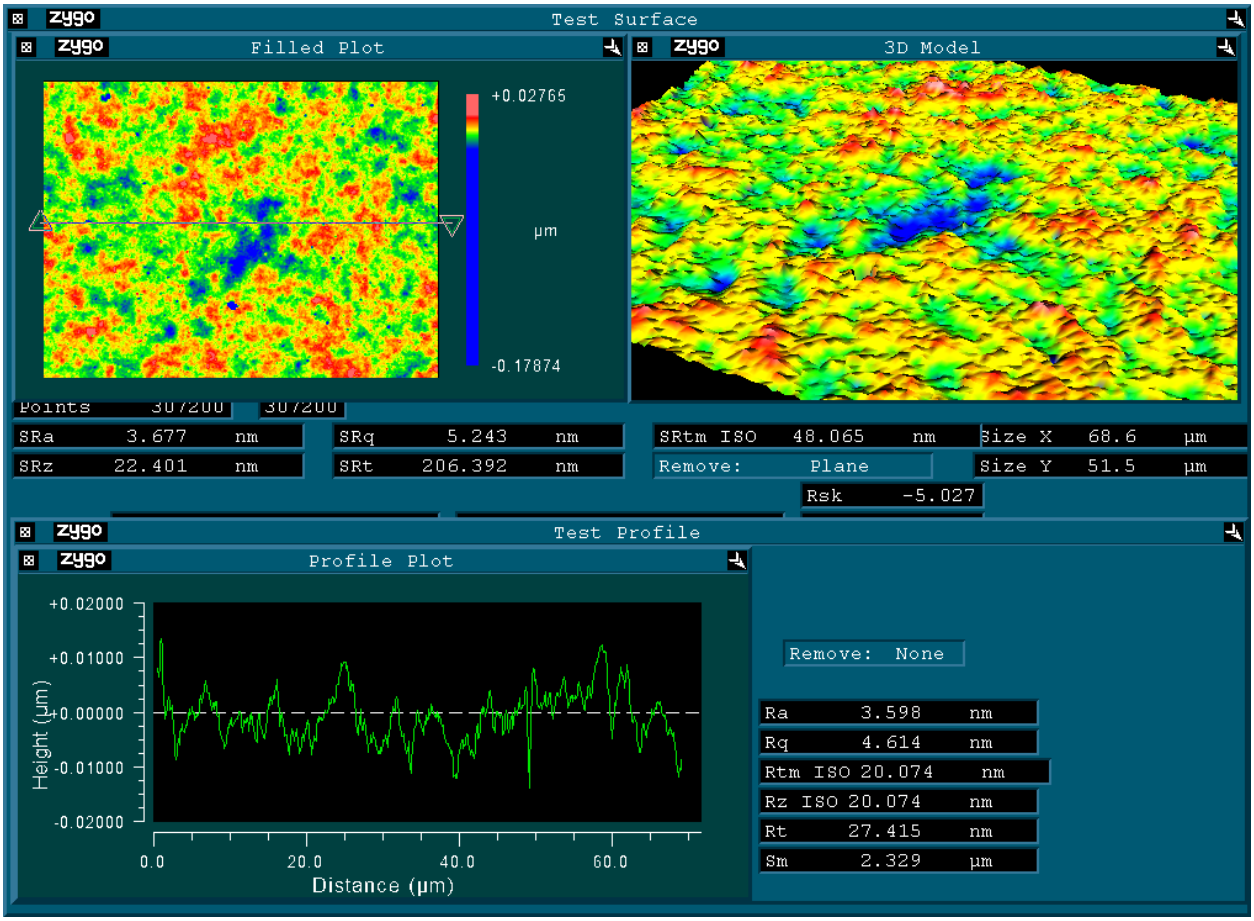

Figure 71: Image of SWLI roughness measurement for samples with 6% Indium under 1000 A^{o} Gold after annealing

7.8.3 SWLI roughness measurement for samples with 7.5% Indium under 2000 A^{o} Gold

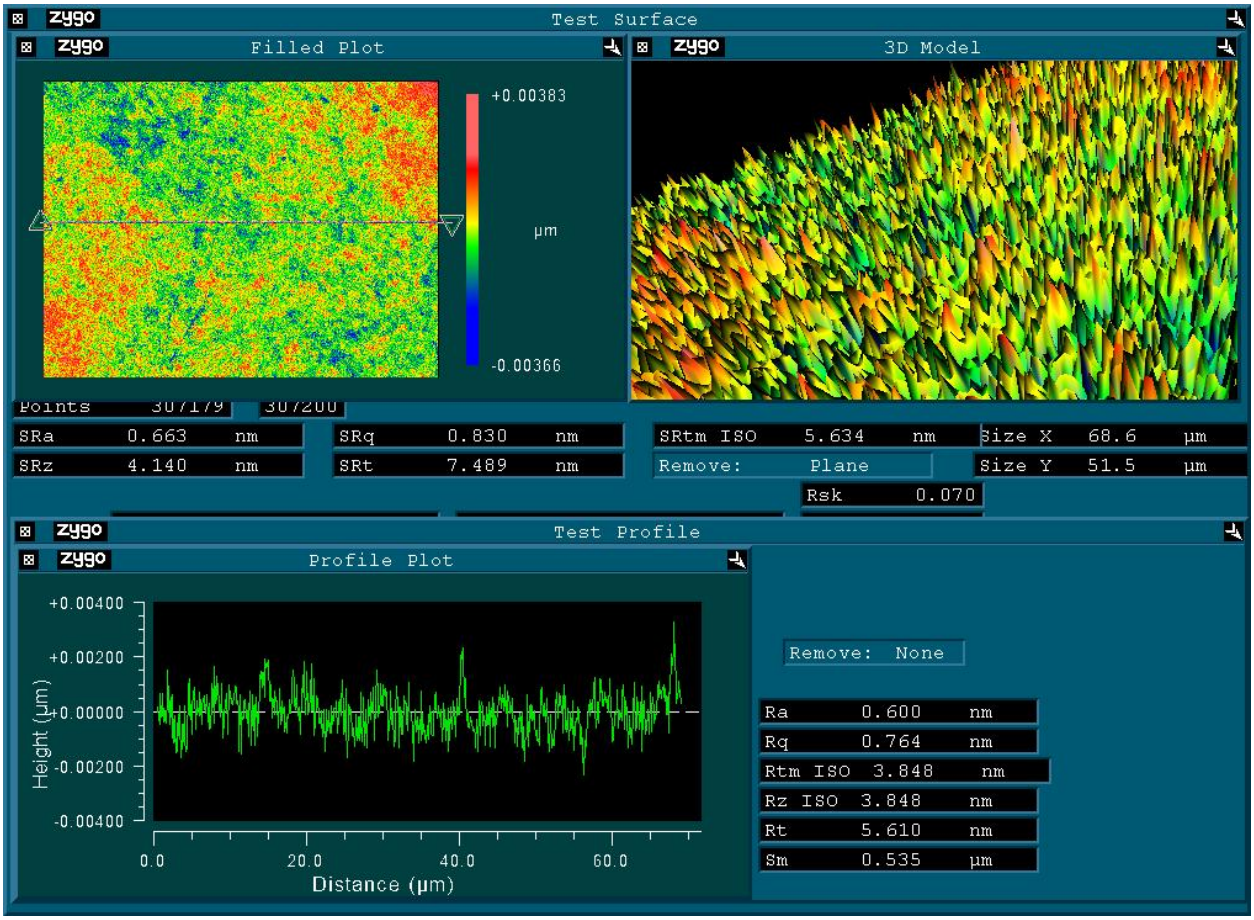

Figure 72: Image of SWLI roughness measurement for samples with 7.5% Indium under 2000 A^{o} Gold before annealing

SWLI surface roughness measurement again provides support to the study that 7.5% Indium underlay with a little thicker (2000 A^{o}) Gold film gives the best performing thin Gold film mirror. The mean roughness is much lower than all the other films by a significant value. Mean roughness is about 5 nm before annealing while it gets to only 20.068 nm after annealing. This also means that there would be lower scattering of radiation that is reflected after being incident on the surface.

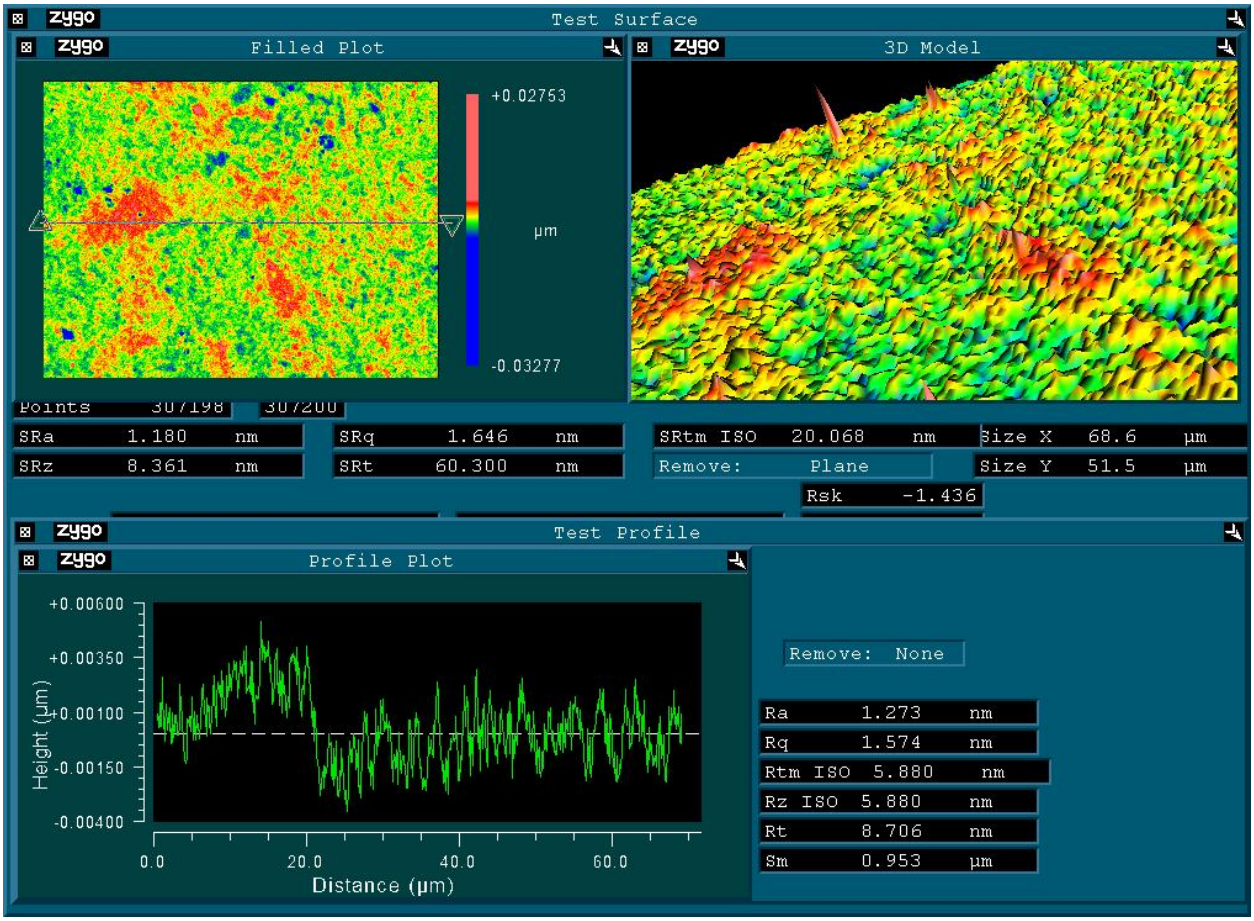

Figure 73: Image of SWLI roughness measurement for samples with 7.5% Indium under 2000 A^{o} Gold after annealing

All the tests and analysis suggest that among the combinations tested the mirror with 7.5% Indium underlay with 2000A^{o} of Gold gives the best performing mirror. Reflection measurements provide a metric that allows evaluation of the performance. After annealing, the mirror performs better in the infrared spectrum which is the area of interest. The SEM, EDS and SWLI analysis provides the understanding of what makes this a better combination of proportion and film thickness.

The reason for better performance of the film can be thus explained. Melting point of Indium is at 156.59^{o}C which is way lower than that of Gold and the operating temperature. However, Indium Oxide has a melting temperature of 1910^{o}C. Also, the maximum solubility of Indium in Gold is 6%. When exposed to high temperature it is possible that molten Indium takes up the spaces between the grains of

Gold and acts as an adhesive. When it comes in contact with the ambient environment and spontaneously forms an oxide. This oxide has a very high melting point and thus provides the layer underneath protection against physical deformation. All of these contribute to maintain the film composition and keep Gold film from undergoing grain boundary separation that ultimately leads to island formation.

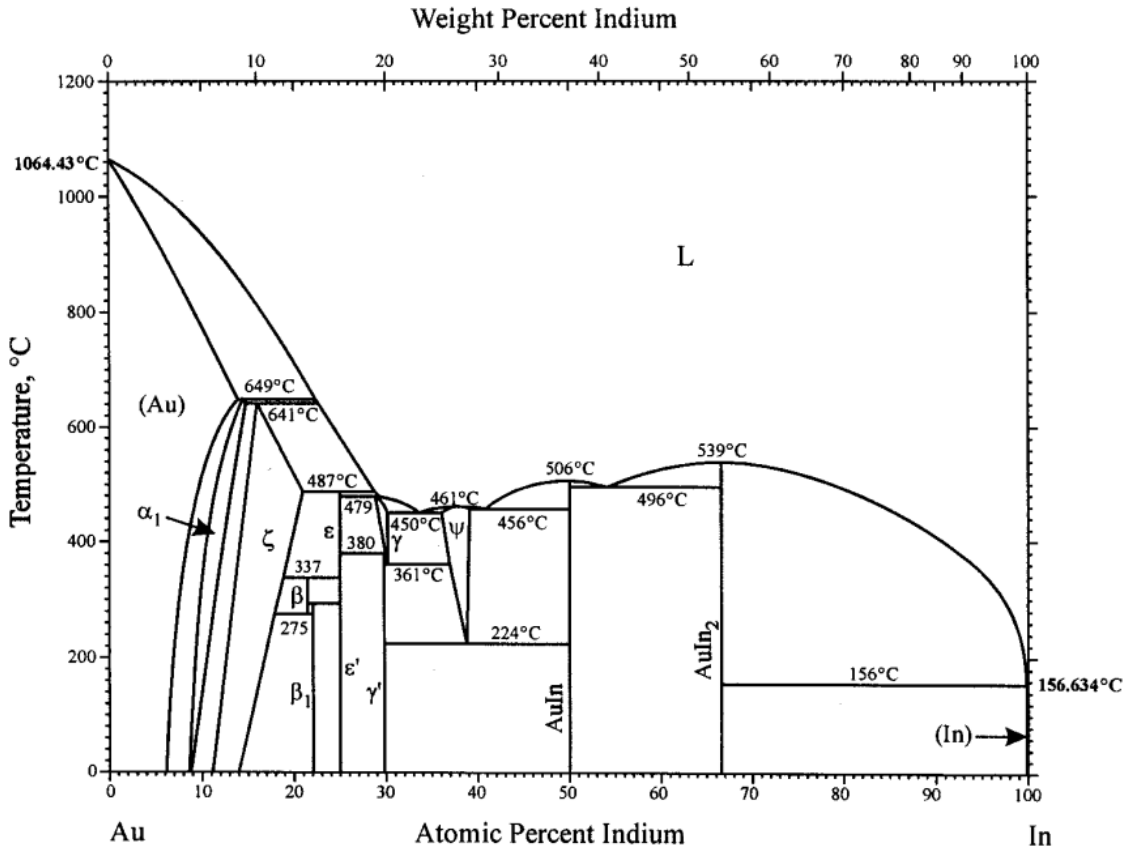

Figure 74: Indium Gold phase diagram.

CHAPTER 8. CONCLUSION AND FUTURE PROSPECT OF STUDY

8.1 Table of observations:

	IR Reflectivity	SEM imaging	EDS mapping	SWLI
Edmund Optics	Falls to below 50% after annealing	Clear island formation post annealing. Renders the film transparent and loss of luster.	Shows various phases with uneven material distribution after annealing.	Root mean square surface roughness changes from 3.673 nm to 5182.197nm. A very large change.
Thor labs	Improves after annealing but is still below 80%	Does not show signs of island formation. Maintains luster but film and SiO layer seem to be separating and pealing. Cracking of SiO layer.	Shows various phases with uneven material distribution after annealing.	Avery clear difference cannot be explained by numbers. But images and surface morphology show considerable increase in surface roughness after annealing.
50% In with 800 A^o Au	Falls below 50% after annealing	Film didn't show any deformation or blisters after annealing but lacks consistency.	In, Si and Au visible before and after annealing.	Root mean square surface roughness remains at approximately 102 nm. No change but not too good to start with.
6% In with 1000 A^o Au	Improves after annealing and is around 97%.	After annealing the close to optimum film looks similar to 50% In with 800 A^o Au film. Performs better but has signs showing deformation.	Only Au visible before annealing but In and Au show up after annealing. Shows oozing of In to the surface.	Root mean square surface roughness changes from 11.497 nm to 48.065 nm. A very small change. Shows lower scattering of reflected radiation.
7.5% In with 2000 A^o Au	Improves after annealing and stays above 98%.	Nearly no change from the surface before annealing. Film remained almost completely intact.	Nearly no difference between the EDS before and after annealing. No In visible in either case.	Root mean square surface roughness changes from 5.634 nm to 20.068 nm. A very small change. Shows lower scattering of reflected radiation.

8.2 Conclusion

Gold thin films are highly chemically stable but undergo deformation on exposure to temperatures in excess of 300^{o}C. This is because of the phenomenon called grain boundary separation that ultimately leads to diffusion and island formation. This is not desirable for gold thin films to be used as a reflector for infrared radiation at high temperature, in spite of gold itself possessing excellent emissivity characteristics.

To use Gold thin films for radiation shield application it is necessary to have an underlay of another metal that has a lower melting temperature and is more ductile. Under most circumstances chromium and tin serve the purpose[15]. However in excess of 500^{o}C, both chromium and tin prove to be ineffective. In this situation it was shown that Indium underlay provides adhesive characteristics, not only between the film and the substrate but also between the grains of gold. This resists grain boundary separation.

This study was aimed at finding out combination of underlay metal with gold, optimum proportion and film thickness that together would provide the best resistance to the above stated phenomenon of deformation. At the end of this study, it was discovered that out of various combinations that were considered, 7.5 % indium by weight underlay with 2000 A^{o} of Gold provides the best resistance against grain boundary separation. This shows its potential application as an industrial radiation shield, in situations where the primary mode of heat loss is radiation.

8.3 Scope of Future Study

- Although literature suggests that gold thin films have nearly the same reflectivity in the infrared spectrum at elevated temperatures as at room temperature[26], an appropriate apparatus would allow measurement of reflectivity at operating temperature. This would provide a concrete proof that these shields can be used as an industrial solution to avoid radiation heat loss and thus provide higher thermal efficiency to the operating system.

- The duration of the tests were limited due to the availability of laboratory apparatus. More cycles of 200 hours and their analysis using techniques like SEM, EDS, SWLI, etc. would give a better estimate of the life of these shields and the associated economics.
- If it is necessary to reduce the temperature of the first radiation shield, possibility of using high reflectivity Accuflect Ceramic materials as the first radiation shield can be researched[27]. Subsequent shield should be still made out of gold on glass substrate so that the advantage of high emissivity of gold is not eliminated. Such a setup can also be used for substantially higher temperatures than used in this study.

REFERENCES

1. Administration, U.S.E.I., *International Energy Outlook.* U.S. Department of Energy, Washington, D.C., 2010.
2. Solomon, S., et al., *Technical summary*. 2007.
3. Solar, H.S.G.-F., *First Solar revenues decline, margins maintained in 3Q 2012 as manufacturing prices fall.* Solar Server - Online Portal to Solar Energy, 2012.
4. Barth, K.L., R.A. Enzenroth, and W.S. Sampath, *Apparatus and processes for the massproduction of photovotaic modules*. 2002, Google Patents.
5. Mochizuki, K., *Vapor growth of CdTe at low temperatures.* Journal of Crystal Growth, 1985. **73**(3): p. 510-514.
6. Teramoto, I., *Vapour growth patterns of CdTe crystals.* Philosophical Magazine, 1963. **8**(87): p. 357-366.
7. Aksyutov, L.N., *Normal spectral emissivity of gold, platinum, and tungsten.* Journal of engineering physics, 1974. **27**(2): p. 913-917.
8. Noblelight, H., *High Reflective Properties of Gold.*
9. Contributors, W., *Black Body.* Wikipedia, The Free Encyclopedia, 2012.
10. contributors, W., *Black-body radiation.* Wikipedia, The Free Encyclopedia, 2013.
11. www.spectralcalc.com, B.b.r.c.-. *High Resolution Spectral Modeling.* GATS, Inc.
12. Howell, J., *A Catalog of Radiation Configuration Factors, McGraw-Hill, New York, 1982.*
13. Hummel, R., et al., *Thermal grooving, thermotransport and electrotransport in doped and undoped thin gold films.* Thin Solid Films, 1981. **78**(1): p. 1-14.
14. Sharma, S.K. and J. Spitz, *Thermal grooving in thin silver films.* Journal of Materials Science, 1981. **16**(2): p. 535-536.
15. Kim, J. and R. Hummel, *The effects of tin underlays on the stability of gold thin films during isothermal annealing.* physica status solidi (a), 1991. **124**(1): p. 211-219.

16. Kim, J.Y., *The Effects of Cu-, Sn-, V-, and Ti-Underlays on the Stability of Gold Thin Films During Isothermal Annealing.* Diss. Abstr. Int., 1990. **50**(7): p. 185.

17. Reimer, L., *Image Formation in Low-Voltage Scanning Electron Microscopy.* SPIE - International Society of Optical Engineering, 1993.

18. Reimer, L., *Scanning Electron Microscopy : Physics of Image Formation and Microanalysis.* Springer-Verlag Berlin Heidelberg, 1985.

19. Liverpool, M.-U.o., *Electron Sources (gun).* 2000.

20. Company, F., *Schottky Field Emission Electron Source.*

21. The Michael J. Drake, E.M.L., University of Arizona, *Brief Introduction to the Electron Microprobe.* Department of Planetary Sciences, Lunar and Planetary Laboratory.

22. Personal Communication with Dr. Patrick McCurdy at Central Instrumentaion Facility, Colorado State Univeristy, Fort Collins

23. Personal communication with Jack Clark at Department of Mechanical Engineering, Colorado State University, Fort Collins.

24. Woods, S., *Understanding scanning white light interferometry.* MICROmanufacturing and Cutting Tool Engineering magazine, 2009. **2**(4).

25. Personal communication with Russell Geisthardt and John Raguse at CSU PV Lab, Colorado State University, Fort Collins, 2012.

26. Bennett, J.M. and E. Ashley, *Infrared reflectance and emittance of silver and gold evaporated in ultrahigh vacuum.* Applied Optics, 1965. **4**(2): p. 221-224.

27. Accuratus, *Accuflect: Light-Reflecting Ceramic.* 2010.

APPENDIX I

C language code for calculation of number of steel radiation shields from starting temperature of 620^{o}C at first shield and 25^{o}C at the last shield. In this program, initial values of temperature were measured after careful calculations for the first and the second shield. Then a loop is created that takes the temperature value of the second shield as the first shield for next round of calculation. This loop is terminated once the final temperature of 25^{o}C is reached.

{\rtf1\ansi\ansicpg1252\cocoartf1038\cocoasubrtf350

{\fonttbl\f0\fnil\fcharset0 Menlo-Regular;}

{\colortbl;\red255\green255\blue255;\red100\green56\blue32;\red196\green26\blue22;\red170\green13\blue145;

\red28\green0\blue207;\red0\green116\blue0;}

\paperw11900\paperh16840\margl1440\margr1440\vieww9000\viewh8400\viewkind0

\deftab720

\pard\tx720\pardeftab720\ql\qnatural\pardirnatural

\f0\fs30 \cf2 \CocoaLigature0 #include \cf3 <stdio.h>\cf2 \

#include \cf3 <sys/types.h>\cf2 \

#include \cf3 <sys/socket.h>\cf2 \

#include \cf3 <stdlib.h>\cf2 \

#include \cf3 <netinet/in.h>\cf2 \

#include \cf3 <arpa/inet.h>\cf2 \

#include \cf3 <unistd.h>\cf2 \

#include \cf3 <sys/utsname.h>\cf2 \

#include \cf3 <netdb.h>\cf2 \

#include \cf3 <string.h>\cf2 \

#include \cf3 <sys/types.h>\cf2 \

#include \cf3 <sys/stat.h>\cf2 \

```
#include \cf3 <fcntl.h>\cf2 \

#include \cf3 <math.h>\cf2 \

\cf0 \

\

\

\cf4 int\cf0  main(\cf4 int\cf0  argc, \cf4 char\cf0  *argv[])\

\{\

	\cf4 float\cf0  theta;\

	\cf4 float\cf0  e1,e2,a1,a2,f1,f12,sig,t1,t2, t24, A, B, C, t3,t4;\

	e1 = \cf5 0.94\cf0 ;\

	e2 = \cf5 0.94\cf0 ;\

	a1 = \cf5 0.184\cf0 ;\

	a2 = \cf5 0.184\cf0 ;\

	theta = \cf5 520.4\cf0 ;\

	f12 = \cf5 0.9\cf0 ;\

	sig = \cf5 5.6704\cf0 /\cf5 100000000\cf0 ;\

	\cf6 //t1 = 893;\cf0 \

	t1 = \cf5 298\cf0 ;\

	\

	\cf6 //theta = (1/ ( ((1-e1)/e1) + ( (a1+a2-(2*a1*f12)) / (a2 - (a1*(f12)*(f12))) ) + (((1-
e2)/e2)*(a1/a2)) )) * (sig*((t1*t1*t1*t1)-(t2*t2*t2*t2)));\cf0 \

   \

	\

	A = ((\cf5 1\cf0 -e1)/e1);\

	B = (a1+a2-(\cf5 2\cf0 *a1*f12)) / (a2 - (a1*(f12)*(f12)));\
```

```
C = (((\cf5 1\cf0 -e2)/e2)*(a1/a2));\

\cf4 int\cf0  count=\cf5 0\cf0 ;\

\cf4 while\cf0  (t1<=\cf5 893\cf0 ) \{\

        count++;\

t24 = t1*t1*t1*t1 ; \

t1 = ((theta * ( ((\cf5 1\cf0 -e1)/e1) + ( (a1+a2-(\cf5 2\cf0 *a1*f12)) / (a2 - (a1*(f12)*(f12))) ) + (((\cf5 1\cf0 -e2)/e2)*(a1/a2)) ) ) / sig) + t24;\

t1 = pow(t1,\cf5 .25\cf0 );\

\

printf(\cf3 "t1 = %.6f \\n"\cf0 ,t1);\

\}\

printf(\cf3 "Count = %d \\n"\cf0 ,count);\

\cf6 /*\

t24 = t1*t1*t1*t1 ;\

e1 = 0.03;\

e2 = 0.03;\

\

t1 = ((theta * ( ((1-e1)/e1) + ( (a1+a2-(2*a1*f12)) / (a2 - (a1*(f12)*(f12))) ) + (((1-e2)/e2)*(a1/a2)) ) ) / sig) + t24;\

t1 = pow(t1,.25);\

\

printf("t1 = %.6f \\n",t1);\

\

t24 = t1*t1*t1*t1 ;\

e1 = 0.8;\
```

```
	e2 = 0.94;\

	\

	t1 = ((theta * ( ((1-e1)/e1) + ( (a1+a2-(2*a1*f12)) / (a2 - (a1*(f12)*(f12))) ) + (((1-
e2)/e2)*(a1/a2)) ) ) / sig) + t24;\

	t1 = pow(t1,.25);\

	\

	printf("t1 = %.6f \\n",t1);*/\cf0 \

	\cf6 //t2 = t14  - ((theta * (A+B+C))/sig);\cf0 \

	\cf6 //printf("Q = %.6f \\n",theta);\cf0 \

	\

\}\

\

\

}
```

Temperature at each shield in Kelvin

t1 = 369.884674	t1 = 652.438171	t1 = 765.665283	t1 = 843.475708
t1 = 414.610870	t1 = 661.977600	t1 = 771.628296	t1 = 847.952637
t1 = 448.278778	t1 = 671.121582	t1 = 777.456177	t1 = 852.359741
t1 = 475.716644	t1 = 679.906372	t1 = 783.155884	t1 = 856.699524
t1 = 499.090820	t1 = 688.363281	t1 = 788.733765	t1 = 860.974365
t1 = 519.577393	t1 = 696.519470	t1 = 794.195801	t1 = 865.186462
t1 = 537.892456	t1 = 704.398804	t1 = 799.547424	t1 = 869.337952
t1 = 554.507324	t1 = 712.022278	t1 = 804.793640	t1 = 873.430786
t1 = 569.750122	t1 = 719.408447	t1 = 809.939270	t1 = 877.466858
t1 = 583.859253	t1 = 726.573914	t1 = 814.988647	t1 = 881.447998
t1 = 597.013916	t1 = 733.533447	t1 = 819.945862	t1 = 885.375916
t1 = 609.352356	t1 = 740.300354	t1 = 824.814758	t1 = 889.252258
t1 = 620.983765	t1 = 746.886597	t1 = 829.598938	t1 = 893.078552
t1 = 631.996033	t1 = 753.303040	t1 = 834.301758	Total Count = 58
t1 = 642.460999	t1 = 759.559631	t1 = 838.926331	